UC-34b
LBL-17279
c.1

Lawrence Berkeley Laboratory

UNIVERSITY OF CALIFORNIA

Physics Division

RECEIVED
LAWRENCE
BERKELEY LABORATORY
MAR 14 1984
LIBRARY AND
DOCUMENTS SECTION

A MEASUREMENT OF THE INTENSITY OF THE COSMIC BACKGROUND RADIATION AT 3.0 cm

S.D. Friedman
(Ph.D. Thesis)

January 1984

For Reference

Not to be taken from this room

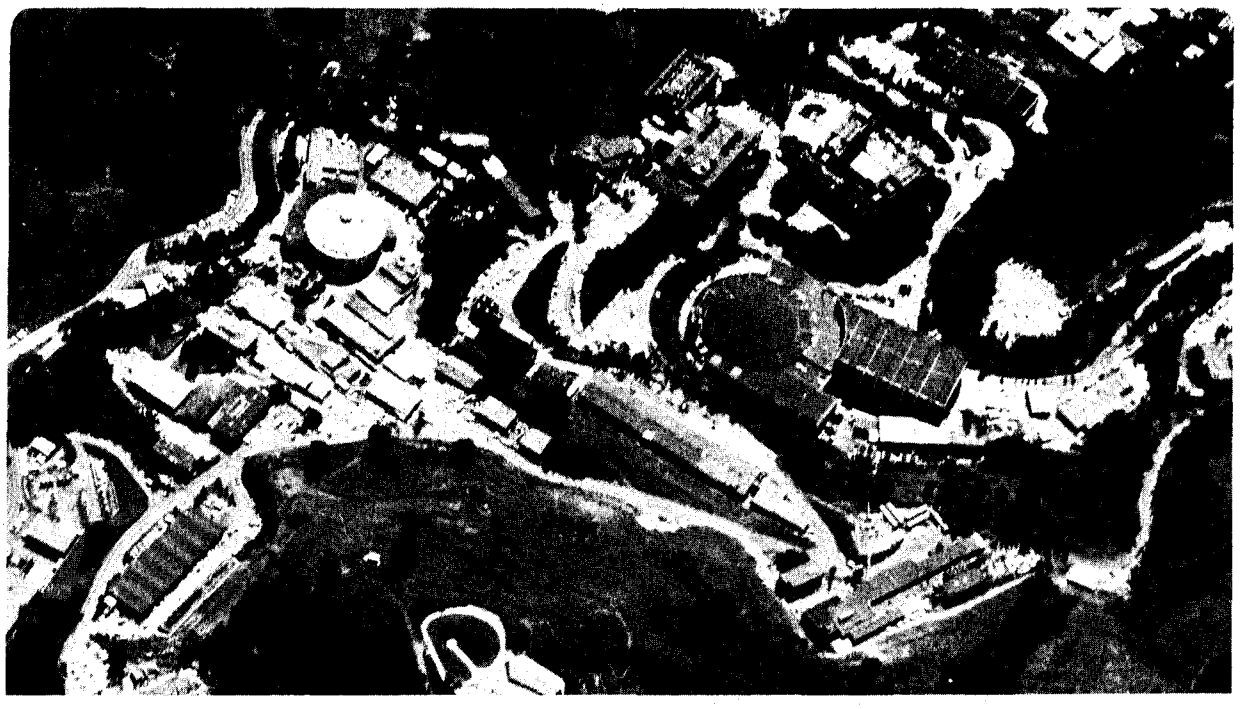

LBL-17279
c.1

Prepared for the U.S. Department of Energy under Contract DE-AC03-76SF00098

DISCLAIMER

This document was prepared as an account of work sponsored by the United States Government. While this document is believed to contain correct information, neither the United States Government nor any agency thereof, nor the Regents of the University of California, nor any of their employees, makes any warranty, express or implied, or assumes any legal responsibility for the accuracy, completeness, or usefulness of any information, apparatus, product, or process disclosed, or represents that its use would not infringe privately owned rights. Reference herein to any specific commercial product, process, or service by its trade name, trademark, manufacturer, or otherwise, does not necessarily constitute or imply its endorsement, recommendation, or favoring by the United States Government or any agency thereof, or the Regents of the University of California. The views and opinions of authors expressed herein do not necessarily state or reflect those of the United States Government or any agency thereof or the Regents of the University of California.

LBL-17279

A MEASUREMENT OF THE INTENSITY OF THE COSMIC BACKGROUND RADIATION AT 3.0 cm

Scott David Friedman
(Ph.D. Thesis)

Lawrence Berkeley Laboratory
University of California
Berkeley, California 94720

January 1984

This work was supported by the Director, Office of Energy Research, Division of High Energy Physics of the Office of High Energy and Nuclear Physics of the United States Department of Energy under Contract Number DE-AC03-76SF00098 and NSF Grants PHY-8015694 and AST-8302843.

A Measurement of the Intensity of the Cosmic Background Radiation at 3.0 cm

Scott David Friedman

Abstract

The intensity of the cosmic background radiation (CBR) has been measured at a wavelength of 3.0 cm as part of a program to measure the Rayleigh-Jeans spectrum of the CBR at five wavelengths between 0.33 cm and 12 cm. The instrument used is a dual-antenna Dicke-switched radiometer with a double-sideband noise temperature of 490 K and a sensitivity of 46 mK/Hz$^{1/2}$. The entire radiometer is mounted on bearings. The atmospheric emission was measured by rotating the radiometer, and thus directing one antenna to zenith angles of $\pm 30^{\circ}$ and $\pm 40^{\circ}$.

The CBR temperature is found by direct comparison with a liquid-helium-cooled absolute-reference load. This load consists of a large cylindrical waveguide, 70 cm in diameter and 130 cm long, terminated by a microwave absorber immersed in LHe. Only two thin polyethylene windows are between the antenna and the LHe. The load has extremely low loss at all five wavelengths of observation. At 3.0 cm reflected power and insertion loss from the walls and windows contribute an additional 20 ± 10 mK to the antenna temperature of the LHe.

Measurements were initially made at White Mountain, Ca. on 5 and 6 July

1982 and repeated with improved equipment on 4, 5, and 6 September 1983. The thermodynamic temperature of the CBR at 3.0 cm is $T_{CBR} = 2.64 \pm 0.14$ K, in good agreement with previous measurements. The error is primarily due to changes in the radiometer output as it rotates during zenith scans.

The weighted mean of our five measurements is $T_{CBR} = 2.70 \pm 0.09$ K. Fitting these five measurements to a Bose-Einstein spectrum yields a thermodynamic temperature of 2.75 ± 0.15 K and a chemical potential $\mu = (2.30 \pm 5.29) \times 10^{-3}$. There is no evidence for a bremsstrahlung repopulation of photons at long wavelengths.

The data are consistent with a blackbody spectrum of the CBR.

Table of Contents

Chapter I - Cosmology and the Cosmic Background Radiation

I.1 Introduction 1
I.2 The Standard Big Bang Model 3
I.3 Possible Causes of Distortions of the CBR 5
I.4 The Spectrum Experiment 10
I.5 Anisotropy and Polarization of the CBR 11

Chapter II - Experimental Design and Description of Apparatus

II.1 Fundamental Concepts 13
II.2 The Observing Site 17
II.3 Description of the Radiometer 19
II.4 The Liquid-Helium-Cooled Reference Load 27
II.5 The Ambient Temperature Load 30
II.6 Data Recording System 30
II.7 The Power Source 31

Chapter III - Preparation and Data Acquisition

III.1 LHe Test in Berkeley 33
III.2 Observation Times 35
III.3 Data Taking 36

Chapter IV - System Performance Tests

IV.1 Introduction 38
IV.2 Integration Tests 38
IV.3 Atmospheric Stability 39
IV.4 Flip Tests 41
IV.5 Other Tests 47
IV.5.a Sidelobe Reception 47
IV.5.b Magnetic Sensitivity 48
IV.5.c Gain Stability 49
IV.6 CBR Measurements With LN 49

Chapter V - Data Reduction and Analysis

V.1 Data Reduction 51
V.2 Calibration Constant 52
V.3 Vertical Sky Temperature 54
V.4 Vertical Atmospheric Antenna Temperature 56
V.4.a Measurement Theory 56
V.4.b Measurement Results 58
V.4.c Rotation of the Quarter Wave Plate 62
V.5 CBR Temperature 63

Chapter VI - Results and Astrophysical Interpretation

VI.1 Results of This Experiment 77
VI.2 Comparison With Previous Results 78
VI.3 Astrophysical Interpretation 81
VI.4 Suggestions For Future Experiments 87

Appendix A - Intensity-Temperature Relations 90

Appendix B - Quarter Wave Plate 92

Appendix C - Emission From LHe Reference Load

C.1 Wall Emission 100
C.2 Reflected Power 103
C.3 Windows 105
C.4 LHe Reference Load Temperature 105

Appendix D - Galactic Background 107

Appendix E - Atmospheric Correction 111

Appendix F - Error Analysis

F.1 Systematic Errors 116
F.1.a Calibration Constant 116
F.1.b Vertical Atmospheric Temperature 117
F.1.c Cosmic Background Temperature 119
F.2 Statistical Errors 120
F.3 Total Experimental Error 120

Acknowledgments 124

References 126

Figures

II.1	Galactic background emission versus wavelength	15
II.2	Vertical atmospheric temperature versus wavelength	16
II.3	Schematic of radiometer	21
II.4	Components of receiver	22
II.5a	Measured E-plane antenna pattern	23
II.5b	Measured H-plane antenna pattern	24
II.6	Liquid-helium-cooled reference load	28
IV.1	RMS fluctuations versus integration time	40
IV.2	Signal average of $\pm 40^{\circ}$ flip test	44
IV.3	Signal average of $-40^{\circ}/+30^{\circ}/+40^{\circ}/+90^{\circ}$ Eccosorb/Sky flip test	45
V.1	T_{40} versus T_{30} (1983 data)	64
V.2a	Cosmic background temperature versus run number (1983 data)	71
V.2b	Cosmic background temperature versus run number (1982 data)	72
V.3a	Cosmic background temperature versus vertical atmospheric temperature (1983 data)	73
V.3b	Cosmic background temperature versus vertical atmospheric temperature (1982 data)	74
V.4a	Histogram of cosmic background temperature values (1983 data)	75
V.4b	Histogram of cosmic background temperature values (1982 data)	76
VI.1	Spectrum measurements of cosmic background radiation	79
VI.2	Results of Woody and Richards spectrum measurement	80
B.1a	Reflection with electric field normal to the plane of incidence	93
B.1b	Reflection with electric field parallel to the plane of incidence	93
B.2	Quarter wave plate	96
B.3	Emissivity of reflector versus radiometer rotation angle	99
D.1	Estimated galactic background temperature at 3.0 cm	109

Tables

I.1	1982 spectrum experiment measurements of the CBR temperature	12
II.1	Data recorded on magnetic tape	32
III.1	Atmospheric measurements in Berkeley	34
III.2	Observation times for LHe measurements of the CBR	37
V.1	Temperature differences between vertical sky and LHe-cooled load	55
V.2	T_{VA} and predicted values of precipitable water vapor	61
V.3	Universal Time, calibration constant, vertical atmospheric temperature, and CBR temperature	67
V.4	Series averages of T_{VA} and T_{CBR}	70
VI.1	Results of this experiment	78
VI.2	Fits of CBR temperature to μ_o and T_1	84
B.1	Emission from aluminum reflector at temperature 275 K	98
B.2	Emission from aluminum reflector for R = 0.53	98
C.1	Resistivity of aluminum and attenuation of an annulus	103
D.1	Estimated galactic background temperature at 3.0 cm	110
E.1	Atmospheric numerical constants	115
F.1	Systematic errors	122
F.2	Parameters used in error analysis	123

Chapter I - Cosmology and the Cosmic Background Radiation

I.1 Introduction

The fields of physics that tend to hold the most interest are those in which there is a good balance between theoretical and experimental advances. Each pushes the other toward greater understanding and new insights. This, however, has not been the state of affairs in cosmology. Formidable technical and observational problems have limited the number of experimental results that have sufficient accuracy to permit a choice between competing theories. The theorists are starved for data, but the experimentalists have not been able to supply it with confidence.

This situation is now changing. More sensitive and precise experiments are producing results which can now constrain some theories dealing with the entire range of cosmology, from the conditions of the universe 10^{-30} seconds after the initial singularity to the mechanisms of galaxy formation. The observational aspect of cosmology is growing out of its infancy.

The study of the origin and ultimate fate of the universe was first cast into a quantitative framework with the introduction of the General Theory of Relativity, by Einstein in 1916 (Lorentz et al., 1952). Among the models which have been extensively studied within the framework of General Relativity is one which obeys the Cosmological Principle. This principle states that the universe is spatially homogenious and isotropic (Weinberg, 1972) and can be described by the Robertson-Walker metric :

$$ds^2 = dt^2 - R^2(t) \left\{ dr^2(1 - kr^2)^{-1} + r^2 d\theta^2 + (r^2 \sin^2\theta) d\phi^2 \right\} .$$

Here $k = 0, \pm 1$ is a parameter which describes the curvature of space. $R(t)$ is called the cosmic scale factor, and is a measure of the change in distance between two points as a function of time.

At about the same time that these theoretical results became known the first spectroscopic observations of nebulae showed that the great majority were shifted toward the red, indicating that they were receding from us. As methods of measuring astronomical distances improved it was found that these nebulae were really galaxies, external to our own Milky Way galaxy. Modern experimental cosmology dates from the announcement by Hubble (1929) of the linear relation between the distance D to a galaxy and its recessional velocity V: $V = H(t)D$. This relationship is a natural outcome of the Robertson-Walker metric, and may also be expressed as

$$H(t) = \frac{1}{R(t)} \frac{dR(t)}{dt} .$$

The function $H(t)$ is constant in space at a given epoch, and is called the Hubble parameter. (Hubble called it K in his work.)

In 1965 Penzias and Wilson (1965) made another great experimental contribution, the discovery of the cosmic background radiation (CBR). It was immediately interpreted (Dicke et al., 1965) as a remnant of an early, hot, highly condensed state of the universe. This was the observation which finally led to the acceptance by most cosmologists of one theory of the early universe above all others. This theory is called the Big Bang.

I.2 The Standard Big Bang Model

The "standard" big bang is a remarkably elegant theory which can account for several important characteristics of the observed universe (Weinberg, 1972; Harrison, 1973). Very briefly, it holds that the universe evolved from an initial state undergoing rapid expansion and cooling. The origin of this state is not known. At a temperature $T \simeq 10^{12}$ K the primary constituents of the universe were a thermal distribution of photons, the light leptons ($e^{\pm}$, $\mu^{\pm}$, and their associated neutrinos), and a relatively low density of neutrons and protons that remained after most of these had annihilated with their antiparticles. As the temperature dropped below about 10^{10} K, approximately one second after the singularity, the neutron/proton ratio became nearly fixed. Photodissociation was no longer able to prevent the formation of deuterium, and of ^{4}He almost immediately thereafter. The non-existence of stable nuclides with $A = 5$ or $A = 8$ effectively prevented heavier nuclei from forming in great abundance. Furthermore, ^{4}He has a binding energy which far exceeds that for other nuclei with $A < 5$. Therefore, by the time the temperature dropped below 10^8 K the nuclear abundances were essentially fixed, with ^{1}H and ^{4}He by far the most abundant, and all other nuclear species accounting for less than 0.1% by mass.

The universe continued to expand after primordial nucleosynthesis for about 10^6 years when, at a temperature $T \simeq 4000$ K, the electrons and protons combined to form neutral hydrogen, and the opacity of the universe precipitously dropped. The radiation and the matter decoupled, and each continued to cool as the universe expanded according to the relation $T(t) \propto \{R(t)\}^{-1}$. The standard model predicts that the radiation we now observe has almost exactly a blackbody distribution (Weinberg, 1972).

There are three reasons why the standard model has been widely accepted. The model

1) is consistent with the observed Hubble recession of the galaxies;

2) predicts a helium abundance which agrees with observation;

3) predicts the existence of the cosmic background radiation.

The Hubble relation has been verified with the observations of hundreds of galaxies over vast distances. Determining the present value H_o of $H(t)$ is the subject of current research. Two careful investigations have yielded widely different results:

$H_o = 50 \pm 7$ km sec^{-1} Mpc^{-1} (Sandage and Tammann, 1982).

$H_o = 93 \pm 10$ km sec^{-1} Mpc^{-1} (Buta and de Vaucouleurs, 1983).

Despite this disagreement there is very little doubt that the observations of the expansion of the universe are valid.

The primordial abundance by mass of ^{4}He, designated Y, depends only weakly on cosmological parameters that are difficult to measure, such as the Hubble parameter and the baryonic mass density of the universe (Yang et al., 1979). This is why the helium abundance is a strong test of the standard model. The model predicts $Y \simeq 0.25$, and this is almost independent of the mass density of the universe over reasonable ranges (unless the number of lepton families is large). Using a wide variety of measurement techniques the experimental results have largely fallen in the range $0.20 < Y < 0.25$ (Bohm-Vitense and Szkody, 1973; Rood, 1973; Hinshfeld, in Yang et al., 1979). These results are from observations of regions both within our galaxy and in other galaxies. Thus they are unlikely to be due to local effects only. This agreement is an important success for the standard model.

Finally, the model predicts that there is a thermal, isotropic radiation background throughout the universe. This radiation, the CBR, is continuously

being redshifted as the universe expands, and is now seen in the microwave and infrared spectral regions. Its observation is perhaps the greatest triumph of the theory.

Despite these successes it is obvious that the standard model is not complete, for it does not describe the events at extremely early times in the universe ($T > 10^{12}$ K), and it does not account for structures which formed much later, such as galaxies and stars.

There is now intensive research underway to understand the conditions in the universe when the temperature was above 10^{12} K. Inflationary universe models (Guth, 1981; Press, 1981; Barrow and Turner, 1982) incorporating Grand Unified Theories (GUTs) of elementary particles, have had some success at explaining, among other things, the observed isotropy of the CBR and the energy density in the universe. These results are still very tentative. However, the spectrum of the CBR is determined by processes that occurred after this early epoch. Thus the uncertainties associated with these models do not affect the predictions about the CBR, as long as the Cosmological Principle is valid.

To account for structures like galaxies and stars, it has been necessary to modify the standard model. Most of these modifications result in some release of energy after the CBR is established. This extra energy may cause a departure of the CBR spectrum from a thermal distribution. The shape and magnitude of such a distortion can reveal its source, providing valuable information about conditions in the early universe. This is why an observed distortion would be so interesting and important.

I.3 Possible Causes of Distortions of the CBR

Above the temperature $T \simeq 5 \times 10^9$ K matter and radiation in the universe

were tightly coupled, and thermal equilibrium was easily maintained. As the temperature fell below this value the e^+e^- pairs quickly annihilated. We first consider the effects of a large energy release after the epoch of $e^\pm$ annihilation. Possible sources of this energy will be considered later.

The extra energy is distributed in the background radiation by the processes of Compton scattering and bremsstrahlung (Kompaneets, 1957; Weymann, 1965). Since $n_\gamma \gg n_e$, Compton scattering, whose rate is proportional to $n_e n_\gamma$, is very efficient compared to bremsstrahlung, whose rate is proportional to n_e^2 (Danese and De Zotti, 1977; Illarionov and Sunyaev, 1975). Here n_γ and n_e are the number densities of photons and electrons (and positrons), respectively. While bremsstrahlung produces photons, and therefore tends to maintain an equilibrium distribution, Compton scattering shifts the energy of photons but preserves their number. Thus the photon number density remains nearly unchanged and the average energy per photon increases. The result is a Bose-Einstein spectrum. Although bremsstrahlung tends to make up for this low photon density, starting first at the long wavelengths, in general there will not be sufficient time to re-establish a blackbody distribution. Thus a distortion in the CBR spectrum may result from any large energy release that occurred after the temperature dropped below 5×10^9 K.

Since the release of energy increases the average energy per photon, measurements of the CBR would yield higher temperatures at short wavelengths (the Wien region of the spectrum) and lower temperatures at long wavelengths (the Rayleigh-Jeans region). The transition wavelength, though model dependent, is typically about 0.3 cm. If the energy were released early enough then bremsstrahlung would begin to raise the temperature again at even longer wavelengths, greater than about 10 cm. The predicted distortions are quite broad so that observations at several wavelengths are required (Weymann, 1966).

The maximum deviation from a blackbody spectrum occurs at a wavelength λ which depends on the redshift z at which the energy was released and on $\Omega = \rho / \rho_c$, the ratio of the density of the universe to the critical density. Here z is the redshift parameter, defined as

$$1 + z = \frac{T(t)}{T_o} = \left\{ \frac{R(t)}{R_o} \right\}^{-1} ,$$

where T(t) and R(t) are the radiation temperature and the scale factor of the universe at the time t of interest, and T_o and R_o are the present values of these parameters. In most cases the distortions are largest in the microwave region, $1 < \lambda < 100$ cm, if $\Omega < 0.1$ and the energy is released at $z < 10^5$ (Illarionov and Sunyaev, 1975; Chan and Jones, 1975).

The magnitude of the distortion is model dependent. In general it is proportional to the ratio of the energy released to the energy present in the radiation field at the time of release. Since the energy density of the radiation is proportional to T^4, and T decreases as the universe expands, a given amount of energy causes a larger fractional distortion if it is released late in the evolution of the universe.

The physical processes that might release a sufficient amount of energy to cause an observable distortion in the CBR spectrum have been discussed by many authors. These processes include dissipation of primordial turbulence (Bontz et al., 1981; Matsuda et al., 1971), isotropization of an anisotropic universe (Doroshkevich et al., 1968), shock waves that accompany matter inhomogeneities (Zeldovich and Illarianov, 1975; Peebles, 1970), fragmentation of protogalaxies and protoclusters (Sunyaev and Zeldovich, 1972), matter-antimatter annihilation (Harrison, 1967), primordial nucleosynthesis, and hydrogen recombination. Although these last two processes release a

considerable amount of energy, neither is likely to cause an observable distortion, as we now show.

Nucleosynthesis occurs at $z \simeq 10^9$. At the time there were about 10^9 photons per nucleon, each with an average energy of $kT_o(1 + z) \simeq 10^5$ eV, where T_o is the present temperature of the CBR. The synthesis of free protons and neutrons into ^{4}He releases about 6 MeV per nucleon. The ratio of the energy released to the energy in the radiation field was

$$(6 \times 10^6 \text{ eV}) / (10^9)(10^5 \text{ eV}) \simeq 10^{-7} .$$

Thus the fractional distortion of the CBR, due to this source, is expected to be far too small to see.

The second source is the energy released at recombination, at $z \simeq 1500$, which liberates 13.6 eV per nucleon. The mean energy per CBR photon was $kT_o(1 + z) \simeq 10^{-1}$ eV, and there were about 10^9 such photons per nucleon. The ratio of the recombination energy to the CBR energy was

$$(13.6 \text{ eV}) / (10^9)(10^{-1} \text{ eV}) \simeq 10^{-7} ,$$

which again is extremely small (Peebles, 1971). One might expect to see this today as a small but sharp bump in the infrared, at a wavelength of

$$\lambda = hc(1 + z) / (13.6 \text{ eV}) \simeq 150 \text{ microns},$$

far in the Wien portion of the spectrum. However, the feature is considerably smoothed because the recombination photons excite the hydrogen atoms, which are then easily ionized by relatively soft photons. The result is that the

recombination process lasts until $z \simeq 150$ (Zeldovich et al., 1969), and produces photons with a range of energies. Thus, the distortion due to recombination is unobservably small.

The mechanisms discussed above tend to produce distortions which are quite different from that reported in the infrared part of the spectrum by Woody and Richards (1981). They observed a flux enhancement at wavelengths near the peak ($\lambda \simeq 0.18$ cm) and a steep drop in flux shortward of the peak. Considerable theoretical work has been done to try to explain such a spectrum. The most straightforward model invokes the existence of a pregalactic generation of stars (Population III) at a redshift $z \simeq 200$ (Negroponte et al., 1981). These hot stars lived for only a short time, and then ejected dust which came to equilibrium with the radiation in the universe. The absorption features at 10 microns of several types of materials were studied. Negroponte found that dust composed of amorphous silicate, obsidian, and basaltic glass would emit radiation which, when redshifted, could account for the observed distortion.

To summarize, the spectrum of the CBR may be distorted, if certain conditions are met, by the release of energy in the early universe. In most models the energy is distributed by Compton scattering, which tends to cause higher flux at short wavelengths, lower flux at long wavelengths, and perhaps high flux again at still longer wavelengths due to bremsstrahlung.

Detection of distortions would be of great value in understanding the conditions that existed in the distant past. This fact was recognized immediately after the discovery of the CBR. Most early experiments to measure the temperature were made in the wavelength region $0.3 < \lambda < 75$ cm. The results of these measurements, which will be discussed in Chapter VI, give no indication of a distortion in the spectrum (Figure VI.1). However these measurements were not sufficiently accurate to rule out distortions even as

large as 15%. More recently Danese and De Zotti (1977) again stressed the importance of knowing with greater accuracy the shape of the CBR spectrum. At their instigation N. Mandolesi and G. Sironi began preparations in Italy for new measurements of the CBR temperature. At the same time, but independently, plans were being made in Berkeley for a similar investigation. A meeting by the parties at a conference in 1977 at Copenhagen, Denmark resulted in an agreement to collaborate on this spectrum experiment, a large coordinated effort to measure the intensity of the CBR at five wavelengths in the Rayleigh-Jeans region.

I.4 The Spectrum Experiment

This experiment was a collaboration of researchers from four institutions, Consiglio Nazionale delle Ricerche (Italy), University of Padova (Italy), Haverford College (Pennsylvania), and University of California (Berkeley). Two radiometers were made in Italy, one was made at Haverford, and most of the rest of the equipment came from Berkeley.

The initial spectrum measurements were made on 5 and 6 July 1982 (Smoot et al., 1983; Sironi et al., 1984; Mandolesi et al., 1984; Friedman et al., 1984; De Amici et al., 1984; Partridge et al., 1984). The results are summarized in Table I.1. The weighted mean of these five measurements is T_{CBR} = 2.79 ± 0.10 K. No evidence for a distortion was seen.

We recognized that each of the radiometers could be modified to give significantly improved results. Thus, we repeated the measurements on 4, 5, and 6 September 1983.

The subject of this thesis is the measurement of the intensity of the CBR at a wavelength of 3.0 cm. Although the emphasis will be on the data taken in

1983, there are only small differences in the procedures and equipment between the 1982 and 1983 measurements. Descriptions of these differences will be given where appropriate.

The result of the new measurement at 3.0 cm is

$$T_{CBR} = 2.64 \pm 0.14 \text{ K.}$$

The results of the 1983 measurements at the other four wavelengths are not yet available.

I.5 Anisotropy and Polarization of the CBR

Two other properties of the CBR which have been measured deserve mention.

The large-scale anisotropy has been measured most recently with balloon-borne radiometers. Epstein (1983) reports a dipole amplitude of 3.48 ± 0.23 mK, in the direction RA = 11.3 hours, declination = -5.7° , from observations at a wavelength of 0.33 cm. This is in very good agreement with the data at 1.2 cm (Fixsen et al., 1983). This is interpreted as a Doppler shift due to our motion relative to the comoving frame of the universe. No significant quadrupole has been seen (Lubin et al., 1983a).

The polarization of the CBR has been most accurately measured at a wavelength of 0.9 cm (Lubin et al., 1983b). No significant component of linear polarization was found at the level of 0.1 mK.

The results of measurements made prior to 1980 of the intensity, large-scale anisotropy, and polarization of the CBR are summarized in the excellent review article by Weiss (1980).

Table I.1 - 1982 spectrum experiment measurements of the CBR temperature. T_{VA} is the antenna temperature of the vertical atmosphere. The 3.2 cm wavelength radiometer was used only to measure the atmospheric emission.

Wavelength (cm)	T_{VA} (K)	T_{CBR} (K)
12.0	0.95 ± 0.05	2.62 ± 0.25
6.3	1.0 ± 0.1	2.71 ± 0.2
3.2	1.03 ± 0.03	———
3.0	0.93 ± 0.16	2.91 ± 0.19
0.9	5.0 ± 0.14	2.87 ± 0.21
0.33	12.3 ± 0.8	2.4 ± 1.0

Chapter II - Experimental Design and Description of Apparatus

II.1 Fundamental Concepts

A measurement of the intensity of the CBR is made by comparing the radiation received from the vertical sky with the radiation received from a known reference source. If the gain of the receiver is known then the power from the vertical sky can be determined. This power is the sum of contributions from the CBR, galactic sources, the atmosphere, the nearby ground, and other sources. The CBR intensity can be determined by carefully accounting for all these contributions.

The experiment was designed to reduce the magnitude of these extraneous contributions to minimal levels. The difficult part of the experiment was to measure the remaining important contributions, with small systematic errors, so that their effects could be correctly removed. Systematic errors dominate the statistical errors, and thus determine the accuracy of the measurement.

In this experiment we measured the CBR temperature at five wavelengths, 12, 6.3, 3.0, 0.9, and 0.33 cm. These wavelengths were chosen primarily to minimize two of the most important systematic effects, the galactic and atmospheric backgrounds.

Figure II.1 shows the galactic background emission as a function of wavelength. It is highly anisotropic, with maximum emission generally in the direction of the galactic plane. The non-thermal component is almost entirely synchrotron radiation, and the thermal component is HII emission. Because of its rapid rise with increasing wavelength and its directional dependence, accurate measurements for $\lambda > 20$ cm are difficult.

The atmospheric emission seen from a mountain elevation (≈ 4000 meters) is shown in Figure II.2. At long wavelengths it is dominated by oxygen emission which is constant in time, and is relatively insensitive to water vapor which changes with time. Therefore, the atmospheric temperature is almost constant in the range $2.5 < \lambda < 30$ cm. We take advantage of this by observing at 12, 6.3, and 3.0 cm.

For $\lambda < 2.5$ cm useful measurements can be made only between the O_2 lines (0.5 and 0.25 cm) and the H_2O lines (1.35 and 0.16 cm). The measurements at 0.9 cm and 0.33 cm fall in these windows. In addition, $\lambda = 0.33$ cm slightly overlaps the Woody and Richards spectral range. This allows a direct comparison of the two experiments.

The design of the experiment incorporated the following features to reduce or eliminate some of the systematic errors present in previous measurements.

1. The measurements of the CBR at all five wavelengths were made simultaneously from the same location, the Barcroft Facility, White Mountain Research Station, of the University of California (118° west longitude, 38° north latitude; elevation 3800 meters). This allows a correlation of the results and accurate modeling of the atmospheric emission.

2. Since the atmospheric emission is the largest extraneous background seen by all five radiometers, an additional radiometer was used as an atmospheric monitor only. This instrument made continuous, automated measurements of the atmospheric emission at a wavelength of 3.2 cm.

3. All of the radiometers used corrugated horn antennas with excellent sidelobe suppression. Those at wavelengths of 12, 6.3, and 3.0 cm were scaled triplicates, with 12.5° half-power beamwidths. Thus each had the same beam shape. Those at 0.9 and 0.33 cm were also scaled duplicates, with 7.5° HPBW.

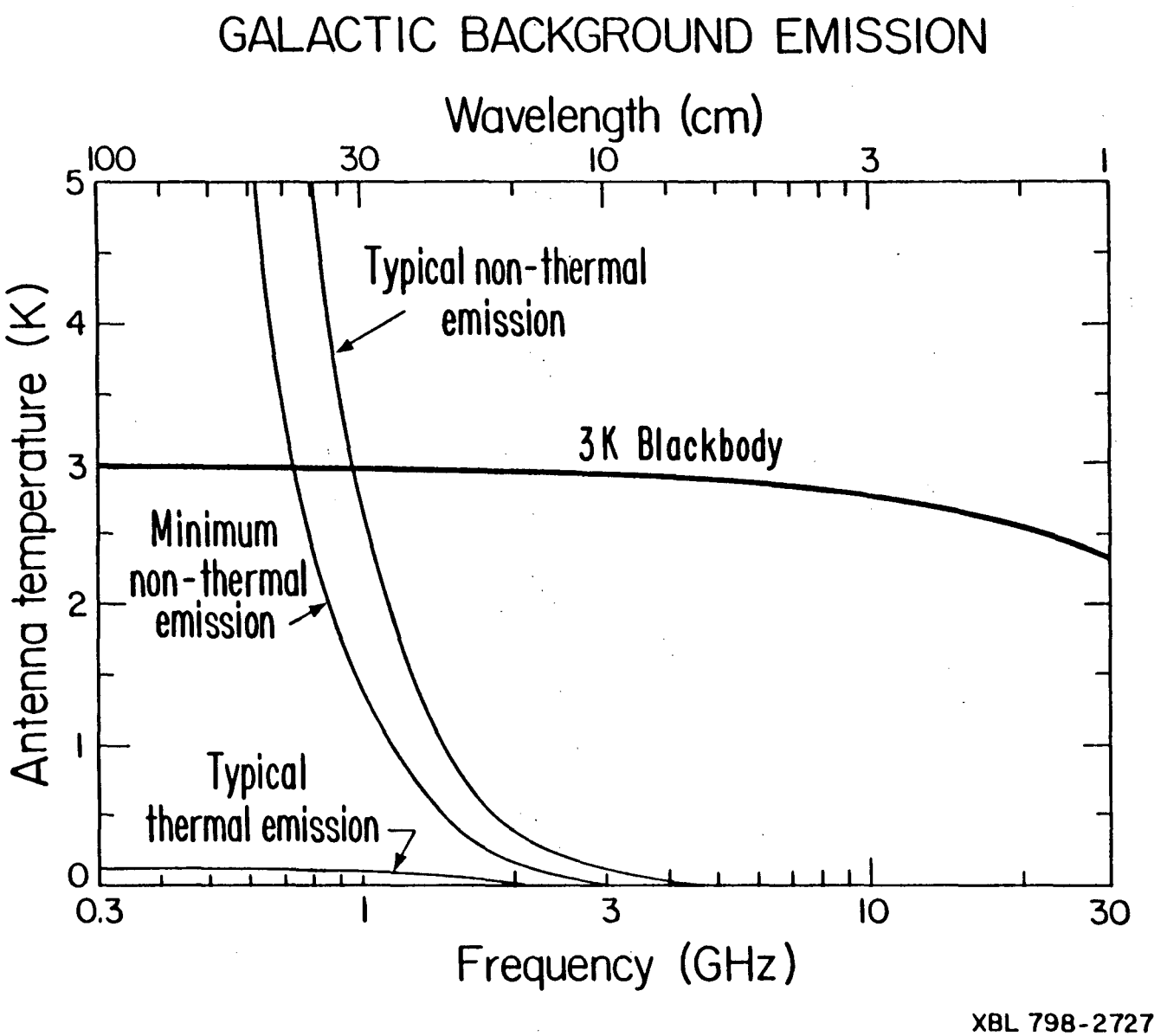

Figure II.1 - Galactic background emission versus wavelength

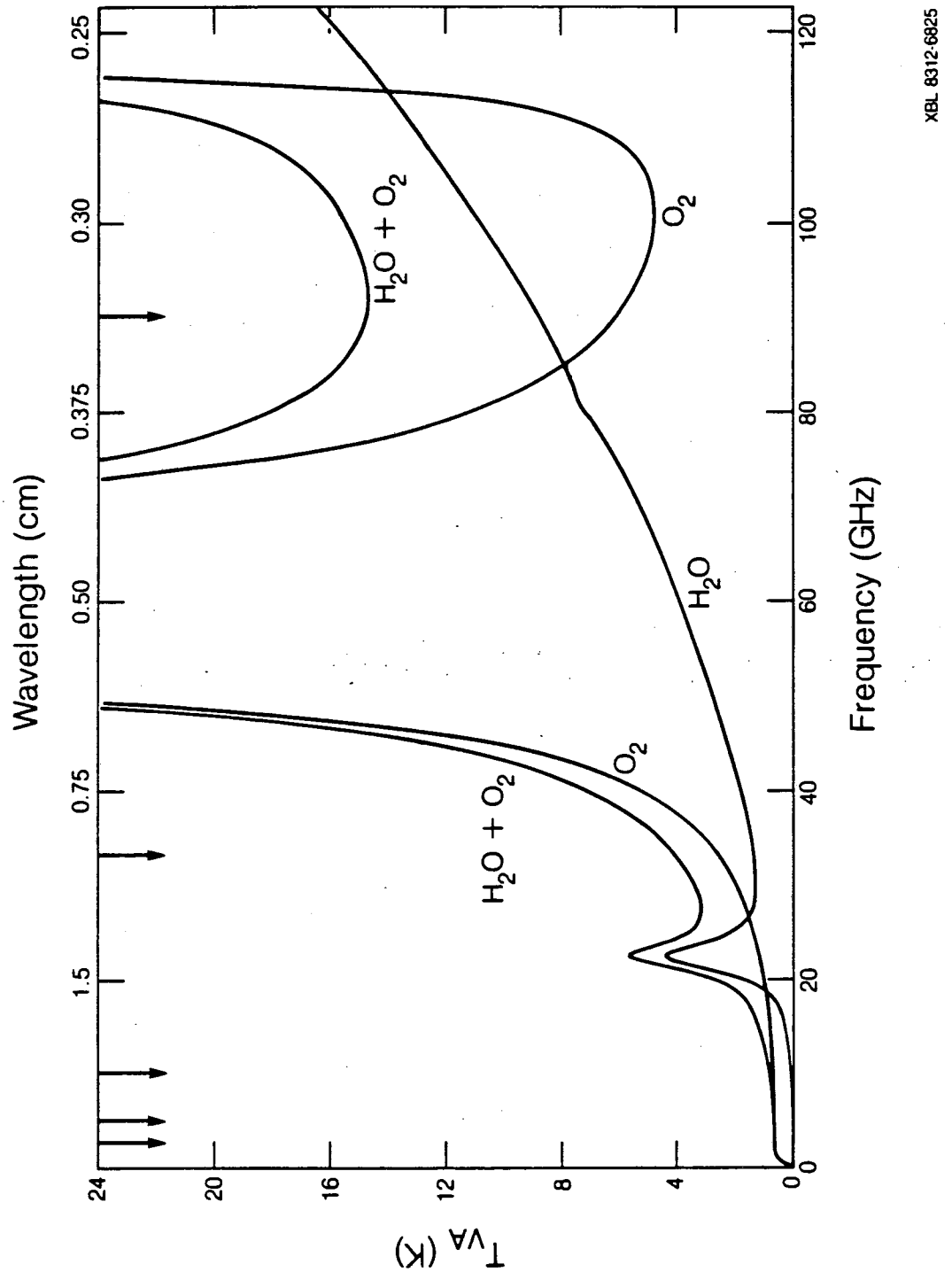

Figure II.2 - Approximate vertical atmospheric temperature versus wavelength (4000 meter elevation). The arrows indicate the wavelengths of observation in this experiment.

4. A single liquid-helium-cooled absolute-reference load was used for all five radiometers. (The atmospheric monitor radiometer does not require a LHe load.) For the 12 cm wavelength radiometer the internal antenna diameter exactly matched the inside diameter of the reference load. With the other four radiometers the reference load acted as a very large waveguide and therefore had very low insertion loss.

II.2 The Observing Site

Barcroft proved to be a good choice as an observing site for several reasons.

It is necessary to go to a high altitude site in order to reduce the intensity of the atmospheric emission. Oxygen and water vapor are the only two constituents of the atmosphere which significantly radiate at the wavelengths of observation. Oxygen is well mixed, but water vapor is variable both in direction and time. Since the ambient temperature at Barcroft on summer nights is usually about $0^{o}C$, most of the water vapor is frozen out of the air. A typical value for the column density of precipitable water is 0.25 gm/cm^2. This is roughly a factor of four lower than on a clear, dry day at Berkeley (sea level).

There is an established high-altitude research station at Barcroft. The presence of a Quonset hut, with living and work rooms, a cook, and electrical power (albeit from a rather unreliable generator) made the site attractive. The support we received from the station personnel proved indispensable.

White Mountain is about 575 km from Berkeley, only a one day drive. This convenient location permitted us to make several trips to Barcroft to test the equipment in the two years preceeding the measurements.

Finally, the site is isolated from urban areas and their multitude of radio

transmitters. Once we unplugged the microwave oven in the Barcroft kitchen we found only low levels of radio-frequency interference. However, as technology improves, satellites which broadcast at wavelengths even shorter than 0.5 cm may make an experiment like this one impossible.

The ideal time for these observations is the middle of winter. The atmospheric emission is very low then since virtually all water vapor is frozen out. The galactic background is at its minimum at night, since the galactic plane passes overhead during the day (Figure D.1). However, deep snow and low temperatures make it is impossible to work outdoors at Barcroft in the winter. In most years data can be taken only between late June and early October. To avoid the galactic plane as much as possible, and to get maximum sky coverage, we made the 1982 measurements in early summer, and the 1983 measurements in late summer.

The Barcroft area is a plateau set in a mountainous region. On one of the flat areas, relatively free from rocks, we erected in the east/west direction a 20-meter-long pair of rails, parallel to each other and spaced 1.9 meters apart. Each of the five radiometers was mounted on a separate cart which rolled freely on the rails. The LHe reference load was suspended just below the center of the rails, in a hole in the ground. When a particular radiometer was making CBR measurements it was positioned at the center of the rails, so that observations of the LHe load could be made without moving the cart. At the same time one or more of the other radiometers made atmospheric zenith scans, so that atmospheric emission could be correlated at different wavelengths. At the end of about 45 minutes of running the first radiometer was rolled out of the LHe position and another took its place.

About five meters to the south of the rails was a shed for the support equipment, including a magnetic-tape data recorder, batteries to power the

apparatus, and chargers for the batteries. The atmospheric monitor radiometer was about ten meters southwest of the shed.

II.3 Description of the Radiometer

The 3 cm wavelength radiometer is mounted on bearings so that it can rotate in a vertical plane (Figure II.3). The primary antenna can swing through 360° to view any desired zenith angle, in order to make atmospheric zenith scans. The rotation axis is coincident with the axis of the horizontal secondary antenna whose beam is reflected by a fixed mirror toward the vertical sky.

The function of the secondary antenna is to provide a constant, low temperature reference signal; the sky serves as a convenient source. It is important that the response of this antenna be independent of the rotation position of the radiometer. Although the cosmic background radiation is unpolarized, a small linear polarization is introduced when it is reflected from the mirror. This polarized signal modulates the power accepted by the secondary antenna as the radiometer rotates. To prevent this modulation a microwave quarter-wave plate was permanently installed in the throat of the secondary antenna. If the quarter-wave plate were perfect then this antenna would respond only to circular polarization, and the signal into the antenna would be independent of the rotation position. However, the quarter-wave plate is not quite ideal and there is a small residual response to linear polarization. These effects are discussed more fully in Appendix B.

A system of aluminum sheets and screens around both antennas shields against thermal emission from the ground. The ground shields used in the 1983 measurements had the same general shape as the 1982 shields, but were larger. The shields around the primary antenna were lengthened in 1983 to allow zenith

scans at larger angles. The horizontal shield below the secondary antenna was found to be intercepting an excessive fraction of the beam, and was moved farther away from the antenna.

A low noise superheterodyne receiver is alternately connected to one of the two antennas by means of a Dicke switch. Details of the receiver are shown schematically in Figure II.4.

The two identical antennas were made by the firm CSELT, of Torino, Italy. They are scalar-feed corrugated horn antennas, made of aluminum, and have a half-power beamwidth of 12.5°. They have excellent sidelobe suppression. For example, when the radiometer is at its maximum tilt (40°) from vertical during atmospheric zenith scans, the local horizon comes to within 35° of the beam axis in the west. However, more than 99.7% of the power is received by the inner 35° cone of the beam. With the additional shielding of the ground screens the contribution from the ground is 7 mK, even in the 40° tilt orientation.

The E and H plane response patterns of the antennas are shown in Figures II.5a and II.5b.

The Dicke switch (Electromagnetic Sciences model 540B) is a latching ferrite three-port circulator. It has a measured insertion loss of less than 0.3 dB between any two ports, and has greater than 25 dB isolation. The switching frequency is 100 Hz.

The isolator (Passive Microwave Technology model XYC1020) is actually a three port ferrite circulator with one port permanently terminated. The measured isolation is greater than 36 dB, and the insertion loss is 0.1 dB.

The Gunn-diode local oscillator (Central Microwave model CMF 410 AK) has a power output of approximately 18 mW. The noise of the mixer is reduced if it receives less power from the LO. Therefore, a waveguide attenuator is

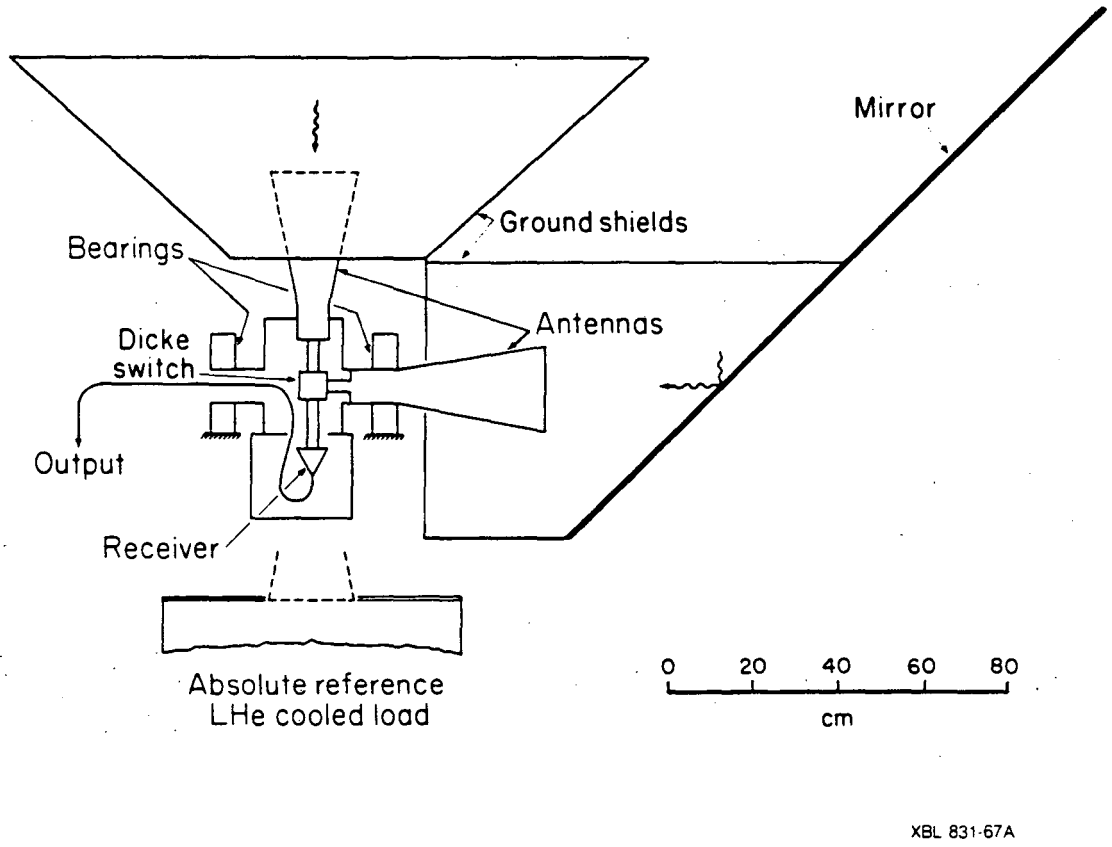

Figure II.3 - Schematic of radiometer in the 1983 configuration

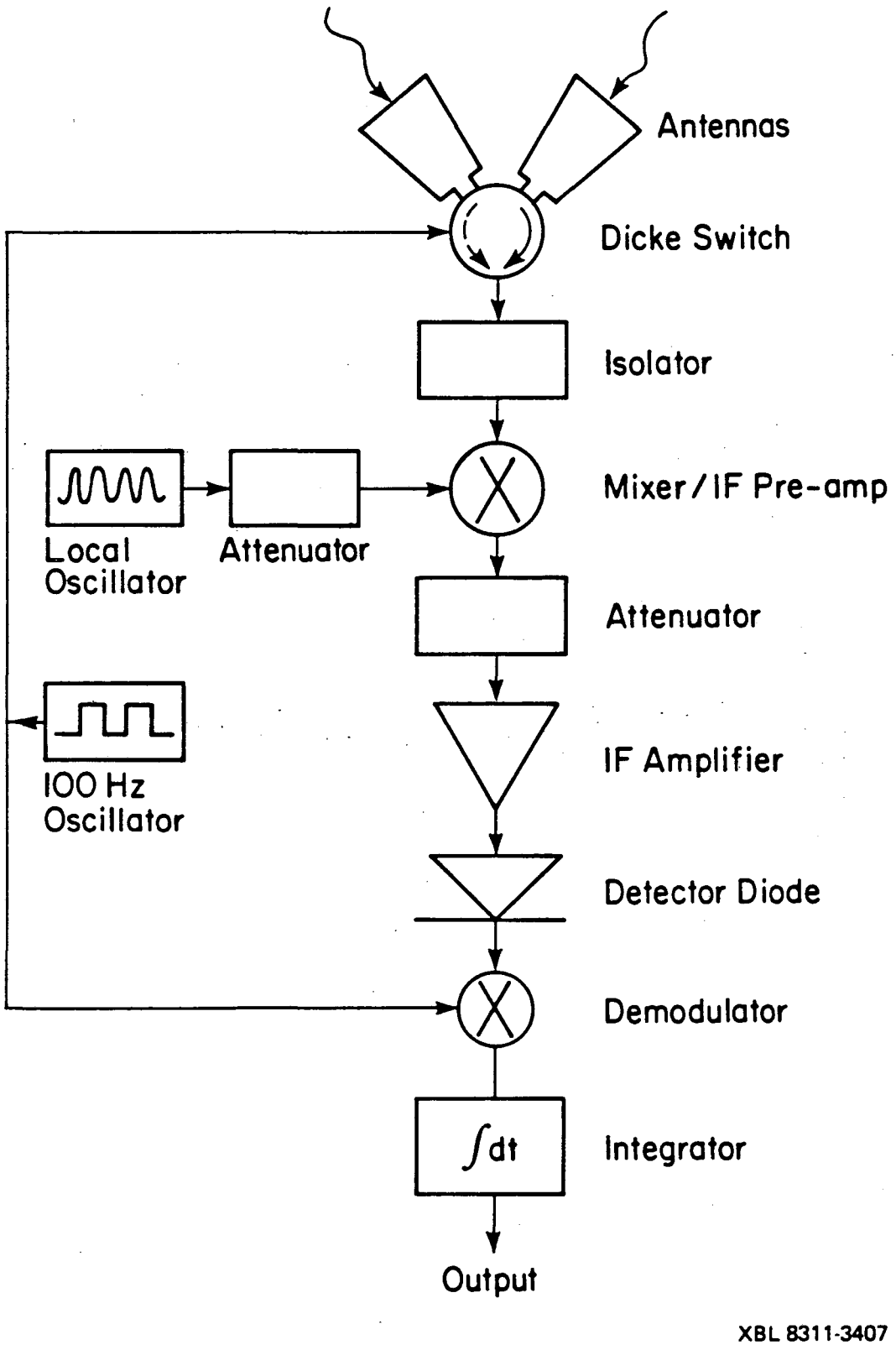

Figure II.4 - Components of receiver

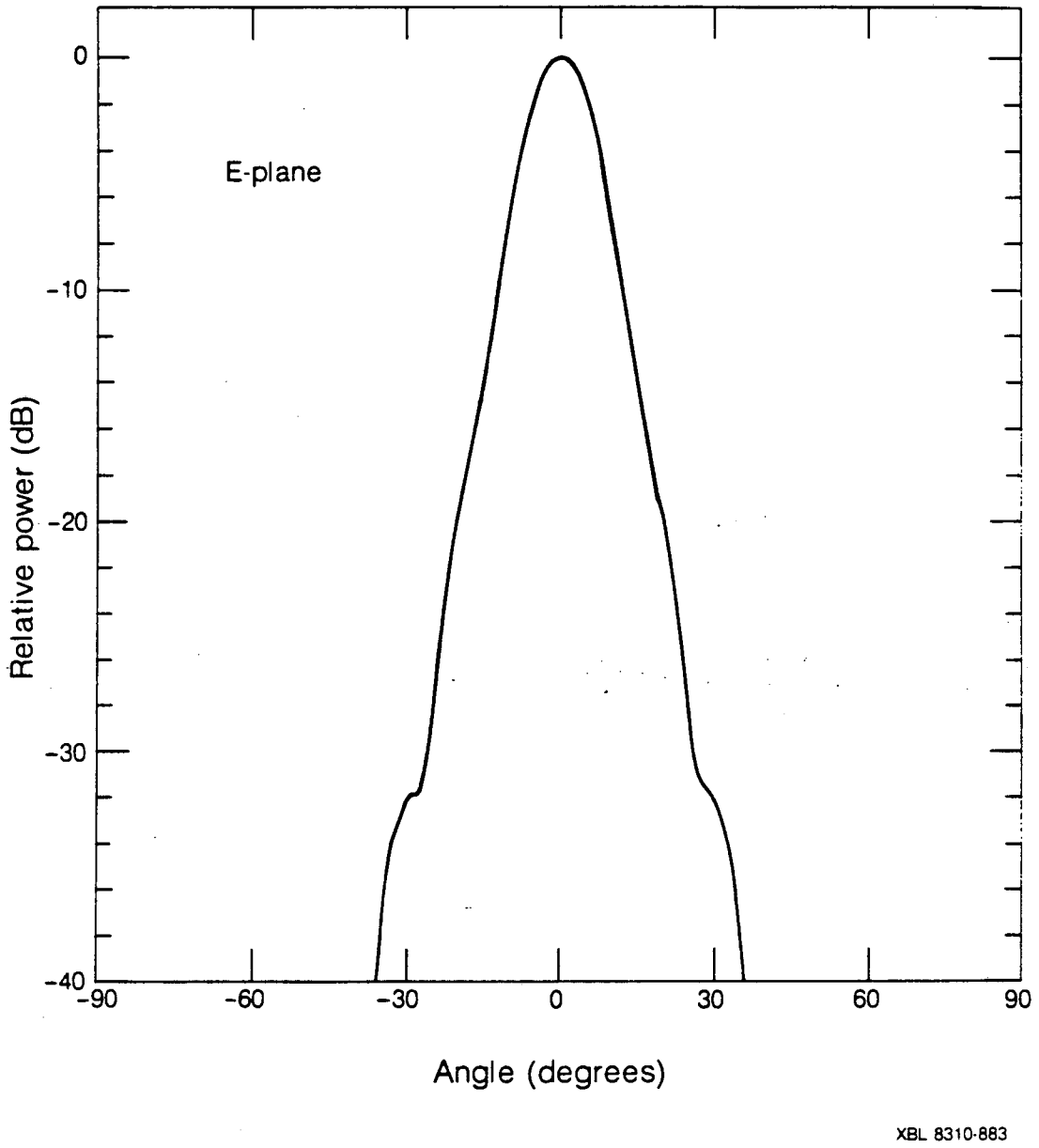

Figure II.5a - Measured E-plane antenna pattern

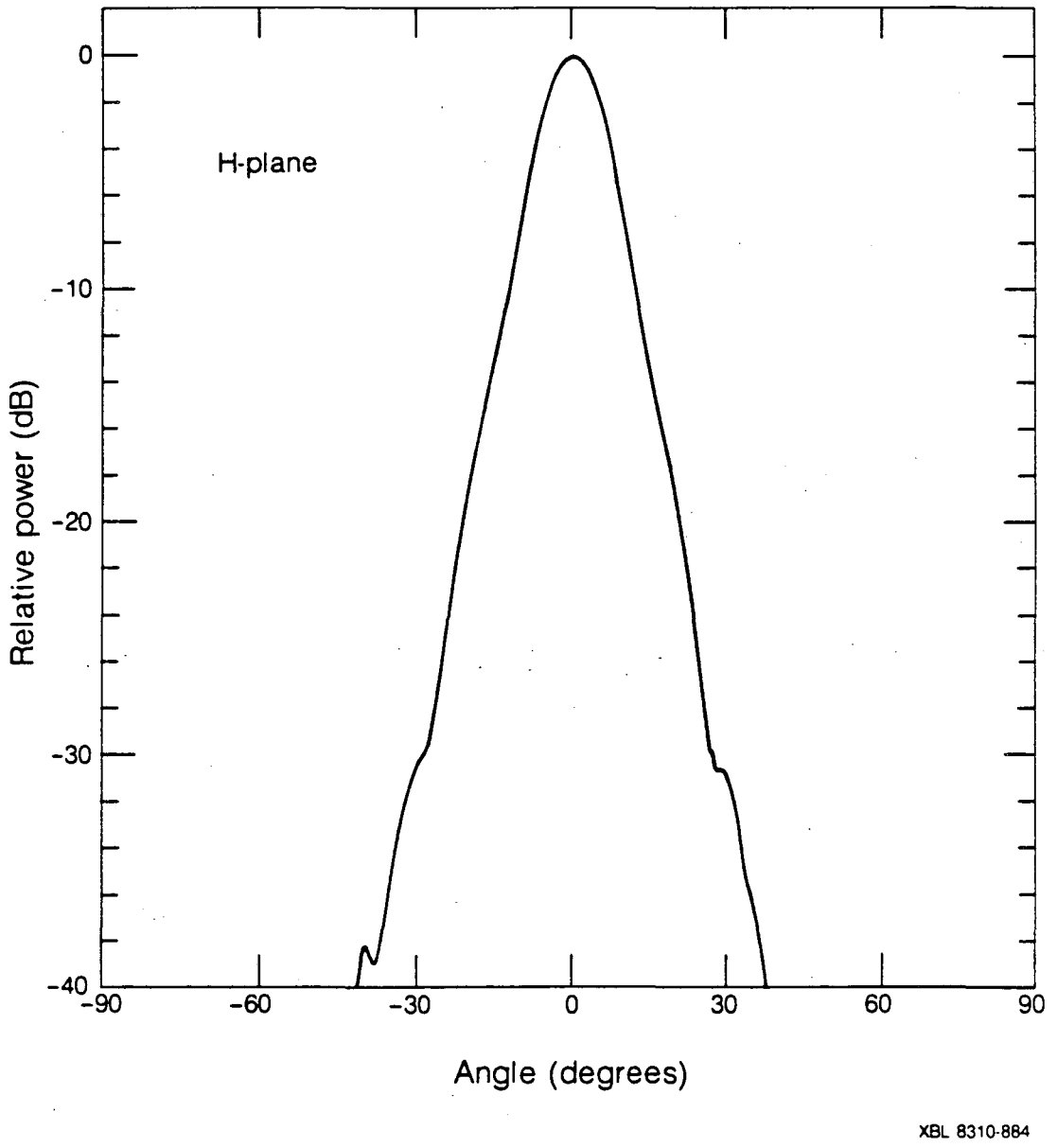

Figure II.5b - Measured H-plane antenna pattern

placed between these two components to reduce the LO power by approximately a factor of two. The frequency of the LO is tuned over a small range using a tuning screw which changes the resonant frequency of the internal cavity. It was set to 10.00 ± 0.01 GHz using an FXR cavity frequency meter, and confirmed with a spectrum analyzer.

The mixer/intermediate-frequency pre-amplifier (Honeywell-Spacekom model R10-U), a single unit, has a nominal bandpass of 10-550 MHz. The measured RF-to-IF gain is greater than 24 dB, and the measured double-sideband noise figure is less than 3.4 dB across the band.

The IF amplifier (Amplica model 401 USL) has a nominal bandpass of 5-500 MHz. The gain is greater than 41 dB and the noise figure less than 2.6 dB.

Inserted between the amplifiers is a 6 dB attenuator which reduces non-linear saturation in the radiometer. It also serves to decouple the amplifiers in order to prevent oscillations.

Following the IF amplifier is a Hewlett-Packard 8472B crystal Schottky-barrier detector diode, whose output voltage is proportional to input power. The conversion factor in the operating regime is approximately 1 mV/μW. The output voltage from the diode is about 3 mV.

The lockin amplifier was built by our electronics engineer. It consists of a demodulator followed by an "ideal" boxcar integrator. The voltage gain of the lockin amplifier is approximately 1.5×10^4. The output is digitized and recorded on magnetic tape.

The power supplies for the amplifiers, Dicke switch, and associated electronics are housed in an RF shielded box fixed to the cart.

The gain of the radiometer is sensitive to changes in temperature of the various components. We monitored the temperature at five locations: the two antennas, the Dicke switch, the power supply box, and the plate on which the

mixer, IF amplifier, and detector diode are mounted. The antennas and Dicke switch are too large and exposed to thermally regulate, but their temperature changed less than 1°C/hour because they are so massive. The other components were thermally regulated with proportional heaters. Their temperatures varied by less than 0.4°C during the entire three nights of CBR observations. The temperature drifts in the radiometer were small enough that the resulting gain change was insignificant.

The sensitivity of a Dicke radiometer is defined as the input temperature difference ΔT which gives rise to an output voltage equal to the RMS thermal noise fluctuations due to the radiometer itself. For a system with square wave switching and wide band detection this is given by (Kraus, 1966)

$$\Delta T = 2 \frac{T_{sys}}{(B\tau)^{1/2}}$$

where T_{sys} is the system noise temperature, B is the IF bandwidth, and τ is the postdetection integration time. For this system T_{sys} = 490K and B = 455 MHz, giving ΔT = 46 mK for an integration time τ = 1 sec. This value has been confirmed by measurement. (The power from a source can be expressed in terms of antenna temperature. Appendix A gives the relation between antenna temperature, thermodynamic temperature, and power.)

Seven targets were observed for an average of about 26 seconds each during every measurement of the CBR temperature. The mean RMS noise output for a single target was about 12 mK. This is approximately a factor of ten lower than the systematic errors in the measurement. Thus, statistical errors due to radiometer noise make only a small contribution to the total measurement error.

II.4 The Liquid-Helium-Cooled Reference Load

The LHe-cooled load (Figure II.6) has two functions. Most importantly it is used as an absolute-temperature reference. Secondly, it is used for gain calibrations.

The intensity of the CBR is determined by directly comparing the power received from the vertical sky with the power received from the LHe-cooled load. It is therefore critically important to know the total emission from the load with high accuracy. Any error contributes an equal error to the measured CBR temperature. The emission from the load is almost entirely from a blackbody source submerged in LHe. There are additional small contributions from the windows, the walls, and any power which comes out of the radiometer and is reflected by the load. Since these are difficult to determine with great accuracy, the load was designed to minimize such contributions. These contributions total 20 ± 10 mK (see Appendix C).

Calibration of the radiometer requires the use of two loads at different temperatures. If they are at widely different temperatures, then the precision with which each must be known is reduced. For calibration we used the LHe-cooled load and an ambient temperature load. The temperature difference is approximately 270 K, so that a gain measurement accurate to 1% requires that this difference be known to within 2.7 K. We measured this difference to an accuracy of better than 0.2 K. Furthermore, since the temperature difference is large, the small contributions from the windows, walls, and reflection from the LHe-cooled load cause a negligible error in the gain calibration.

The LHe-cooled reference load consists of a large open mouth dewar with an interior diameter of 70 cm. The interior radiometric walls are made of aluminum-coated mylar. The aluminum is 13 microns thick or 15 skin depths at

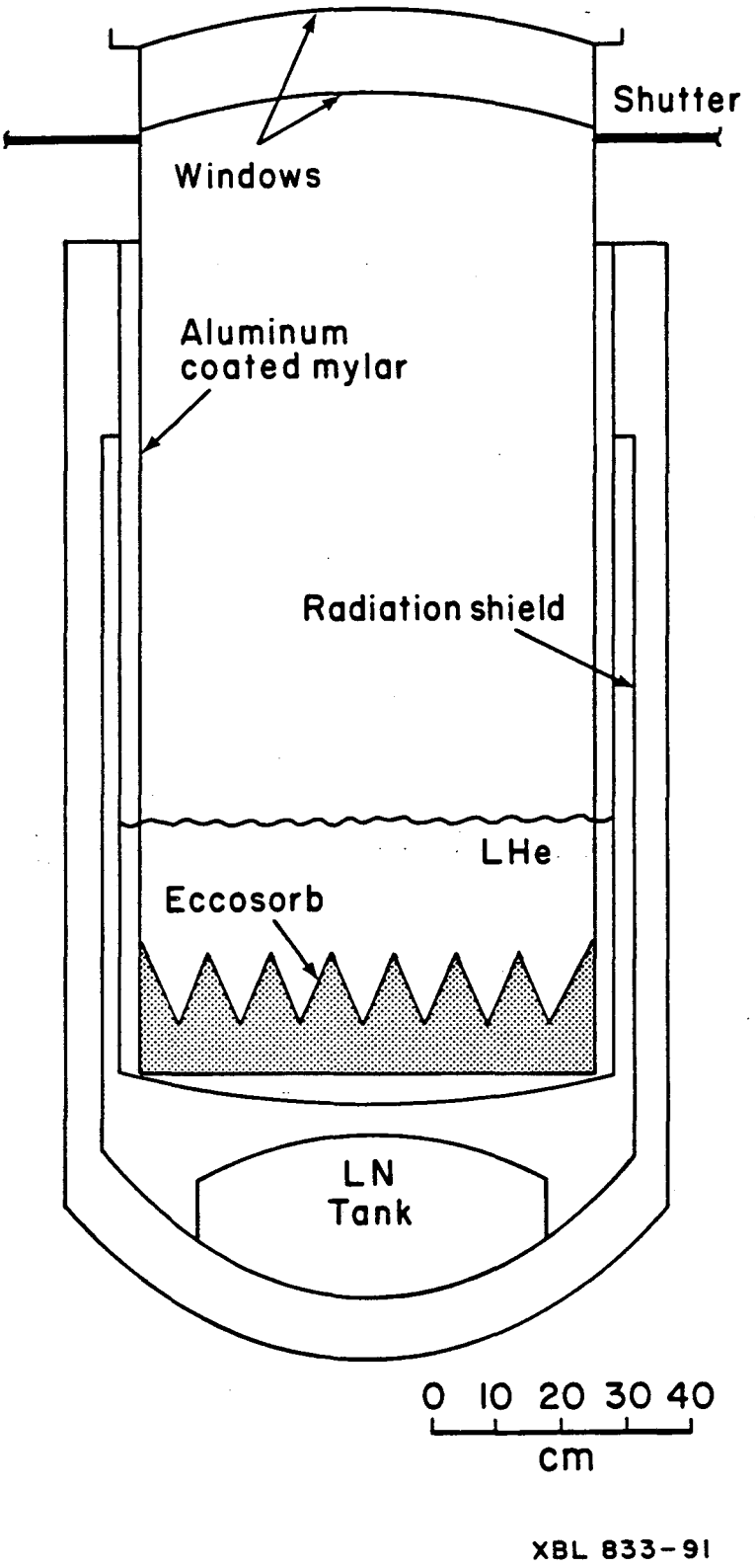

Figure II.6 - Liquid-helium-cooled reference load

the 3 cm wavelength. Completely covering the floor of the load is a 20 cm thick circular slab of Eccosorb (Emerson & Cuming VHP-8), a microwave absorber. The Eccosorb has a microwave emissivity greater than 0.999. During operation we maintained at all times between 100 and 200 liters of LHe in the calibrator; 90 liters are required to completely cover the Eccosorb. The distance from the antenna aperture to the top of the Eccosorb is approximately 130 cm.

The liquid helium temperature was estimated from the ambient barometric pressure. The ambient pressure during all CBR measurements was 486 ± 1 mm Hg. The pressure in the LHe-cooled load was maintained about 2 mm above ambient in order to ensure positive outflow of gas. Thus the total internal pressure was 488 ± 2 mm Hg. At this pressure the boiling point of LHe is 3.773 ± 0.004 K (Donnelly, 1967). The corresponding antenna temperature at 3 cm wavelength is 3.538 ± 0.004 K.

There were also two calibrated silicon diode temperature sensors (Lakeshore Cryotronics model DT-500KL) embedded directly in the Eccosorb. These indicated temperatures of 3.77 K and 3.79 K, respectively. However, the accuracy of the current source driving these sensors was 1%, which limited the temperature accuracy to about 0.2 K. Thus we use only the barometric pressure reading to give the LHe temperature.

Two polyethylene windows, 23 microns thick and spaced about 15 cm apart, cover the top of the load. Helium boil-off gas was warmed in a heat exchanger and passed between the windows. This kept the top window warm enough to prevent condensation of moisture from the outside air. The insertion loss of the windows is 5 ± 2 mK. No other objects were between the antenna and the LHe.

There are additional small contributions to the temperature of the load from resistive losses in the aluminum walls (9 ± 5 mK) and from power reflected

by the load (7 ± 4 mK). The antenna temperature of the load is the sum of the LHe temperature and these small terms:

$$T_{cla} = 3.56 \pm 0.01 \text{ K} .$$

When no radiometers were viewing the LHe load a shutter across the top was closed in order to reduce the radiative heat input. With the shutter closed the total heat input was about 12 watts, causing a boil-off rate of approximately 17 liters/hour. The rate was much higher when the shutter was open, especially when the large radiometers were viewing the load. In 1983 we bought 2500 liters of LHe, of which perhaps 2000 liters remained after transport to the mountain. We used it all in 2½ nights of observation. Apparently we cornered the west coast LHe market for a few days with our purchase.

II.5 The Ambient Temperature Load

The ambient temperature load is used in conjunction with the LHe-cooled load for gain calibrations. It consists of a 7.6 cm thick piece of Eccosorb CV-3, encased in a thermally insulating styrofoam box. The target is backed by an aluminum sheet to prevent transmission. The emissivity of the Eccosorb, as measured by its reflection coefficient, was 0.9998. The temperature of the Eccosorb was measured with a small sensor buried within it and was recorded every 16 seconds with an accuracy of 0.1°C.

II.6 Data Recording System

All data for the 3.0, 0.9, and 0.33 cm radiometers and the LHe-cooled

load were automatically recorded on magnetic cassette tape with a Datel LPS-16 Incremental Tape Recorder. The analog words were digitized with a 16 bit analog/digital converter prior to being recorded. Plus/minus full scale corresponded to an input voltage of ±10 V. Thus each digitized unit (du) equaled approximately 3.1 mV.

The maximum output of the 3.0 cm radiometer corresponded to an input temperature difference of approximately ±300 K, so the least significant bit from the analog/digital converter corresponded to 300 K / 2^{15} = 9 mK. Thus, the dynamic range was large enough that no lockin amplifier scale change was required even during calibration with the ambient temperature load.

The basic cycle time for the data recorder was 16 seconds, and two cycles transpired for each target observed. All timing commands, including those for the Dicke switch and lockin amplifier, were slaved to the same crystal controlled clock.

A list of the sampling periods of each of the data words recorded that are relevant to the 3 cm radiometer is given in Table II.1.

II.7 The Power Source

Electrical power to the equipment was supplied by in-series pairs of Sears 12 volt deep-cycle marine batteries. Normally the batteries were simultaneously connected to a charger to keep the voltage level in the acceptable range. The capacitance of the batteries was sufficient to eliminate any significant voltage ripple, even under conditions of changing load. Separate sets of batteries powered the radiometer electronics and heaters, in order to keep these systems electrically isolated from each other.

Table II.1 - Data recorded on magnetic tape.

Data Words	Sampling Period
DIGITAL	
Universal Time: Day, Hour	16 Seconds
Universal Time: Minutes, Seconds	16
Radiometer Rotation Position and Sense Switches	16
Barometric Pressure	16
ANALOG	
Lockin Amplifier Output	2
Temperature of Primary Antenna	16
Temperature of Secondary Antenna	16
Dicke Switch Temperature	16
Mixer/IF Amplifier Temperature	16
Support Electronics Temperature	16
Ambient Eccosorb Temperature	16
Radiometer Heater Current	16
Support Electronics Heater Current	16
LHe Temperature Sensor 1	16
LHe Temperature Sensor 2	16
LHe Load Wall Temperature	16
LHe Level	16
Electronics Battery Voltage	16
Heater Battery Voltage	16

Chapter III - Preparation and Data Acquisition

In preparation for the 1982 CBR measurements we had a full-scale test of all equipment in Berkeley. This test was successful. Immediately afterward we took the equipment to White Mountain, where we made even more extensive tests to be certain that nothing had been damaged during shipment. After we were satisfied that everything was working properly, we awaited the first nights of good weather and made the CBR measurements with LHe.

The preparations for 1983 were similar, except that we had no full-scale test in Berkeley with the Haverford and Italian equipment prior to the White Mountain tests.

III.1 LHe Test in Berkeley

On 14 June 1982, we assembled the equipment in Berkeley for a full scale test. We had four objectives, and at least three were completed.

The first objective was to ensure compatibility of the equipment. This was the first assembly of the rails with the reference cold load suspended in a hole in the ground. We verified that the antennas properly mated to the top of the cold load, and that the radiometers did not interfere with each other. As a result of this test we lengthened the rails by about three meters. Otherwise there were no serious problems.

The second objective was to test the cold load with LHe. A prior LHe test about eight months earlier was unsuccessful because the heat input to the LHe was excessively high, causing it to boil away too rapidly. As a result we installed a shutter at the top of the load. This was the first test of the shutter with LHe and it proved very successful. The shutter reduced the heat input to

about 12 watts, and made the load much easier to use.

The third objective was to establish measurement procedures. In this test we learned which sequence of observations allowed most efficient use of the limited LHe supply.

The last objective was to measure the atmospheric temperature. Unfortunately, the RF interference in Berkeley was so strong that no useful data could be obtained with the 12 cm wavelength radiometer. The design of the 6.3 cm radiometer (Mandolesi et al., 1984) prohibited simple independent measurements of the atmosphere. This design was changed to permit such measurements in the 1983 experiment. The other radiometers obtained results which are listed in Table III.1.

Table III.1 - Atmospheric measurements in Berkeley, 14 June 1982.

Wavelength (cm)	T_{VA} (K)
3.2	4 ± 1
3.0	3.3 ± 0.4
0.9	12 ± 1
0.33	53 ± 1

III.2 Observation Times

After completing this test the equipment was packed into three large trucks and taken to White Mountain. The first of our party of 20 physicists, technicians, and students arrived on 25 June 1982.

The next six days were spent digging a hole for the LHe dewar, installing the shutter on the LHe load, erecting and leveling the rails, and unloading the radiometers. After these preparations we began a series of performance tests of the radiometers to be sure that they had not been damaged during transit. These included integration, sidelobe, and flip tests, and are discussed in Chapter IV. On 3 July we made CBR measurements using LN as the cryogen in the absolute reference load. Although the accuracy of the CBR measurements was not as high as with LHe, we were able to practice the procedures which we used a few days later with LHe. We thus identified and solved several small problems with the radiometers prior to the high quality CBR measurements. The LHe measurements were made on 4 and 5 July 1982. After completion of the measurements we packed the equipment for shipment back to Berkeley, Haverford, and Italy. We left the rails and the LHe load in place, chained down and covered for protection against the upcoming winter weather. We returned to Berkeley on 11 July.

For the 1983 measurements the groups met at Barcroft, beginning on 20 August 1983. Our immediate concern was the LHe dewar. The previous winter was one of the most severe in recent years. The deep snowpack led to an unusually heavy runoff the following spring. On one warm spring day the snow melted so rapidly that the hole for the dewar began to fill with water. The dewar started to float, and rose more than one foot, lifting hundreds of pounds of rails with it, before the water was pumped out. However, our fears that the

integrity of the vacuum seals was lost were not realized. The dewar and the LHe-cooled load inside were not damaged.

The first several days on the mountain were spent preparing the radiometers, re-installing the shutter on the LHe load, and aligning and leveling the rails. We made the same systems tests as described above, with particular attention to the flip tests. On 30 August 1983 the cooled load was filled with LN for preliminary CBR measurements. We took data with LHe in the load on 4, 5, and 6 September 1983. We returned to Berkeley on 10 September.

III.3 Data Taking

A complete "run" of data was taken every 224 seconds. Each run consisted of seven 32-second periods with a different target observed during each period. The targets were always viewed in the same order: LHe-cooled load, vertical sky, -40° sky, -30° sky, +30° sky, +40° sky, and ambient temperature load. (Negative angles refer to west of zenith, positive to east of zenith). The radiometer was well balanced to allow it to rotate from one position to the next in a short time, usually less than six seconds. Each run of seven measurements was sufficient for a complete determination of the CBR temperature.

In the 1982 experiment the atmospheric emission was measured only at ±30° zenith angles. The measurement accuracy of this emission improves by using greater zenith angles, provided that the sidelobes of the antenna do not receive an excessive amount of thermal radiation from the ground. By enlarging the ground shields around the primary antenna we were able to tilt to ±40° in 1983, yet keep the ground contribution to a low level.

There was a sufficient amount of liquid helium for 2½ nights of

observations in 1983, and 2 nights in 1982. Each radiometer in turn made a series of measurements lasting approximately one hour, before yielding the LHe load to another radiometer. The 3.0 cm wavelength radiometer made four series of observations for a total of 59 runs in 1983, and five series of observations for 82 runs in 1982. The observation times and local sidereal times for each series are shown in Table III.2.

Table III.2 - Observation times for LHe measurements of the CBR at 3.0 cm.

Observation Series		Observation Times (UT)	Local Sidereal Time	Number of CBR Runs
1983	I	4 Sept, 8:25 - 9:21	23:24 - 00:20	15
	II	5 Sept, 3:31 - 4:20	18:33 - 19:22	13
	III	5 Sept, 9:00 - 9:41	00:03 - 00:44	10
	IV	6 Sept, 7:02 - 8:20	22:08 - 23:27	21
1982	V	5 July, 5:08 - 5:48	16:06 - 16:46	15
	VI	5 July, 12:00 - 12:30	22:59 - 23:29	12
	VII	6 July, 3:09 - 3:54	14:12 - 14:57	18
	VIII	6 July, 6:25 - 7:21	17:28 - 18:24	22
	IX	6 July, 11:44 - 12:22	22:48 - 23:26	15

Chapter IV - System Performance Tests

IV.1 Introduction

Numerous tests of the radiometer and associated apparatus were made in order to measure the magnitude of the various effects that may contribute to the error budget. In some cases the effects are large enough to require a specific correction to the data, while in other cases they are sufficiently small that no correction is necessary.

All tests were initially made in Berkeley with the radiometer on the roof of our laboratory. On clear and cool nights the atmosphere was stable enough to get excellent results, in spite of its relatively high radiometric temperature ($\approx$ 3 K). Such nights are frequent in the spring and summer. Thus each test described here was done at least twice, and in some cases many times, giving us confidence in the results.

Several of the most critical systems tests were repeated at White Mountain to verify that no changes had occurred during the difficult trip to the observing site.

We made extensive use of a computer software package we wrote called RADTST to analyze the test results immediately after completion of the test. RADTST calculates the Fourier transform, autocorrelation, and signal average of the radiometer output, and shows whether the radiometer noise "integrates down" properly. The results are presented in both numerical and graphical form.

IV.2 Integration Tests

The sensitivity, or minimum detectable temperature, of a radiometer is

inversely proportional to the square root of the integration time. RADTST calculates the RMS fluctuations as a function of integration time. Figure IV.1 shows the results of a typical test, made in Berkeley on 20 June 1983, in which both antennas viewed the vertical sky. The fluctuations have been normalized to the value for an integration time of one second, which was 46 mK. At an RMS of about 5 mK, corresponding to an integration time of about 64 seconds, the system no longer integrates down proportional to $t^{-1/2}$. This is due to non-Gaussian fluctuations in either the atmosphere or the radiometer itself. In either case this is at a sufficiently low level that statistical noise makes little contribution to the error in the computed CBR temperature.

IV.3 Atmospheric Stability

An important observing parameter was the length of time that each of the seven targets was observed during the CBR measurements. A period of 32 seconds was used. We now discuss the basis of this choice.

The integration tests described above were made with both antennas viewing the vertical sky. The radiometer output was proportional to the difference in power entering the antennas. Since they viewed the same portion of the atmosphere, fluctuations in the atmospheric emission caused almost no change in the radiometer output. Thus integration tests provide little information about the stability of the atmosphere.

We tested for atmospheric stability by performing integration tests with the primary antenna directed at an angle other than vertical (usually 30° from vertical). The results are similar to those in Figure IV.1, but with the departure from the straight line typically at 10 mK, corresponding to an integration time of 20 - 25 seconds. At this point the radiometer noise is roughly equal to the

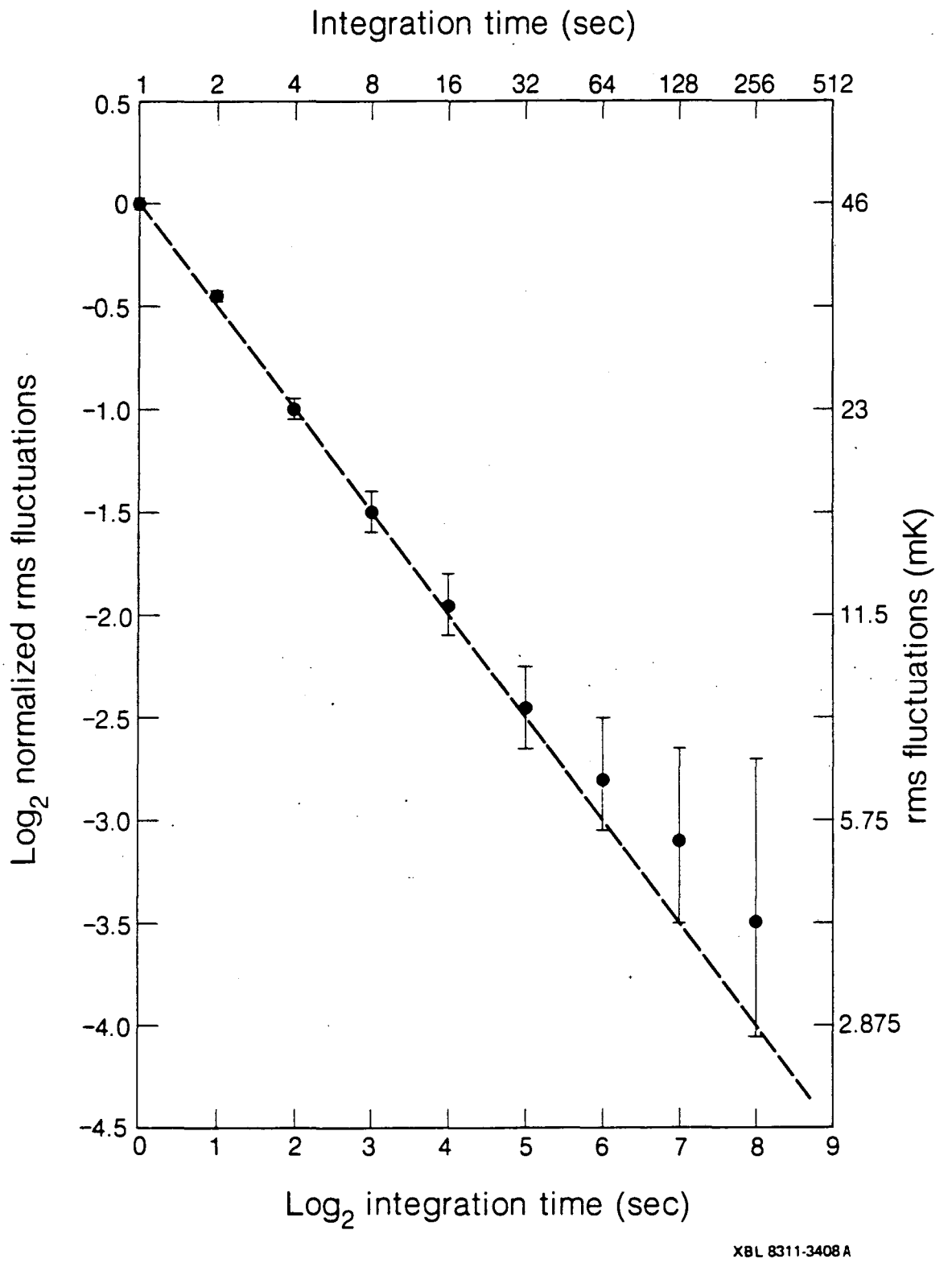

Figure IV.1 - RMS fluctuations versus integration time

noise from atmospheric fluctuations. For longer integration times the noise stayed at about the same level. Thus observing for a longer period would have been a waste of time. Shorter periods would have meant that a greater fraction of observing time was lost since no data was collected while the radiometer was rotating. Therefore observing for 32 seconds was an appropriate choice. Since the secondary antenna viewed the sky for all rotation positions, this period was also appropriate when the primary antenna was viewing the LHe load or ambient temperature load.

IV.4 Flip Tests

The entire radiometer rotates on a pair of bearings. As the primary antenna moves from target to target the gravitational stresses on the components change. It is critically important that the gain and offset of the radiometer do not change excessively as it is rotated or flipped from one orientation to another.

Extensive tests were made to measure the level of the flip asymmetry. We first did this by firmly attaching ambient temperature Eccosorb CV-3 targets to each antenna, completely covering the apertures. As the radiometer was rotated through each position the output changed by 12 ± 8 mK.

Certain kinds of flip asymmetries, however, will be revealed only by using loads which are not at ambient temperature. We tested for these in several ways.

Horizontal flip tests were made by alternately directing the primary antenna horizontally east and west. Large reflectors on each side of the radiometer, mounted at 45°, redirected the beam toward the zenith. The output difference between looking east and looking west is compared to the same

difference when the reflectors were interchanged, in order to remove the effect of asymmetric reflectors. This double difference is a measure of the intrinsic change within the radiometer, due to rotation, when it is directed horizontally. The horizontal flip asymmetry was measured to be 30 ± 5 mK.

Vertical flip tests were made with the primary antenna in either the straight up (0°) or straight down (180°) positions. A piece of Eccosorb CV-3 which had been dipped and saturated with LN was placed in front of the primary at each position. The secondary antenna viewed the sky via its mirror, as usual. We were able to set a 55 mK limit on the change in output as the primary antenna was rotated from 0° to 180°. The dipped Eccosorb stayed cold for about 15 seconds. The radiometer thermal noise is about 12 mK for this integration time, so that statistical noise did not make a large contribution to this limit.

The 55 mK value is an upper limit, set by the mechanical and thermal stability of the dipped Eccosorb target. The true vertical asymmetry may be less than this. In fact, due to the way in which the antennas and receiver are mechanically supported, the greatest stress exists when the primary is horizontal, and we may expect this to be the worst case.

More accurate tests were made in a way similar to the horizontal flip tests previously described. ±40° flip tests were made by directing the primary antenna alternately to +40° and -40°, stopping at each position for 32 seconds. This was done for approximately 20 minutes. The output difference corresponding to the two positions was compared to the same difference when the entire cart was rotated by 180°. These differences were determined very accurately by signal averaging for the entire 20 minute period. Figure IV.2 shows such a signal average for a test made at White Mountain on 30 August 1983. Each point represents an integration time of 38 seconds. The data from the three anomolous points were taken while the radiometer was rotating, and

are neglected. The result of this test is a flip asymmetry of 18 ± 24 mK. Identical tests in Berkeley gave the results 14 ± 4, 11 ± 2, and 18 ± 7 mK; and tests at ±30° gave 15 ± 5 and 25 ± 6 mK.

The ±40° and ±30° flip tests have the important virtue that they directly measure what we want to know — the change in radiometer output due to rotation. However, they are limited for two reasons: they don't sample all rotation positions and they are insensitive to gain changes in the radiometer.

The last procedure, called Eccosorb/Sky flip tests, addressed these problems. A target of ambient temperature Eccosorb CV-3 was attached to the aperture of the primary antenna. The Eccosorb and the end of this antenna were then completely wrapped in aluminum foil to prevent reception of extraneous RF interference. The secondary antenna viewed the sky, as usual. In this configuration the radiometer was set at many positions to measure changes in the output due to rotation.

In an individual test four positions were observed. Figure IV.3 shows the signal average for an Eccosorb/Sky flip test, made at White Mountain on 2 September 1983, in which the primary was successively positioned at -40°/+30°/+40°/+90°. Each point represents 38 seconds of integration time. Another test was done at the positions 0°/+40°/+90°/+180°. (+90° is the position at which the ambient temperature load is observed during gain calibrations, and +180°, or straight down, is the position for looking into the LHe-cooled load). In these two tests the largest output difference between any two positions was 18 ± 10 mK and 18 ± 16 mK, respectively. The same kind of tests in Berkeley yielded maximum differences of 10 ± 3, 23 ± 5, 29 ± 6, and 24 ± 5 mK.

The advantage of Eccosorb/Sky flip tests is that they test the sensitivity to rotation of the <u>entire</u> radiometer, including the quarter wave plate in the secondary antenna, except for the primary antenna arm upstream of the Dicke

10 GHZ +/-40 DEGREE FLIP TEST WITH CART IN NORMAL ORIENTATION
Date & time: 30d 1:44:56 Record numbers 86 through 161
Data from 10 GHz Radiometer has mean value of 61.4

NO.	AVERAGE	RMS
1	16.5	1.1
2	15.2	0.8
3	14.7	0.8
4	15.9	0.8
5	14.1	0.4
6	15.3	0.9
7	15.1	0.8
8	13.8	0.6
9	16.3	0.8
10	15.2	1.1
11	28.6	1.4
12	1522.1	*****
13	11.2	1.0
14	11.6	1.3
15	11.1	0.8
16	12.2	1.0
17	10.0	0.7
18	10.7	0.7
19	11.9	1.3
20	11.8	0.9
21	10.9	0.9
22	11.8	0.7
23	11.9	0.6
24	11.1	1.0
25	9.7	1.1
26	11.4	1.0
27	31.5	0.9
28	14.8	0.8
29	14.5	0.4
30	14.3	0.5
31	15.5	0.6
32	14.8	0.8

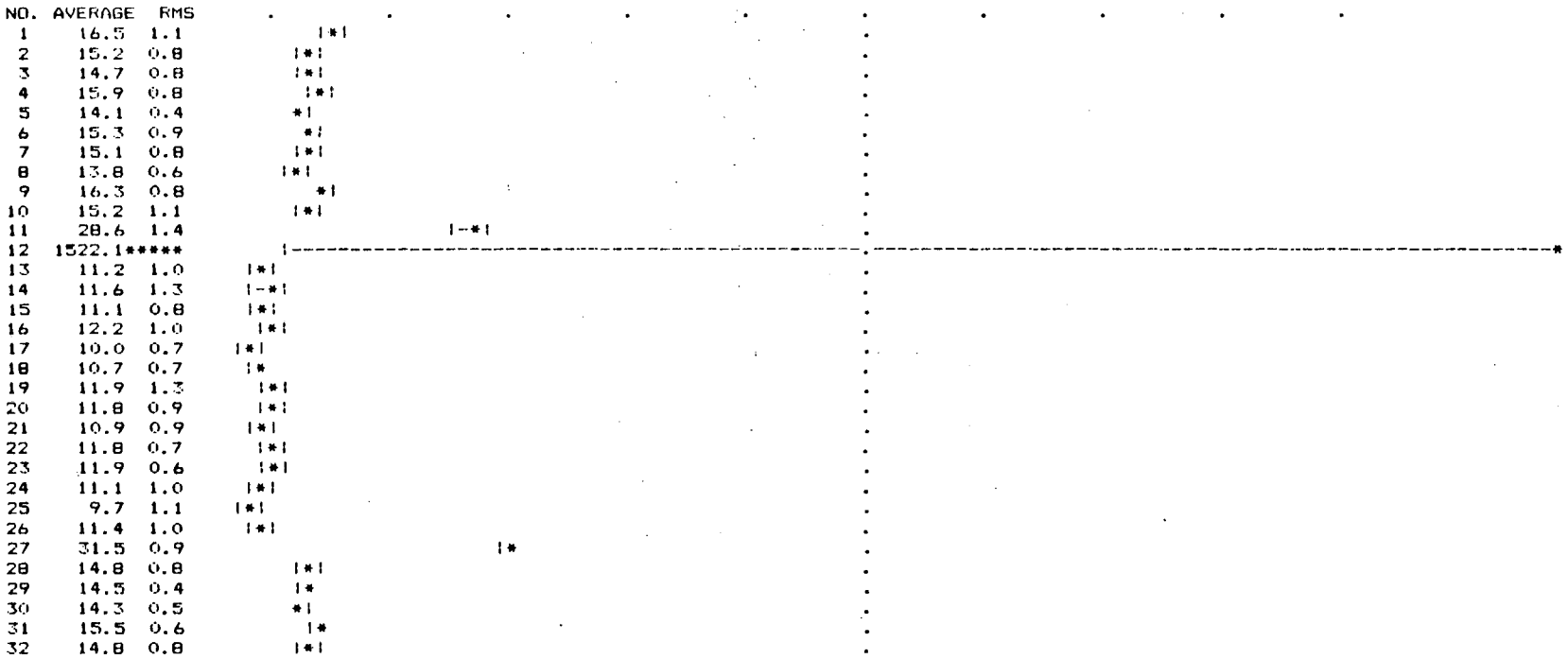

Figure IV.2 - Signal average of ±40° flip test

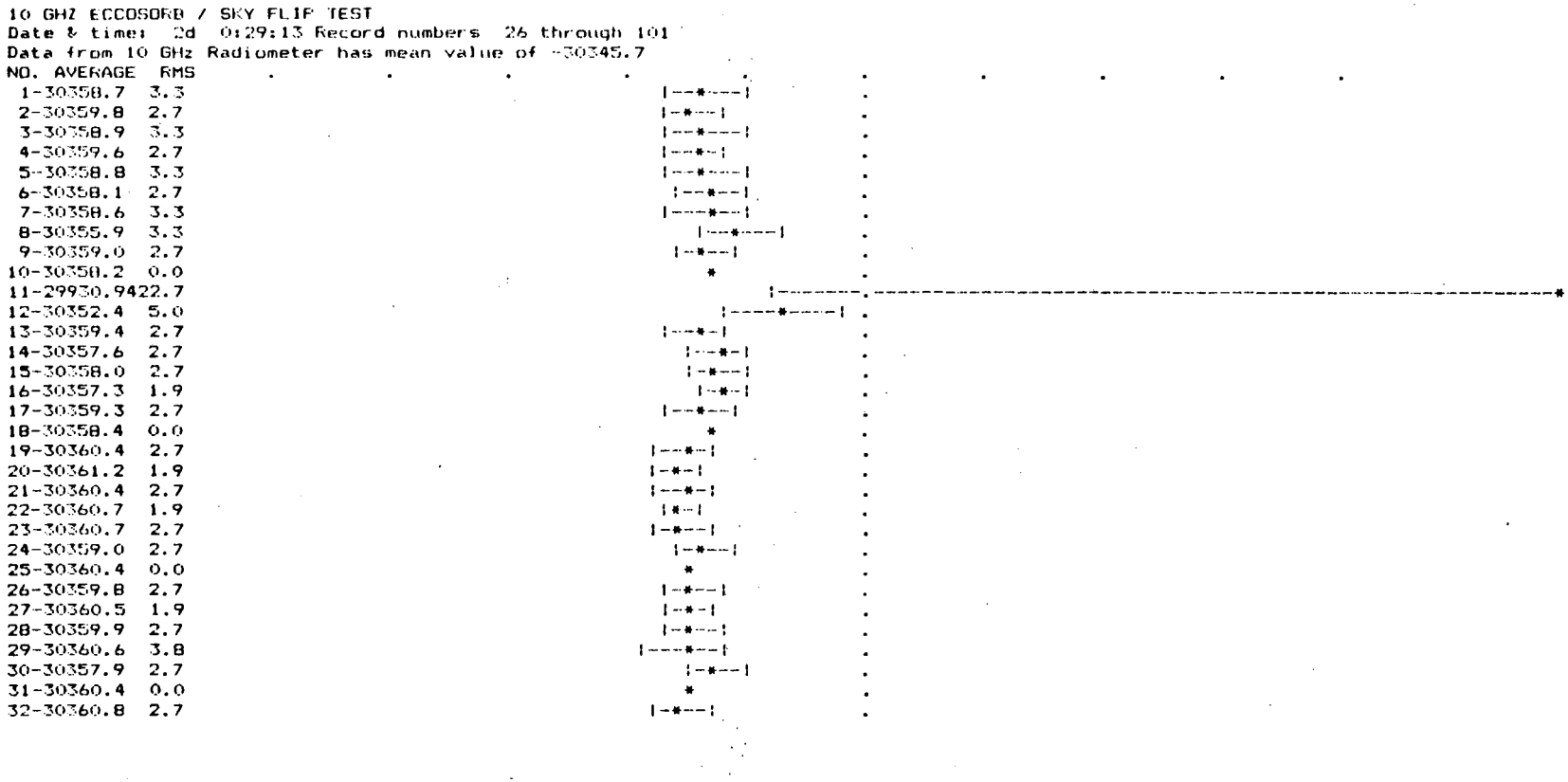

Figure IV.3 - Signal average of -40°/+30°/+40°/+90° Eccosorb/Sky flip test

switch. Sensitivity of all other parts of the radiometer is revealed by this test. We tested for effects arising from the primary antenna by fixing the radiometer in a particular position and physically pushing on the antenna. No measurable output change was observed even though the applied force was far greater than it is subject to in any of its seven positions.

Although differences in the radiometer output between two given positions were not constant from test to test, the result of more than 15 independent flip tests, both at Berkeley and at White Mountain, sampling more rotation positions than are used in the CBR measurements indicates that the amplitude of the difference never exceeds 30 mK. Therefore, in the error budget we take ±30 mK as the maximum amplitude of the flip asymmetry between any two rotation positions.

Since the input temperature difference during the Eccosorb/Sky flip tests is approximately 300 K, we also conclude that the maximum change in gain due to flipping the radiometer is (30 mK)/(300 K) = 10^{-4}, a negligibly small value.

The cause of the 30 mK flip asymmetry is not known. Reception of ground emission in the beam sidelobes was not the cause since we measured this contribution (Section IV.5.a) to be at most 7 ± 3 mK. The polarization effect from the mirror of the secondary antenna cannot account for it since the quarter-wave plate caused the antenna to respond to circular polarization with very high efficiency, as was verified with a polaroid.

However, it is likely that the quarter-wave plate was at least partially responsible for the flip asymmetry. Prior to the 1983 series IV runs the plate was rotated by 90° in the antenna feed. In an ideal system this would have no effect on the flip asymmetry. However, a significant change was observed in the measured atmospheric temperature. It is possible that the plate caused a small non-axisymmetric change in the beam pattern of the antenna, so that rotation

would cause a variable response.

It is also likely that mechanical stress induced part of the flip asymmetry. Strain on the radiometer components can cause reflections at waveguide junctions. The antennas are particularly susceptible, since they are massive and mechanically supported only at their small ends (Figure II.3). The flip tests do not reveal small changes in the reflection coefficient between the aperture of the primary antenna and the Dicke switch. No significant change in the output of the radiometer resulted from artificially introducing stress on the antenna by pushing on it. However, it was not possible to stress the other components to simulate the effects of rotating the radiometer.

IV.5 Other Tests

Other systems tests include sidelobe reception, magnetic sensitivity, and gain stability.

IV.5.a Sidelobe Reception

The observing site at White Mountain is located on a plateau with nearby hills in two directions. One rises 10° above horizontal at an azimuthal direction of 0° (north), and the other rises 16° in the direction 265° (almost due west). Reception of thermal radiation from the ground by the beam sidelobes when the primary antenna was tipped to 40° leads to erroneously large computed values of the atmospheric temperature. We tested for this by alternately raising and lowering a large (4 ft. by 6 ft.) aluminum reflector. In the raised position it was held above and parallel to the permanent ground screens around the primary antenna, as if it were an extension of the screens. In the lowered position it was held out of view of the antennas. Each position was held for 32 seconds, and the

test lasted for about 20 minutes. The signal average of the radiometer output indicated that sidelobe reception of ground radiation made the following contributions :

0 ± 3 mK at 0°	0 ± 3 mK at $\pm 30^{\circ}$
7 ± 3 mK at -40°	3 ± 3 mK at $+40^{\circ}$.

A correction to the data is made by subtracting these values at the appropriate angles.

IV.5.b Magnetic Sensitivity

The earth has a magnetic field strength of approximately 0.5 Gauss. The components of this field perpendicular to the axis of rotation of the radiometer could induce an output change as a function of rotation position. To reduce this effect we wrapped the Dicke switch and the isolator in 5 and 2 layers, respectively, of mu-metal (4 mils thick/layer). There are no other magnetically sensitive components in the radiometer. For testing purposes we erected a large (5 ft. diameter) pair of Helmholtz coils around the stationary radiometer. They were alternately turned on and off to produce an external magnetic field. The largest effect was with the field direction perpendicular to both antennas. With the antennas viewing the sky the radiometer offset changed by 41 ± 10 mK and 22 ± 4 mK for applied field strengths of 10 and 5 Gauss, respectively. The sensitivity to the earth's magnetic field is therefore at most 4 ± 2 mK, and is likely to be less than this since the earth's field was not perpendicular to both antennas. The sensitivity is about a factor of four less than this for the case in which the magnetic field was parallel to the primary antenna.

IV.5.c Gain Stability

An error of 1% in the gain α of the radiometer causes an error of approximately 12 mK in both the vertical atmospheric temperature and the CBR temperature. A complete measurement run of the CBR takes 224 seconds. Our requirement was to have gain stability better than 1% for at least this long.

The gain stability of the radiometer was tested by covering the aperture of one antenna with Eccosorb CV-3, while the other viewed the sky. Gain drifts as small as $\Delta\alpha/\alpha = 10^{-3}$ produced output changes far greater than the radiometer noise, and were easily seen. Typical tests indicated a maximum of $\Delta\alpha/\alpha = 4 \times 10^{-3}$ in 17 minutes, easily satisfying the requirement.

Gain drifts are usually caused by temperature changes in the receiver. The most sensitive element is the IF amplifier, which has a thermal gain coefficient of about $10^{-2}/^{o}C$. During each series of CBR runs the temperature of the amplifier changed by a maximum of $0.3^{o}C$, and within a given run by less than $0.1^{o}C$. In addition, the gain of the radiometer, measured during each run, drifted by less than 6×10^{-3} in each series, causing a maximum error in the temperature of the CBR of 7 mK. Thus, the effects of gain drifts were negligible.

IV.6 CBR Measurements With LN

The most important test was the measurement of the CBR temperature. Liquid helium is too difficult to handle and too expensive for use in general testing. Liquid nitrogen is both cheap and convenient to use as a reference cryogen in tests. However, there is a loss of accuracy when using LN which is related to the gain of the radiometer.

Using LN, if the measured gain were in error by 1% then T_{CBR} would be in error by approximately (0.01)(70 K) = 700 mK, since the difference between the temperature of the sky (vertical atmosphere plus CBR) and the temperature of LN is about 70 K. But a gain error of 1% causes an error of only 12 mK if LHe is used.

Measurements of T_{CBR} were made at White Mountain with LN in the cold load on the nights of 30 August, 2 September, and 7 September 1983. A total of 31 runs were made, with a mean of $T_{CBR} = 2.27 \pm 0.04$ K, where the error is statistical only. This value is about 0.35 K lower than the LHe result. The difference can be accounted for entirely by a gain error of 0.5%, which would cause a negligible error in the LHe measurements. This test therefore indicates that the gain of the system was known with sufficient accuracy.

Chapter V - Data Reduction and Analysis

V.1 Data Reduction

On White Mountain the raw data were printed out at the same time they were written on magnetic tape. The printed output was used to make preliminary calculations in real time to verify that the equipment was working properly. The final analysis was done in Berkeley. This analysis is described below.

The digitized lockin amplifier output was sampled and recorded every two seconds. Values recorded while the radiometer was rotating between observing positions were removed, resulting in the loss of about six seconds of data for each 32 second period. The average and RMS of the remaining lockin values were calculated for each of the seven positions. These values, the temperature of the ambient Eccosorb load, and the Universal Time at the beginning of the run are all that is necessary to compute T_{CBPa}, the CBR antenna temperature.

T_{CBRa} is found by comparing the temperature of the vertical sky to the temperature of the cooled load :

$$T_{sky} - T_{cla} = \alpha(V_o - V_{cla}) , \tag{V.1}$$

where

$$T_{sky} = T_{CBRa} + T_{VA} + T_{go} + T_{so} \tag{V.2}$$

and α = calibration constant , in units of K/du ;

V_o = radiometer output when viewing the vertical sky, in du ;

V_{cla} = radiometer output when viewing the LHe-cooled load, in du ;

T_{cla} = antenna temperature of the LHe-cooled load ;

T_{sky} = antenna temperature of the vertical sky ;

T_{VA} = antenna temperature of the vertical atmosphere ;

and T_{go} and T_{so} are the small contributions from the galactic background and sidelobes, received when the primary antenna was in the vertical position. V_o and V_{cla} are directly measured quantities. T_{cla} is known from the physical temperature and emission properties of the LHe-cooled load. The remaining terms in this expression will now be discussed.

V.2 Calibration Constant

The calibration constant α is a measure of the gain of the system. It is measured using the cold and ambient temperature loads:

$$\alpha = g \frac{T_{amb} - T_{cla}}{V_{amb} - V_{cla}} , \qquad (V.3)$$

where g = gain saturation factor ;

T_{amb} = antenna temperature of the ambient calibration load ;

and V_{amb} = radiometer output when viewing the ambient calibration load.

The value of α is approximately 9×10^{-3} K/du.

For large input powers the radiometer output saturated slightly due to non-linear behavior of the detector diode. The level of saturation was determined by comparing the values of the calibration constant measured in two different input temperature regions.

First α_1 was calculated using the loads Eccosorb at ambient temperature and the vertical sky.

$$\alpha_1 = \frac{T_{amb} - T_{sky}}{V_{amb} - V_{sky}} .$$

The ambient temperature Eccosorb, a warm blackbody, is the highest power load presented to the radiometer during the experiment. It is the only load which causes saturation. The temperature of the sky, approximately 5.7 K, was found by estimating an atmospheric temperature, then calculating the gain of the system, and repeating the process in order to get a self-consistent result. The sky temperature included both the atmosphere (in Berkeley) and the CBR.

Next, the calibration constant α_2 was calculated in a similar way using the sky and LN as calibration loads. The temperature of LN was 77.1 K. Since both these loads were cold we assumed that the detector diode was linear in this temperature range. This was supported by precision saturation measurements of the detector diode alone.

The ratio of the two calibration constants gives the gain saturation factor.

$$\alpha_1/\alpha_2 = g = 1.015 \pm 0.01 \ .$$

The primary effect of the saturation correction is to change the measured temperature of the atmosphere by a small amount. On White Mountain the vertical atmospheric temperature was approximately 1.2 K. Thus saturation of 1.5% decreases the computed atmospheric temperature by approximately 0.015 x 1.2 K = 18 mK.

In 1982 there was additional saturation caused by a faulty zener diode in the lockin amplifier. The gain saturation factor was g = 1.06. This problem was fixed prior to the 1983 measurements.

V.3 Vertical Sky Temperature

The antenna temperature of the vertical sky is the sum of contributions of the CBR, the atmosphere, the galactic background, and ground radiation received by the beam sidelobes. These last two contributions are of order ten mK or less, and may be considered as small corrections. Since the calibration constant α is known, the sky temperature can be determined very accurately without having to measure directly the temperature of the atmosphere. This allows a comparison of the data taken in 1982 and 1983.

Table V.1 shows the antenna temperature difference between the vertical sky and the LHe-cooled load. The weighted means of the differences are

$$T_{sky} - T_{cla} = 58 \pm 14 \text{ mK} \quad (1982) ; \qquad T_{sky} - T_{cla} = 13 \pm 11 \text{ mK} \quad (1983) .$$

The antenna temperature of the LHe-cooled load was $T_{cla} = 3.56 \pm 0.01$ K in both years.

The CBR temperature is found by determining the value of each of the terms in Eq. (V.2). This is done separately for each run. It is also useful to compare the mean values of the 1982 and 1983 data sets.

The average galactic background over the regions of the sky surveyed differed by less than 5 mK over the two data sets.

The sidelobe contribution for vertical sky observations was 0 ± 3 mK for both years.

The flip asymmetery was about 40 mK in 1982 and 30 mK in 1983. This improvement resulted from a small modification in the ground screens, and is discussed in the next section.

Therefore, according to Eq. (V.2), the cosmic background temperature is

Table V.1 - Antenna temperature differences between the vertical sky and the LHe-cooled load. The errors are the RMS in each series.

	Series	$T_{sky} - T_{cla}$ (mK)
1983	I	-24 ± 16
	II	46 ± 20
	III	32 ± 23
	IV	106 ± 57
		mean = 13 ± 11 mK
1982	V	48 ± 37
	VI	44 ± 55
	VII	72 ± 26
	VIII	56 ± 23
	IX	55 ± 34
		mean = 58 ± 14 mK

$$T_{CBRa} = (3.61 \pm 0.04\ K) - T_{VA} \qquad (1982)$$

$$T_{CBRa} = (3.57 \pm 0.03\ K) - T_{VA} \qquad (1983)\ .$$

Thus, the antenna temperature of the vertical atmosphere was 40 ± 50 mK warmer in 1982 than in 1983. This conclusion is based only on observations of the vertical sky and the LHe-cooled load, and does not depend on any zenith scan data.

To find the cosmic background temperature it is necessary to measure T_{VA}. This is much larger than the terms T_{go} and T_{so} which appear in Eq. (V.2). The experimental error in T_{CBRa} is largely determined by the error in T_{VA}, since these other terms are known with much greater accuracy.

V.4 Vertical Atmospheric Antenna Temperature

V.4.a Measurement Theory

If the atmosphere were a flat slab and the antenna beam were a delta-function, then the vertical atmospheric antenna temperature would be given by

$$T_{VA} = \alpha \frac{V_o - V_1}{\sec\theta - 1}\ , \qquad (V.4)$$

where V_1 = radiometer output when viewing at angle θ from zenith. (The subscript "1" always refers to observations made at either of the two zenith angles, $\theta = \pm 30^o$ or $\theta = \pm 40^o$.) Since the antennas have half-power beamwidths of 12.5^o and the atmosphere curves to follow the earth's surface, T_{VA} must be found by convolving the antenna beam with the atmosphere, taking into account

atmospheric self-absorption. The result is a generalization of the expression above.

$$T_{VA} = \frac{\Delta T}{F_o} \left\{ F_1 + \frac{\Delta T}{F_o T_{atm}} F_2 + \left(\frac{\Delta T}{F_o T_{atm}} \right)^2 F_3 \right\}, \tag{V.5}$$

where $\Delta T = \alpha(V_1 - V_o) - (T_{g1} + T_{s1}) + (T_{go} + T_{so})$;

T_{atm} = physical temperature of the atmosphere ≃ 240 K ;

and F_o, F_1, F_2, and F_3 are constants, which depend only on θ. In this expression the effects of the galactic background and sidelobes (T_{g1}, T_{s1}; and T_{go}, T_{so}) at the zenith angle θ and at vertical, respectively, have been explicitly subtracted.

In practice V_1 is the mean of the output values at $+\theta$ and $-\theta$. Averaging the data in this way reduces the error that arises from a tilt in the radiometer cart to less than 10 mK, even if the cart is tilted by as much as 1° , provided that the relative angles at $\pm 30^o$ and $\pm 40^o$ are accurate to within 10 arcminutes. On White Mountain we measured the angles and found them to be accurate to better than four arcminutes.

The 1983 vertical atmospheric temperature is computed according to Eq. (V.5) using the data taken at $\pm 30^o$ independently from the data taken at $\pm 40^o$. These atmospheric temperatures are called T_{30} and T_{40}. The final value of T_{VA} for each run is the weighted mean of T_{30} and T_{40} ,

$$T_{VA} = \frac{T_{30}/(\sigma_{30})^2 + T_{40}/(\sigma_{40})^2}{(\sigma_{30})^{-2} + (\sigma_{40})^{-2}} , \tag{V.6}$$

where σ_{30} and σ_{40} are the systematic errors in T_{30} and T_{40} , respectively. It is shown in Appendix F that σ_{30} is approximately twice as large as σ_{40} . Thus T_{VA} is more heavily weighted toward the data taken at $\pm 40^o$.

The galactic background contribution is due to synchrotron and HII

thermal emission. We correct for it with the aid of a model based on surveys and measurements published by other investigators. Details of this model and a map of the galactic emission at a wavelength of 3 cm are given in Appendix D.

The galactic emission is greatest in the direction of the galactic plane. We avoided taking data when the plane was in view, particularly with the long-wavelength radiometers, which are affected most by this background. The largest correction applied to the 3 cm data is 14 mK. However most of the data require a correction of less than 8 mK. These corrections are small enough that the precise accuracy of the model is not critical. If the model were in error by 50% the computed value of T_{CBR} would change by only 2 mK.

The sidelobe corrections were measured on White Mountain. As shown in Section IV.5a, the correction is 7 mK for data taken at a zenith angle of -40°, and less than this at all other angles.

V.4.b Measurement Results

A value of T_{VA} was computed for each run. In 1982 they ranged in value from 0.71 K to 1.19 K, with a mean of 0.93 ± 0.16 K. In 1983 they ranged from 1.08 K to 1.34 K, with a mean of 1.20 ± 0.13 K.

The average value of T_{VA} measured in 1983 was 270 ± 210 mK higher than in 1982. However it was shown in Section V.3 that T_{VA} was 40 ± 50 mK higher in 1982 than in 1983. There is a discrepancy of 310 ± 210 mK between the two measurements.

The reason for this discrepancy is the flip asymmetry, which limited the measurement accuracy of T_{VA} in both years. There are three reasons why the 1983 result is better.

1. Mechanical improvements in the radiometer reduced the flip asymmetry.

2. The flip asymmetry was measured more accurately using improved testing procedures.

3. Measurements of the atmosphere emission were made at larger zenith angles in 1983 than in 1982.

Each of these points will now be discussed.

Shortly after the 1982 measurements were completed we tried to reduce the flip asymmetry with various mechanical modifications. The only one that significantly helped was enlarging the ground shields around the secondary antenna (Figure II.3). The horizontal shield below this antenna was 34 cm away from the beam axis in 1983, but only 18 cm away in 1982. This single change reduced by about 30% the average asymmetry as measured by $\pm 30^{\circ}$ and $\pm 40^{\circ}$ flip tests.

Prior to the 1982 measurements horizontal flip tests provided the most accurate information about the flip asymmetry. These tested the radiometer in what was expected to be the orientation of maximum stress, which was when the primary antenna was horizontal. Prior to the 1983 measurements Eccosorb/Sky flip tests were made. These tests yielded considerably more information since they tested all orientations of the radiometer for sensitivity to rotation, and for rotation induced gain changes. We set a much firmer upper limit on the magnitude of the flip asymmetry, applicable to all rotation positions, with Eccosorb/Sky flip tests.

The most significant improvement in the atmospheric measurement occurred because in 1983 the atmospheric zenith scans were made at $\pm 30^{\circ}$ and $\pm 40^{\circ}$, while in 1982 data were taken at $\pm 30^{\circ}$ only. From Eq. (V.5) the vertical atmospheric temperature computed from observations at $\pm 30^{\circ}$ and $\pm 40^{\circ}$ is

$$T_{VA} = 6.227(\Delta T)\{1 + 0.016(\Delta T) + 0.0006(\Delta T)^2\}$$

$$= 6.227(\Delta T) + 0.098(\Delta T)^2 + 0.0037(\Delta T)^3 \qquad \text{at } 30^\circ ;$$

$$T_{VA} = 3.126(\Delta T)\{ 1 + 0.009(\Delta T) + 0.0002(\Delta T)^2\}$$

$$= 3.126(\Delta T) + 0.028(\Delta T)^2 + 0.0006(\Delta T)^3 \qquad \text{at } 40^\circ .$$

Since the flip asymmetry appears directly in ΔT, the error in T_{VA} was reduced by a factor of two by scanning to $\pm 40^\circ$ instead of $\pm 30^\circ$.

The 1982 flip asymmetry of 40 mK, at zenith angles of $\pm 30^\circ$, produced an error of about 250 mK in T_{VA}. The 1983 flip asymmetry of 30 mK, at zenith angles of $\pm 40^\circ$, produced an error of about 95 mK. This provides a possible explanation for the 310 mK difference between the two measurements of T_{VA}.

To resolve the discrepancy we make another estimate of T_{VA} by using the atmospheric model of Partridge et al. (1984). This model predicts the following values of T_{VA} (in Kelvin) based on emission from oxygen and water vapor :

$$T_{VA} = 1.035 + 0.350W \qquad (3.2 \text{ cm}) ;$$

$$T_{VA} = 1.048 + 0.404W \qquad (3.0 \text{ cm}) ;$$

$$T_{VA} = 3.182 + 3.60W \qquad (0.9 \text{ cm}) ;$$

$$T_{VA} = 4.706 + 21.97W \qquad (0.33 \text{ cm}) .$$

Here W is the precipitable water vapor, in gm/cm^2. Table V.2 lists T_{VA} and the best fit values of W predicted by this model, based on the measured atmospheric temperatures. (The 1983 temperatures given here at 0.9 and 0.33 cm are based on a preliminary analysis of the new data, and are to be taken as approximate. The 1983 data at 3.2 cm is not yet available.) The accuracy of the model is 100 mK at 3.2 and 3.0 cm, 200 mK at 0.9 cm, and 500 mK at 0.33 cm. If this error were contained in the water vapor term only, then W might be in error by

Table V.2 - The vertical atmospheric temperature and predicted values of the precipitable water vapor.

	Wavelength (cm)	T_{VA} (K)	W (gm/cm^2)
4 Sept. 1983	3.0	1.17 ± 0.13	0.302
	0.9	4.20 ± 0.30	0.283
	0.33	9.87 ± 0.40	0.235
5 Sept. 1983	3.0	1.16 ± 0.13	0.277
	0.9	4.65 ± 0.30	0.408
	0.33	11.1 ± 0.40	0.293
6 Sept. 1983	3.0	1.25 ± 0.13	0.500
	0.9	4.60 ± 0.30	0.394
	0.33	12.2 ± 0.40	0.341
4, 5 July 1982	3.2	1.03 ± 0.03	0.0
	3.0	0.93 ± 0.16	0.0
	0.9	5.0 ± 0.14	0.505
	0.33	12.3 ± 0.80	0.346

as much as 0.29, 0.25, 0.056, and 0.023 at the four wavelengths. However, the model should be more accurate in comparing measurements at different times, since only differences in the water vapor are important.

Since water vapor makes a large contribution to T_{VA} at 0.9 and 0.33 cm, observations at these wavelengths provide a good measure of the change in W with time. From Table V.2 we find that the weighted mean value of W was 0.10 ± 0.05 greater in 1982 than in 1983, based on the 0.9 and 0.33 cm data. Thus, the model predicts that at 3.0 cm the vertical atmospheric temperature was (0.10 ± 0.05)(0.404 K) = 40 ± 20 mK greater in 1982 than in 1983. This is in good agreement with the estimates made in Section V.3 based on $(T_{sky} - T_{cla})$.

To summarize, the values of T_{VA} at 3.0 cm measured with zenith scans differ considerably in 1982 and 1983. However, the yearly estimates of T_{VA} from $(T_{sky} - T_{cla})$ are consistant and in good agreement with the changes predicted by the 0.9 and 0.33 cm data and the atmospheric model. The cause of the discrepancy is the flip asymmetry, which has a much larger effect on the zenith scan data than on the vertical sky data. We conclude that the 1982 value of T_{VA} was incorrect, and that it should be 40 ± 50 mK greater than the 1983 result of 1.20 ± 0.13 K. This gives

$$T_{VA} = 1.24 \pm 0.14 \text{ K} \qquad \text{(1982 corrected)}.$$

V.4.c Rotation of the Quarter Wave Plate

The average value of T_{VA} in the series IV data is 1.25 K, or about 90 mK higher than the others in 1983 (see Table V.4). There are two reasons for this, one instrumental and one atmospheric.

The instrumental effect is related to the quarter wave plate in the feed of the secondary antenna. Prior to the series IV runs the plate was rotated by 90°

in the antenna feed. The response of the antenna should not have been affected by this change. Figure V.1 shows a plot of T_{40} vs. T_{30}. It is evident that although T_{40} was roughly constant for all runs, T_{30} has a much larger spread. For the series I, II, and III runs T_{30} was generally less than T_{40}, while the reverse is true for series IV. This shows that the origin of the flip asymmetry is probably the quarter-wave plate. The 30 mK flip asymmetry discussed in Section IV.4 is consistent with the variation observed in T_{30}. T_{VA} exhibits much less variation since it is weighted more toward T_{40}, which is far less susceptible to this problem.

The second reason is that the atmospheric humidity was higher on 6 September. From Table V.2 it is evident that W increased relative to the previous nights, causing higher atmospheric emission. The scatter in the values of W prohibit more quantitative conclusions about the expected temperature increase, especially since T_{VA} is only weakly dependent on W at 3.0 cm.

Thus, although rotation of the quarter wave plate had some effect on the 1983 data, there is no doubt that the increased atmospheric temperature seen on 6 September at 3 cm was partially due to higher humidity. The atmospheric model does not have sufficient accuracy to determine the relative magnitude of the two effects.

The quarter wave plate was not moved during the 1982 measurements. The scatter in the values of T_{VA} was primarily due to variable humidity.

V.5 CBR Temperature

With the measured values of α and T_{VA} the CBR antenna and thermodynamic temperatures have been computed separately for each run. The mean values are

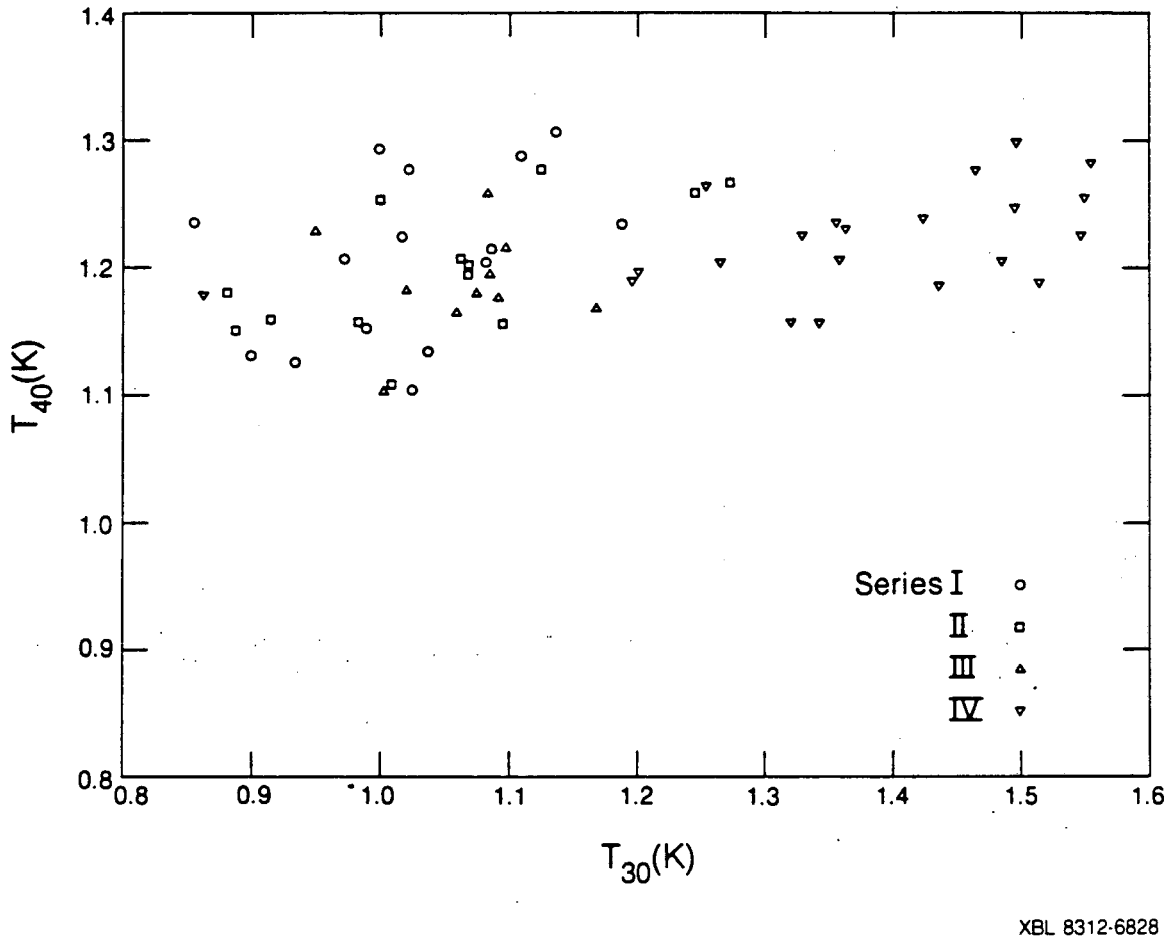

Figure V.1 - The vertical atmospheric antenna temperature: T_{VA} calculated from 40° zenith scans versus T_{VA} calculated from 30° zenith scans (1983 data).

$T_{CBRa} = 2.41 \pm 0.14$ K $\qquad$ $T_{CBR} = 2.64 \pm 0.14$ K $\qquad$ (1983)

$T_{CBRa} = 2.68 \pm 0.19$ K $\qquad$ $T_{CBR} = 2.91 \pm 0.19$ K $\qquad$ (1982) .

The errors here include both systematic and statistical effects. The differences in the 1983 and 1982 results are due to the different computed values of the vertical atmospheric temperatures.

Table V.3 lists the Universal Time, the calibration constant α , T_{30} , T_{40} , T_{VA} , T_{CBRa} , and T_{CBR} for each run. Table V.4 gives the average values of T_{VA} and T_{CBR} for each series. The series IV value of T_{VA} is higher than the others for 1983, but T_{CBR} for series IV is exactly equal to the average for all 1983 data. This indicates that the instrumental problem described above had a small effect.

Figures V.2a and V.2b show plots of T_{CBR} for each run in order for the 1983 and 1982 data, respectively. There is no significant systematic trend in either data set. Since the data were taken at different sidereal times, this shows that the galactic background emission was correctly subtracted from the sky emission.

Figures V.3a and V.3b show plots of T_{CBR} vs. T_{VA}. The highly correlated relationship is easily understood. T_{sky} in Eq. (V.2) is nearly a constant for all runs, and T_{go} and T_{so} are small correction terms. Thus T_{CBRa} and T_{VA} are linearly related with a slope of -1.

Histograms of the values of T_{CBR} are shown in Figures V.4a and V.4b. The RMS is 0.07 K for the 1983 data set, and 0.14 K for the 1982 data set. This factor of two arises because T_{VA} was measured at a larger zenith angle ($\pm 40^{o}$) in 1983 than in 1982, which reduced the measured fluctuations in T_{VA}.

We can estimate a corrected CBR temperature based on the 1982 data.

The 1982 corrected value of T_{VA} was 310 mK greater than the measured value. Therefore, T_{CBR} must be corrected by subtracting the same amount:

$$T_{CBR} = 2.60 \pm 0.15 \text{ K} \qquad \text{(1982 corrected)} .$$

That this is so close to the 1983 result is simply a restatement that T_{sky} was nearly the same in both years.

It is now evident that the 0.19 K error assigned to the 1982 measurement of T_{CBR} was probably an underestimate since in computing the experimental error we took the average of the flip test results as the flip asymmetry. In the analysis of the 1983 data we have taken a more conservative approach by using the highest measured flip test result for the value of the flip asymmetry. Nevertheless, the final error in 1983 is lower than in 1982 because zenith scans were made at $\pm 40^{\circ}$, and because the flip asymmetry was reduced.

Although the 1982 corrected numbers at 3.0 cm are very close to the 1983 results, we use only the 1983 data for the analysis in Chapter VI. The modifications of the equipment, the improved testing, and the superior atmospheric measurement make the newer result substantially more accurate.

Table V.3 - The Universal Time, calibration constant, vertical atmospheric temperature, and cosmic background temperature.

1983		TIME	ALPHA	T30	T40	TVA	TCBRo	TCBR
SERIES I	1	4: 8:25:53	-.00896	0.854	1.235	1.155	2.374	2.607
	2	4: 8:29:37	-.00895	0.999	1.294	1.232	2.308	2.540
	3	4: 8:33:21	-.00894	0.900	1.132	1.083	2.454	2.687
	4	4: 8:37: 5	-.00895	1.022	1.278	1.224	2.302	2.535
	5	4: 8:40:49	-.00895	1.082	1.203	1.178	2.364	2.597
	6	4: 8:44:33	-.00895	0.971	1.208	1.158	2.371	2.604
	7	4: 8:48:17	-.00895	1.135	1.308	1.272	2.241	2.473
	8	4: 8:52: 1	-.00895	1.110	1.289	1.251	2.261	2.493
	9	4: 8:55:45	-.00895	1.037	1.133	1.113	2.395	2.628
	10	4: 8:59:29	-.00895	0.933	1.126	1.085	2.456	2.689
	11	4: 9: 3:13	-.00895	0.988	1.152	1.117	2.418	2.651
	12	4: 9: 6:57	-.00896	1.188	1.234	1.224	2.305	2.538
	13	4: 9:10:41	-.00895	1.026	1.106	1.090	2.477	2.710
	14	4: 9:14:25	-.00895	1.086	1.213	1.187	2.363	2.596
	15	4: 9:18: 9	-.00895	1.017	1.225	1.181	2.356	2.588
SERIES II	16	5: 3:31:50	-.00897	0.880	1.181	1.118	2.478	2.711
	17	5: 3:35:34	-.00895	1.069	1.201	1.173	2.395	2.628
	18	5: 3:39:18	-.00895	1.066	1.204	1.175	2.406	2.639
	19	5: 3:43: 2	-.00894	0.914	1.160	1.109	2.532	2.765
	20	5: 3:46:46	-.00894	1.069	1.197	1.170	2.427	2.660
	21	5: 3:50:30	-.00894	1.271	1.267	1.268	2.317	2.550
	22	5: 3:54:14	-.00894	1.125	1.279	1.246	2.336	2.568
	23	5: 3:57:58	-.00894	0.982	1.153	1.117	2.512	2.745
	24	5: 4: 1:42	-.00895	1.096	1.156	1.143	2.484	2.717
	25	5: 4: 5:26	-.00895	0.888	1.150	1.095	2.521	2.754
	26	5: 4: 9:10	-.00895	1.000	1.252	1.199	2.409	2.642
	27	5: 4:12:54	-.00894	1.244	1.259	1.256	2.360	2.593
	28	5: 4:16:38	-.00894	1.008	1.107	1.086	2.522	2.755
SERIES III	29	5: 9: 0:38	-.00892	1.097	1.217	1.192	2.424	2.657
	30	5: 9: 8: 6	-.00890	1.020	1.181	1.148	2.456	2.689
	31	5: 9:11:50	-.00890	1.081	1.196	1.173	2.418	2.651
	32	5: 9:15:34	-.00890	0.949	1.229	1.172	2.408	2.641
	33	5: 9:19:18	-.00890	1.082	1.259	1.223	2.335	2.567
	34	5: 9:23: 2	-.00890	1.059	1.164	1.143	2.445	2.677
	35	5: 9:26:46	-.00890	1.005	1.107	1.086	2.494	2.727
	36	5: 9:30:30	-.00891	1.091	1.175	1.158	2.415	2.648
	37	5: 9:34:15	-.00891	1.168	1.168	1.168	2.392	2.624
	38	5: 9:37:59	-.00891	1.074	1.180	1.159	2.445	2.678
SERIES IV	39	6: 7: 2:35	-.00887	0.861	1.179	1.112	2.479	2.712
	40	6: 7: 6:19	-.00887	1.200	1.196	1.196	2.422	2.655
	41	6: 7:10: 3	-.00887	1.461	1.277	1.316	2.341	2.573
	42	6: 7:13:47	-.00887	1.341	1.157	1.196	2.474	2.707
	43	6: 7:17:31	-.00888	1.512	1.189	1.256	2.365	2.598
	44	6: 7:21:15	-.00887	1.422	1.239	1.277	2.396	2.629
	45	6: 7:24:59	-.00887	1.547	1.224	1.291	2.397	2.629
	46	6: 7:28:43	-.00888	1.497	1.299	1.341	2.299	2.532
	47	6: 7:32:27	-.00887	1.195	1.189	1.190	2.494	2.727
	48	6: 7:36:11	-.00887	1.436	1.185	1.237	2.419	2.652
	49	6: 7:39:55	-.00887	1.362	1.229	1.257	2.391	2.624
	50	6: 7:43:39	-.00888	1.550	1.254	1.316	2.298	2.531
	51	6: 7:47:23	-.00888	1.554	1.282	1.339	2.262	2.494
	52	6: 7:51: 7	-.00888	1.253	1.264	1.262	2.368	2.601
	53	6: 7:54:51	-.00887	1.359	1.206	1.238	2.370	2.603
	54	6: 7:58:35	-.00887	1.329	1.224	1.245	2.407	2.640
	55	6: 8: 2:19	-.00887	1.266	1.202	1.215	2.459	2.692
	56	6: 8: 6: 3	-.00887	1.483	1.205	1.263	2.413	2.646
	57	6: 8: 9:47	-.00886	1.320	1.156	1.190	2.491	2.724
	58	6: 8:13:31	-.00887	1.493	1.248	1.300	2.416	2.648
	59	6: 8:17:15	-.00887	1.356	1.235	1.261	2.399	2.632

Table V.3 (continued)

		TIME (UT)	ALPHA	TVA	TCBRa	TCBR
1982						
SERIES V	1	5: 5: 8:14	-.00970	1.015	2.602	2.835
	2	5: 5:10:54	-.00971	0.961	2.640	2.873
	3	5: 5:13:34	-.00971	1.085	2.538	2.771
	4	5: 5:16:14	-.00970	0.961	2.677	2.910
	5	5: 5:18:54	-.00970	0.831	2.813	3.047
	6	5: 5:21:34	-.00970	0.844	2.777	3.011
	7	5: 5:24:14	-.00971	0.985	2.633	2.866
	8	5: 5:26:54	-.00971	1.012	2.616	2.849
	9	5: 5:29:34	-.00971	1.178	2.394	2.627
	10	5: 5:32:14	-.00971	0.949	2.683	2.916
	11	5: 5:34:54	-.00971	1.189	2.404	2.637
	12	5: 5:37:34	-.00971	1.000	2.612	2.845
	13	5: 5:42:54	-.00972	0.894	2.716	2.949
	14	5: 5:45:34	-.00972	1.088	2.454	2.687
	15	5: 5:48:14	-.00972	1.078	2.433	2.666
SERIES VI	16	5:12: 0:30	-.00963	1.021	2.529	2.762
	17	5:12: 3:10	-.00964	0.816	2.938	3.172
	18	5:12: 5:50	-.00965	0.865	2.716	2.949
	19	5:12: 8:30	-.00966	1.011	2.602	2.835
	20	5:12:11:10	-.00966	0.889	2.699	2.932
	21	5:12:13:50	-.00966	1.055	2.518	2.751
	22	5:12:16:30	-.00966	0.983	2.585	2.818
	23	5:12:19:10	-.00967	0.734	2.853	3.087
	24	5:12:21:50	-.00966	0.786	2.812	3.046
	25	5:12:24:30	-.00966	0.999	2.582	2.815
	26	5:12:27:10	-.00962	0.834	2.775	3.009
	27	5:12:29:50	-.00962	0.849	2.688	2.921
SERIES VII	28	6: 3: 9: 0	-.00975	0.988	2.635	2.868
	29	6: 3:12: 0	-.00976	0.989	2.602	2.835
	30	6: 3:14: 0	-.00976	0.989	2.634	2.867
	31	6: 3:17: 0	-.00976	1.092	2.468	2.701
	32	6: 3:19: 0	-.00977	0.894	2.697	2.930
	33	6: 3:22: 0	-.00976	0.996	2.595	2.828
	34	6: 3:25: 0	-.00976	0.893	2.730	2.963
	35	6: 3:28: 0	-.00976	0.989	2.732	2.965
	36	6: 3:30: 0	-.00976	1.091	2.502	2.735
	37	6: 3:33: 0	-.00976	1.193	2.400	2.633
	38	6: 3:35: 0	-.00976	0.887	2.738	2.972
	39	6: 3:38: 0	-.00975	0.887	2.738	2.972
	40	6: 3:41: 0	-.00975	0.988	2.605	2.838
	41	6: 3:44: 0	-.00975	0.886	2.771	3.005
	42	6: 3:46: 0	-.00974	1.089	2.504	2.737
	43	6: 3:49: 0	-.00974	1.089	2.536	2.769
	44	6: 3:52: 0	-.00973	0.783	2.842	3.076
	45	6: 3:54: 0	-.00973	1.087	2.537	2.770

Table V.3 (continued)

		TIME (UT)	ALPHA	TVA	TCBRa	TCBR
1982						
SERIES VIII	46	6: 6:25: 6	-.00967	1.139	2.466	2.699
	47	6: 6:27:46	-.00969	0.935	2.696	2.929
	48	6: 6:30:26	-.00970	1.032	2.597	2.830
	49	6: 6:33: 6	-.00970	0.843	2.811	3.045
	50	6: 6:35:46	-.00970	0.875	2.782	3.016
	51	6: 6:38:26	-.00970	1.053	2.569	2.802
	52	6: 6:41: 6	-.00970	0.713	2.950	3.184
	53	6: 6:43:46	-.00970	0.797	2.842	3.076
	54	6: 6:46:26	-.00970	0.829	2.836	3.070
	55	6: 6:49: 6	-.00970	0.965	2.685	2.918
	56	6: 6:51:46	-.00971	1.090	2.500	2.733
	57	6: 6:54:26	-.00970	0.819	2.839	3.073
	58	6: 6:57: 6	-.00970	0.963	2.626	2.859
	59	6: 6:59:46	-.00970	0.824	2.832	3.066
	60	6: 7: 2:26	-.00971	0.721	2.918	3.152
	61	6: 7: 5: 6	-.00971	0.839	2.751	2.985
	62	6: 7: 7:46	-.00964	0.827	2.788	3.022
	63	6: 7:10:26	-.00964	1.123	2.493	2.726
	64	6: 7:13: 6	-.00969	0.760	2.902	3.136
	65	6: 7:16:18	-.00969	0.958	2.651	2.884
	66	6: 7:18:58	-.00970	0.947	2.679	2.912
	67	6: 7:21:38	-.00970	0.778	2.884	3.118
SERIES IX	68	6:11:44:50	-.00966	0.940	2.681	2.914
	69	6:11:47:30	-.00967	0.935	2.680	2.913
	70	6:11:50:10	-.00968	0.963	2.630	2.863
	71	6:11:52:50	-.00968	1.104	2.470	2.703
	72	6:11:55:30	-.00969	0.903	2.694	2.927
	73	6:11:58:10	-.00968	0.859	2.749	2.983
	74	6:12: 0:50	-.00968	0.995	2.620	2.853
	75	6:12: 3:30	-.00969	0.924	2.659	2.892
	76	6:12: 6:10	-.00969	1.000	2.629	2.862
	77	6:12: 8:50	-.00969	0.715	2.928	3.162
	78	6:12:11:30	-.00969	0.761	2.892	3.126
	79	6:12:14:10	-.00969	0.885	2.758	2.992
	80	6:12:16:50	-.00969	0.951	2.657	2.890
	81	6:12:19:30	-.00969	0.710	2.887	3.121
	82	6:12:22:10	-.00969	0.980	2.646	2.879

Table V.4 - Series averages of T_{VA} and T_{CBR}.

	Series	T_{VA} (K)	T_{CBR} (K)
1983	I	1.17	2.60
	II	1.17	2.68
	III	1.16	2.66
	IV	1.25	2.64
1982	V	1.01	2.83
	VI	0.90	2.92
	VII	0.99	2.86
	VIII	0.90	2.96
	IX	0.91	2.94

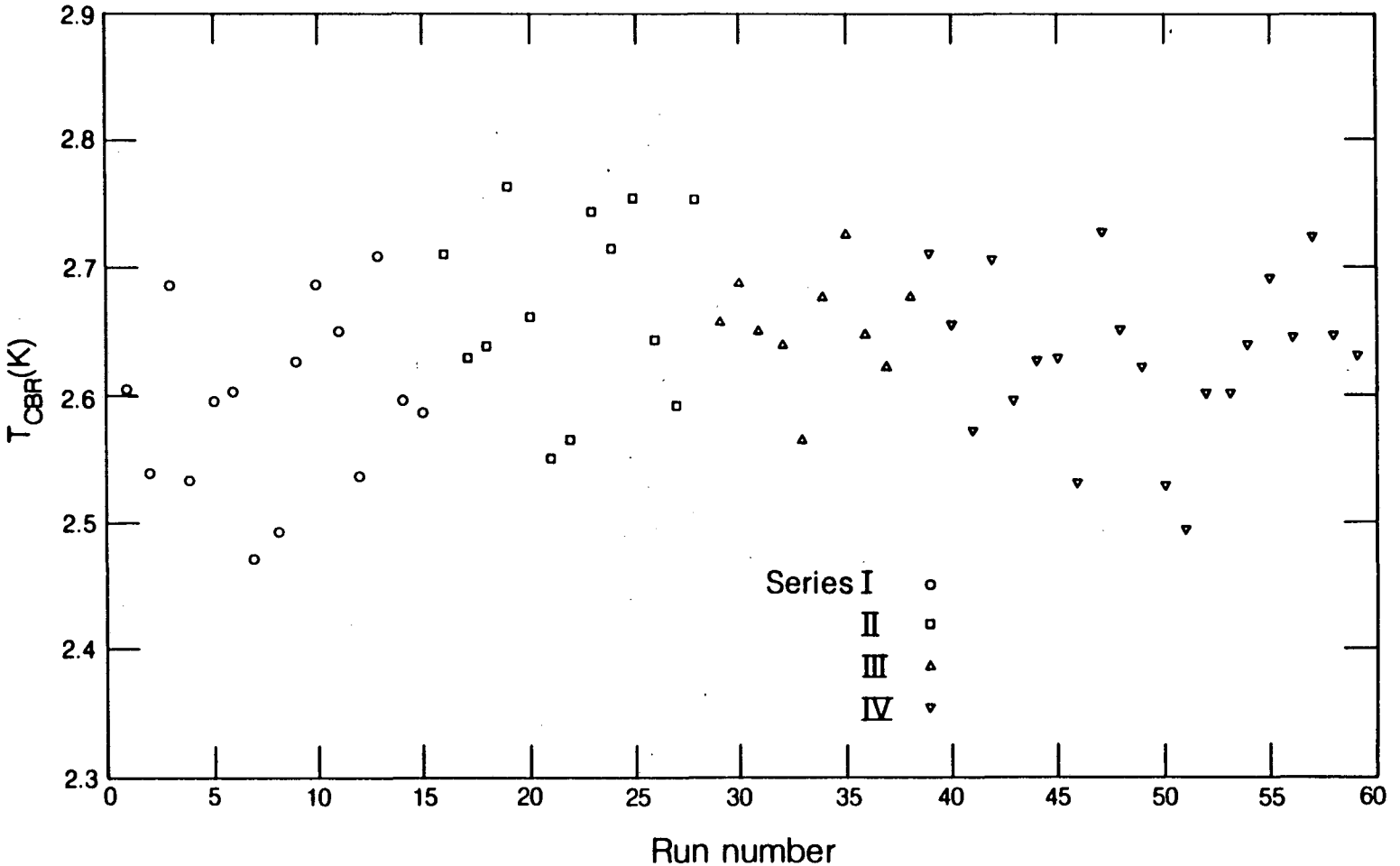

XBL 8312-6829

Figure V.2a - Cosmic background temperature versus run number (1983 data)

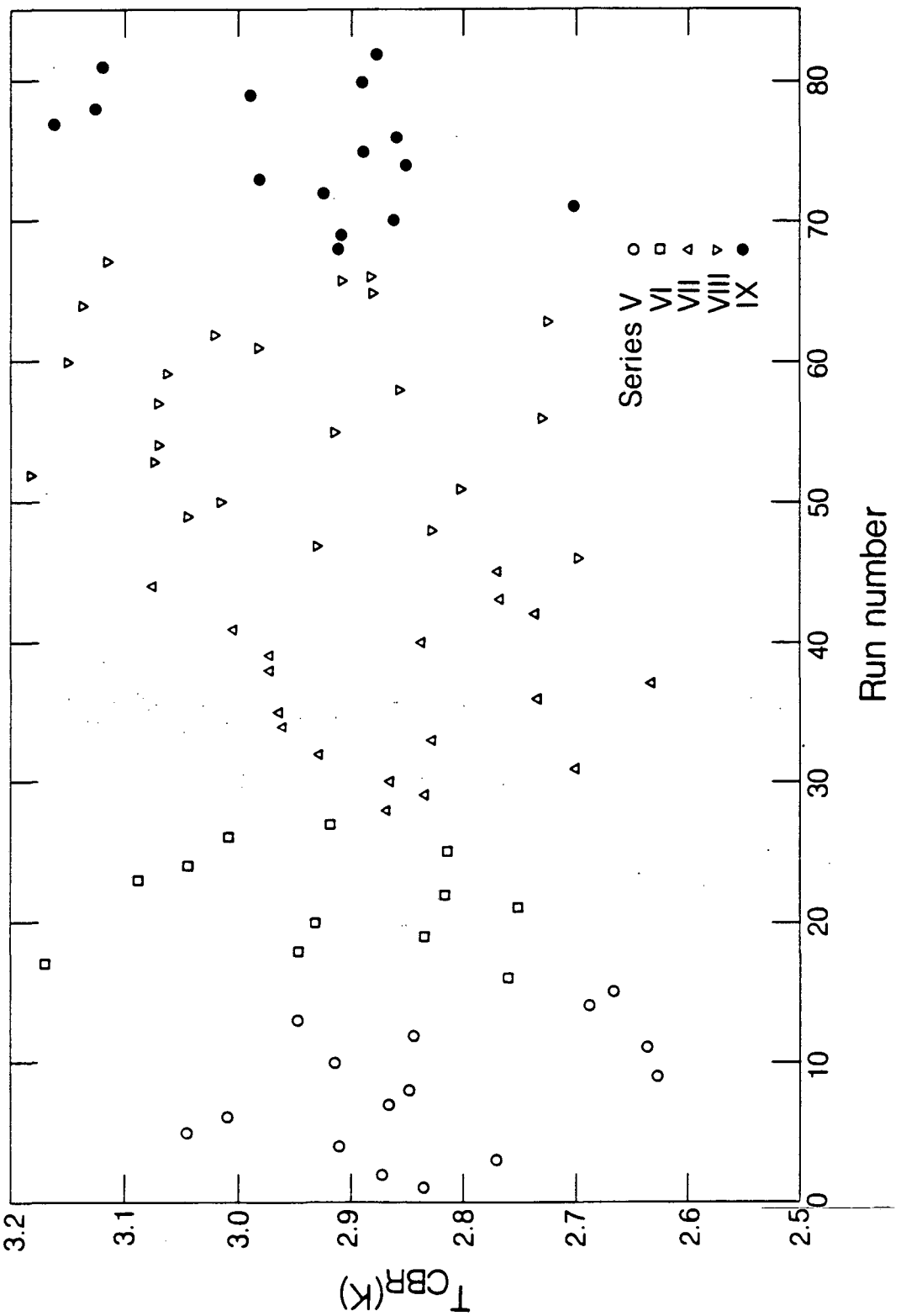

XBL 8312-6837

Figure V.2b - Cosmic background temperature versus run number (1982 data)

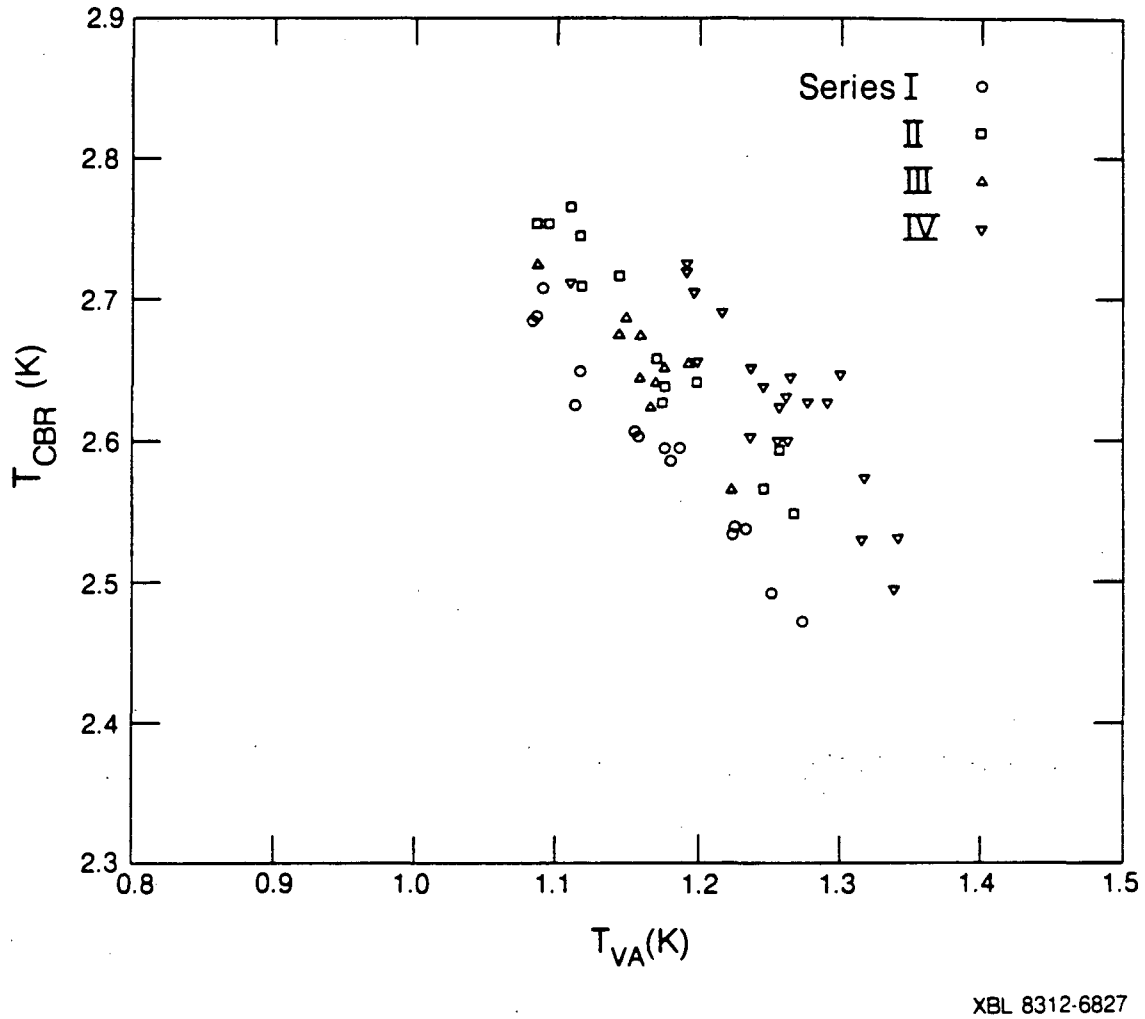

Figure V.3a - Cosmic background temperature versus vertical atmospheric temperature (1983 data)

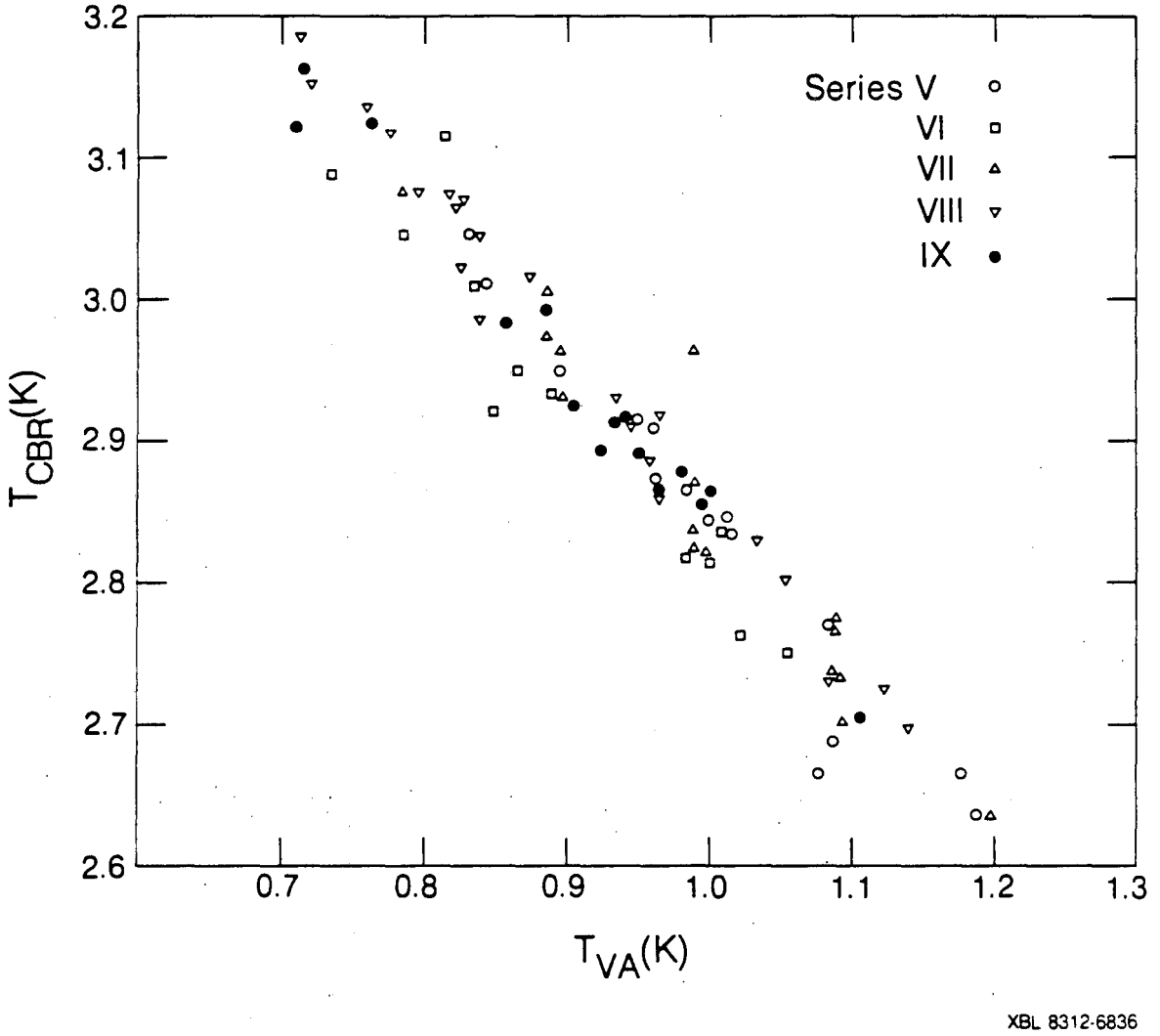

Figure V.3b - Cosmic background temperature versus vertical atmospheric temperature (1982 data)

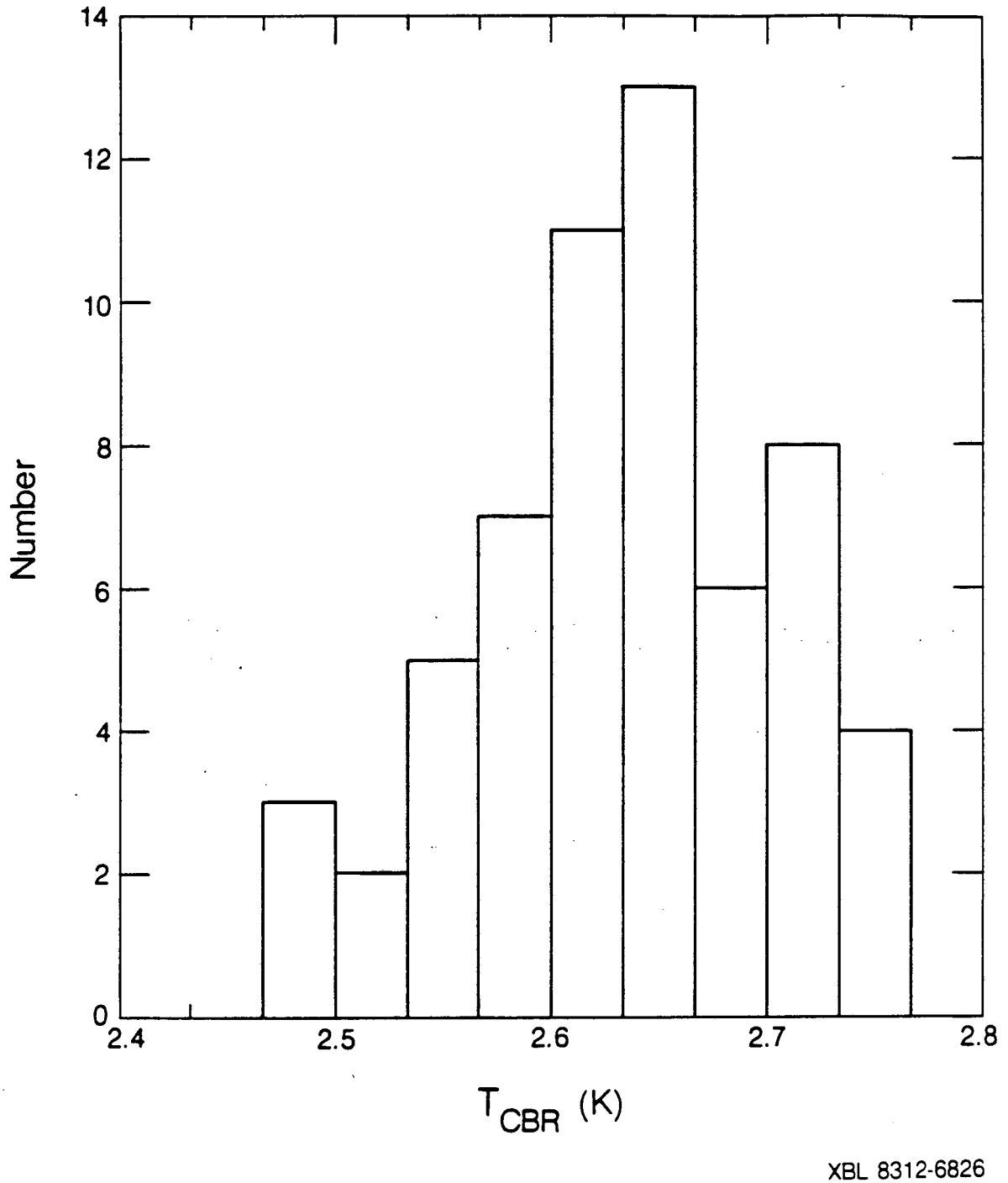

Figure V.4a - Histogram of cosmic background temperature values (1983 data)

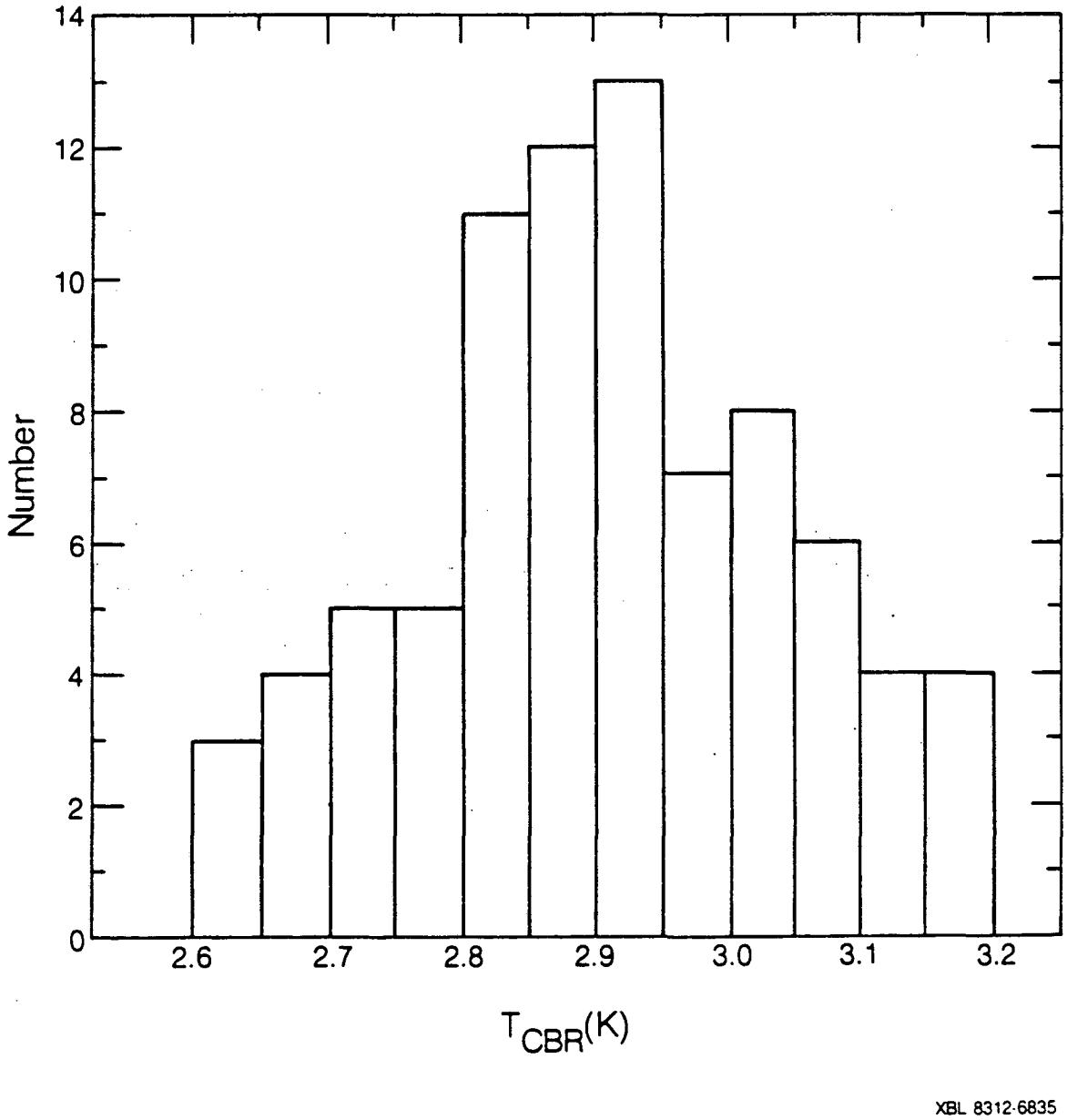

Figure V.4b - Histogram of cosmic background temperature values (1982 data)

Chapter VI - Results and Astrophysical Interpretation

VI.1 Results of This Experiment

At the time of this writing the analysis of data taken in 1983 has been completed only at the 3.0 cm wavelength. The temperature of the cosmic background radiation at 3.0 cm, based on the new data, is

$$T_{CBR} = 2.64 \pm 0.14 \text{ K} \qquad (3.0 \text{ cm}) .$$

Initial analysis at 12 cm indicates that there is no discrepancy between the 1982 and 1983 observations. At the shorter wavelengths the preliminary results are

$$T_{CBR} = 2.83 \pm 0.25 \text{ K} \qquad (0.9 \text{ cm}) ;$$

$$T_{CBR} = 2.6 \pm 0.3 \text{ K} \qquad (0.33 \text{ cm}) .$$

No statements can be made about the measurements at 6.3 and 3.2 cm in time to include in this thesis. Until the final analysis has been completed at these wavelengths we shall use the 1982 results.

Table VI.1 gives a summary of the current results of this experiment. The weighted mean of the five measurements is $T_{CBR} = 2.70 \pm 0.09$ K, using the new value at 3.0 cm. This number may change slightly when the 1983 results from the other four radiometers are included.

A plot of our results is shown in Figure VI.1. This figure is based on the 1982 data except for the new result at 3.0 cm.

VI.2 Comparison With Previous Results

There have been no previous measurements of the CBR temperature at a wavelength of exactly 3.0 cm. There have been two measurements at 3.2 cm. In 1965, shortly after the discovery of the cosmic background radiation, Roll and Wilkinson (1966) found $T_{CBR} = 3.0 \pm 0.5$ K from data taken at Princeton, New Jersey. Stokes et al. (1967) made measurements from White Mountain in 1967 with the result $T_{CBR} = 2.69 \begin{smallmatrix} + 0.16 \\ - 0.21 \end{smallmatrix}$ K. This is in good agreement with our result, even though they measured a vertical atmospheric temperature of 1.37 ± 0.1 K, which is 170 mK higher than our value.

There have been many measurements of the CBR temperature in the wavelength region $0.33 \leq \lambda \leq 73.5$ cm, all of them made before 1968 (Weiss, 1980). The weighted mean is T_{CBR} 2.74 ± 0.09 K, in excellent agreement with our results. These measurements are also shown in Figure VI.1.

Table VI.1 - Summary of results of this experiment.

Wavelength (cm)	T_{VA} (K)	T_{CBR} (K)
12.0	0.95 ± 0.05	2.62 ± 0.25
6.3	1.0 ± 0.1	2.71 ± 0.2
3.2	1.03 ± 0.03	———
3.0	1.20 ± 0.13	2.64 ± 0.14
0.9	5.0 ± 0.14	2.87 ± 0.21
0.33	12.3 ± 0.8	2.4 ± 1.0

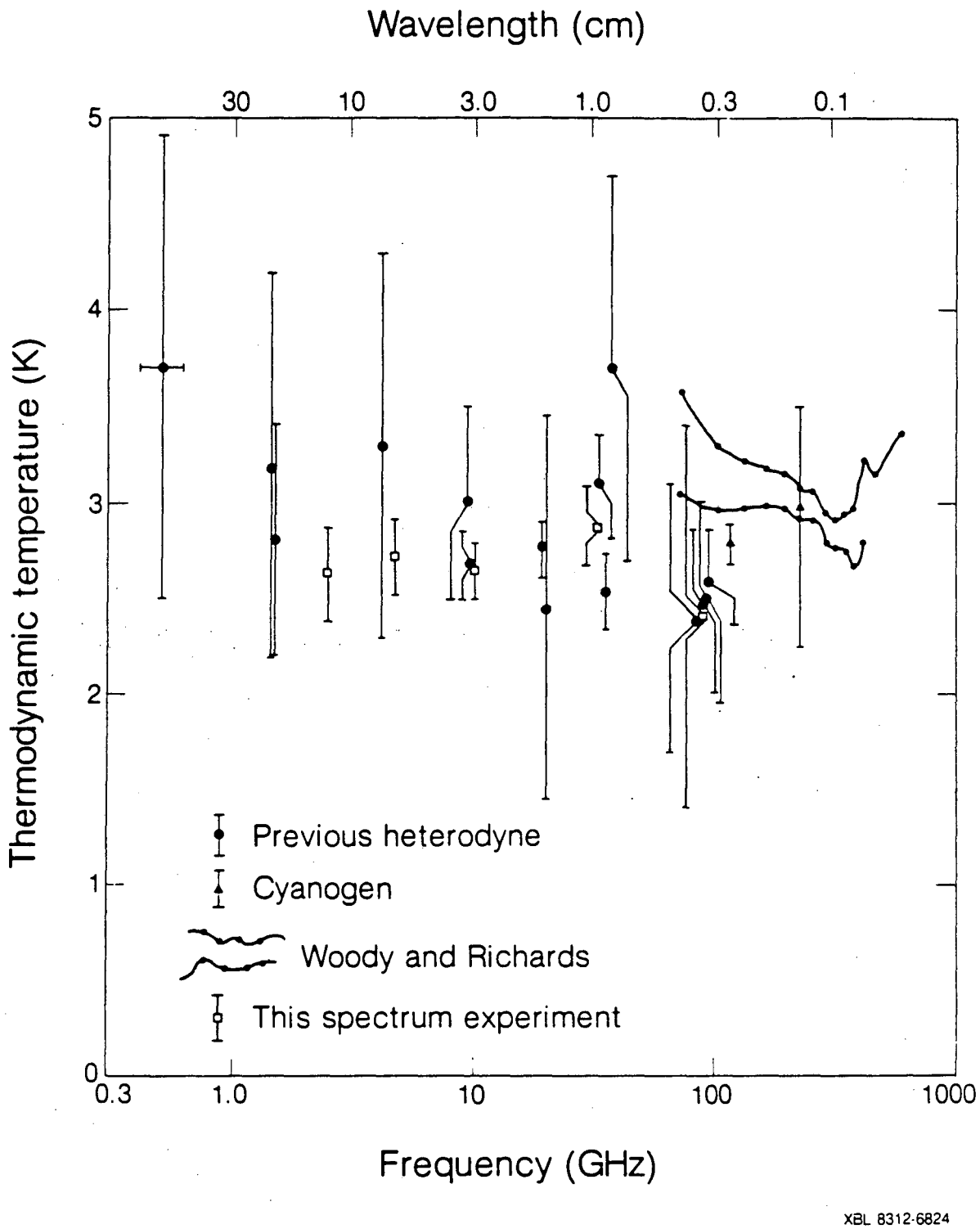

Figure VI.1 - Spectrum measurements of the cosmic background radiation

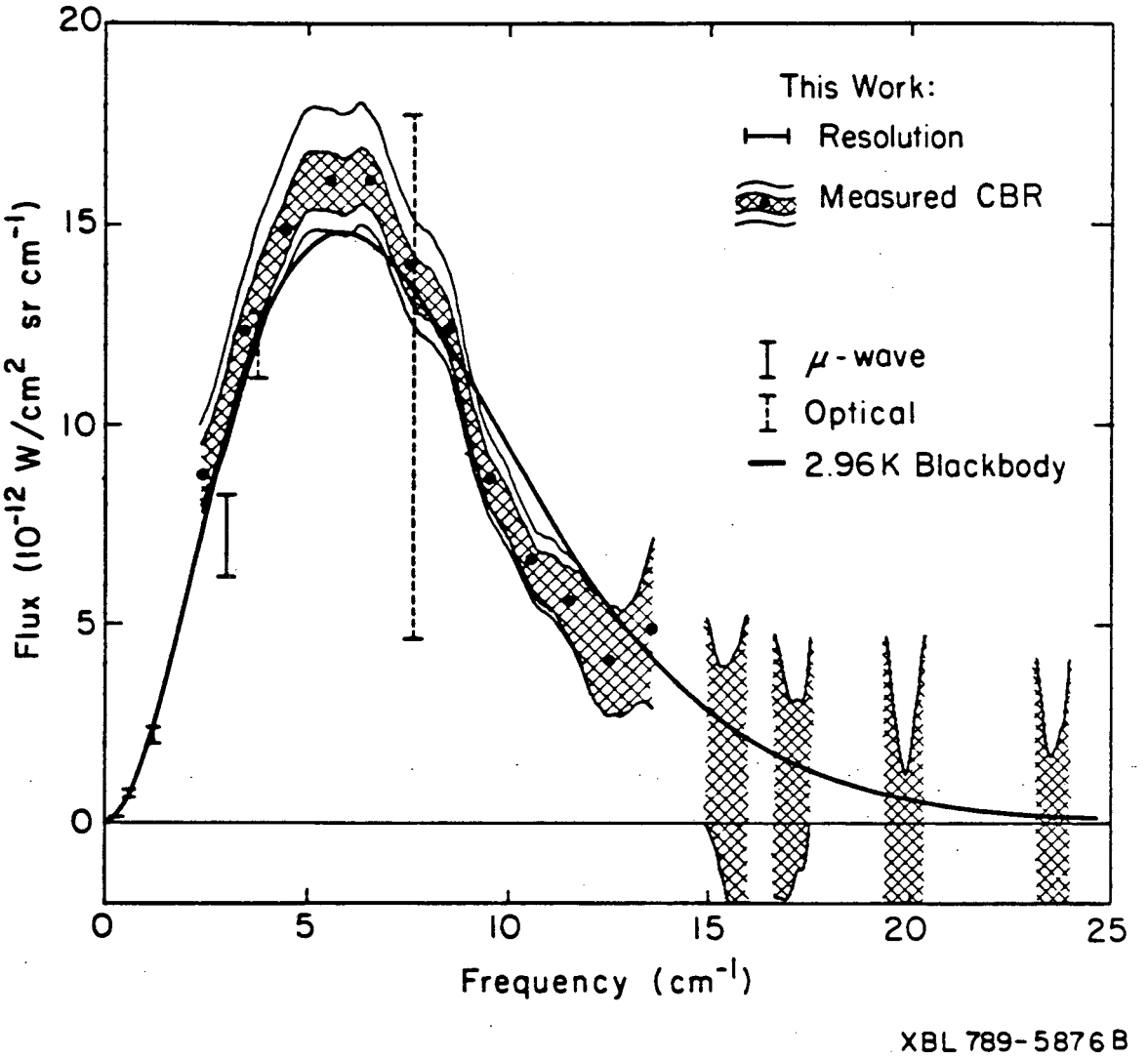

Figure VI.2 - Results of Woody and Richards (1981) spectrum measurement

In the infrared region a distortion has been reported by Woody and Richards (1981), as we previously stated. The instrument used was a balloon-borne polarizing Michelson interferometer, with germanium bolometers. Their results are shown in Figure VI.2. However, recent data are in conflict with this. New high precision measurements of transitions of the interstellar molecule cyanogen (CN) have led to highly accurate estimates of the CBR temperature in the infrared region (Meyer and Jura, 1984). They report CN excitation temperatures of 2.73 ± 0.04 K and 2.8 ± 0.3 K at 2.64 mm and 1.32 mm, respectively, which they interpret as an upper limit on T_{CBR}. The first value is in serious disagreement with Woody and Richards, but agrees quite well with most of the measurements in the Rayleigh-Jeans region.

VI.3 Astrophysical Interpretation

The addition of energy in the early universe may distort the CBR spectrum. The mechanism of Compton scattering tends to produce a Bose-Einstein distribution (Illarionov and Sunyaev, 1975), characterized by a photon occupation number

$$n = \{e^{(x+\mu)} - 1\}^{-1}, \qquad x = h\nu/kT . \tag{VI.1}$$

This differs from a Planck distribution only by the presence of the chemical potential μ. A CBR temperature that is higher in the Wien region than in the Rayleigh-Jeans region is indicative of this photon occupation number. If the energy injection occurs early enough then there is also a temperature rise at long wavelengths, since low energy photons are produced by bremsstrahlung. Given sufficient time, a Planck distribution is re-established.

We can fit the data listed in Table VI.1 to a spectrum that is expected to result from an energy release in the early universe. Since the result at 12 cm, our longest wavelength observation, is the lowest of our four most accurate measurements (the 0.33 cm value is lower, but has much larger errors) it is unlikely that bremsstrahlung has had any effect over our spectral range. We therefore fit to the Bose-Einstein spectrum of Eq. (VI.1). It is linearized by expanding about the temperature $T_o = 2.7$ K, and assuming that $\mu << 1$ and $T = T_o + T_1$, where $T_1 << T_o/x_o$.

$$n_i = \left(e^{x_o} - 1\right)^{-1} \left\{1 + T_1 \frac{x_o}{T_o} \left(1 - e^{-x_o}\right)^{-1} - \mu\left(1 - e^{-x_o}\right)^{-1}\right\},$$

$$x_o = h\nu_i/kT_o .$$

We find the best fit values of μ and T_1 by minimizing

$$\chi^2 = \sum_i \frac{1}{\sigma_i^2} \left(\frac{h}{k} \nu_i n_i - T_i\right)^2 ,$$

where T_i is the measured antenna temperature of the CBR at the frequency ν_i. Fitting our data alone gives

$$\mu = (2.30 \pm 5.29) \times 10^{-3} \qquad T_1 = 0.048 \pm 0.154 \text{ K} ;$$

$$\chi^2/\text{DOF} = 0.27 \text{ for 3 degrees of freedom.}$$

If we include all previous Rayleigh-Jeans measurements, $73.5 \leq \lambda \leq 0.33$ cm, which are tabulated in Danese and De Zotti (1978) and are shown in Figure VI.1, we find

$$\mu = (-1.48 \pm 2.65) \times 10^{-3} \qquad T_1 = -0.013 \pm 0.074 \text{ K};$$

$$\chi^2/\text{DOF} = 0.46 \text{ for 18 degrees of freedom.}$$

Our data alone, as well as all Raleigh-Jeans measurements taken together, are consistent with $\mu = 0$, that is, with a blackbody spectrum.

Because of Compton scattering the spectrum may not be characterized by a constant chemical potential. We can include evolutionary effects by taking a frequency dependent μ (Danese and De Zotti, 1979) :

$$\mu(x) = \mu_o e^{-(2x_1/x_o)}, \tag{VI.2}$$

$$x_1(z_h) = 50 \left(g(x_o)\,\hat{\Omega}\right)^{1/2} z_h^{-3/4},$$

where $\hat{\Omega} = (H_o/50)^2\,\Omega$,

Ω = ratio of density to the critical density in the universe,

H_o = the Hubble parameter, in units of km $\sec^{-1}$ Mpc^{-1},

z_h = redshift at which the energy is released,

and $g(x_o)$ = the frequency dependent Gaunt factor.

(In this analysis we will make the approximation that $g(x_o) = 1$, which is accurate to within a factor of 5 over all relevant values of x_o.) Equation (VI.2) is valid for small values of μ_o, and for energy release at redshifts $z_h > 2 \times 10^4$.

The fits of our data to μ_o and T_1, for various values of $\hat{\Omega}$ and z are given in Table VI.2. If the other Rayleigh-Jeans measurements are included then the fits formally give negative, but statistically insignificant, values of μ_o. This is physically impossible, and indicates that the data are best fit by $\mu_o = 0$.

Table VI.2 - Fits of CBR measurements to μ_o and T_1 (in Kelvin).

	$z = 2 \times 10^4$	$z = 10^5$	$z = 10^6$
$\hat{\Omega} = 1.0$			
μ_o	$(4.33 \pm 2.20) \times 10^{-2}$	$(5.69 \pm 8.17) \times 10^{-3}$	$(2.71 \pm 5.71) \times 10^{-3}$
T_1	0.484 ± 0.266	0.099 ± 0.176	0.055 ± 0.157
χ^2/DOF*	0.88	0.27	0.27
$\hat{\Omega} = 0.1$			
μ_o	$(5.99 \pm 8.38) \times 10^{-3}$	$(3.07 \pm 6.07) \times 10^{-3}$	$(2.42 \pm 5.42) \times 10^{-3}$
T_1	0.103 ± 0.178	0.060 ± 0.160	0.050 ± 0.155
χ^2/DOF*	0.28	0.26	0.27
$\hat{\Omega} = 0.01$			
μ_o	$(3.12 \pm 6.12) \times 10^{-3}$	$(2.52 \pm 5.52) \times 10^{-3}$	$(2.34 \pm 5.33) \times 10^{-3}$
T_1	0.060 ± 0.161	0.052 ± 0.156	0.048 ± 0.154
χ^2/DOF*	0.26	0.27	0.27

*3 degrees of freedom.

It is evident that the data are inconsistent with a chemical potantial larger than about 10^{-2}, and we now consider the implications which follow from such a limit. It is convenient to divide the analysis into three epochs bounded by redshifts z_1 and z_2.

For energy released at $z_h > z_1 \simeq 5.4 \times 10^4 \, \Omega^{-6/5}$ the combination of bremsstruhlung and Compton scattering relaxes a distorted spectrum to a Planck distribution (Chan and Jones, 1975). There is no observable distortion today.

The redshift z_2 is given by

$$z_2 \simeq 2.3 \times 10^4 \, \Omega^{-1/5} \quad \text{for} \quad \Omega > 0.6 \, ;$$

$$z_2 \simeq 1.6 \times 10^4 \, \Omega^{-1/2} \quad \text{for} \quad \Omega < 0.6 \, .$$

Its significance is that for $z_h > z_2$ bremsstrahlung is too slow to completely thermalize a distorted spectrum, although Compton scattering is efficient enough to establish a Bose-Einstein spectrum. For $z_h < z_2$ not even a Bose-Einstein spectrum can be formed. Bremsstrahlung and Compton scattering will continue to modify the spectrum until recombination at $z \simeq 1500$, when the interaction between matter and radiation effectively stops.

Consider first heating at $z_2 < z_h < z_1$. The fractional change in the radiation energy density U is related to the chemical potential (Chan and Jones, 1975)

$$\Delta U/U_o = 0.7 \, \mu < 7 \times 10^{-3} \, ,$$

where U_o is the energy density of the unperturbed spectrum. The greatest temperature deviation in the Rayleigh-Jeans region from a blackbody is

$$\Delta T_{RJ}/T_{RJ} \simeq e^{-1}\,\mu/x_m ,$$

where x_m is the normalized frequency at which the maximum deviation occurs. Our data indicate that $\Delta T_{RJ}/T_{RJ} \leq 0.1$. If, for definiteness, we assume that the equality holds, then

$$x_m < 3.7 \times 10^{-2} \quad \text{or} \quad \lambda_m > 15 \text{ cm} .$$

This is difficult to observe because the synchrotron emission from the galaxy increases rapidly at long wavelengths. If the greatest deviation is less than 10% then it may fall at a more accessible wavelength. However, experiments with greater accuracy would be required to detect such a distortion.

For energy released at later epochs, $z_h < z_2$, the antenna temperature of the CBR is constant at frequencies $x < 1$, which corresponds to $\nu < 56$ GHz, or $\lambda > 0.53$ cm (Jones, 1980). If the primordial plasma density is high enough then bremsstrahlung repopulates the long wavelength portion of the spectrum, but there is insufficient time for the Compton process to scatter these photons to higher energies. The CBR temperature is highest at wavelengths shortward of the peak.

The maximum jump in the CBR temperature in this case is model dependent. If, for example, the energy source were hot electrons resulting from turbulence in the plasma, then the magnitude of the jump would be (Chan and Jones, 1975)

$$\Delta T \simeq (T_e - T_o)(1 - 2y) ,$$

where T_o is the CBR temperature before the perturbation ;

T_e is the temperature of the hot electrons ;

and y is a parameter related to the time of energy release. If the release is prior to recombination then $y \simeq 3 \times 10^{-9} z^2 \Omega$. Thus, by observing the difference in temperature between the Rayleigh-Jeans and Wien portions of the spectrum constraints can be set on the matter temperature T_e and on the time of heat input.

The Woody and Richards result does not support models of this kind since they observed a sharply falling flux shortward of the peak. As stated in Chapter I, models invoking the existence of a pregalactic Population III generation of stars can account for their result. Since the spectral index for dust emission is between -1 and -2 (Weiss, 1980) the spectrum measurements in the Rayleigh-Jeans region are not useful for testing these models.

To summarize, our results are consistent with the previous microwave measurements. The values of T_{CBR} at 12 and 6.3 cm represent a considerable improvement in accuracy in the long wavelength region, and give no evidence for a bremsstrahlung repopulation of photons. An upper limit on the chemical potential $\mu < 10^{-2}$ puts roughly the same limit on the fractional energy release in the early universe. Such a release may cause a distortion, but the maximum temperature deviation could then fall at very long wavelengths. If this is the case then the galactic background could prohibit a sufficiently accurate measurement to observe the distortion.

VI.4 Suggestions For Future Experiments

Atmospheric emission has been the largest background in the measurements of the Rayleigh-Jeans spectrum of the CBR. Use of a high

altitude balloon, rocket, or satellite would reduce this to a negligible level. But this may be prohibitively expensive, since long wavelength radiometers are quite large and heavy. Such platforms are not immediately necessary, since it is possible to make significantly more accurate ground-based measurements, particularly in the 3-15 cm wavelength region.

The first highly accurate measurements of the CBR temperature were made by David Wilkinson and his group at Princeton. Recognizing that moving the radiometer during zenith scans caused flip asymmetries, they chose to direct the antenna beam to various angles with a reflector. This permitted the measurement of the atmospheric temperature with very small errors. However, since it was necessary to use the reflector to view the vertical sky, they were never able to direct their primary antenna straight down. Thus, they had to use a relatively small LHe-cooled load which, during calibrations, was temporarily attached to the antenna at an angle of approximately 30° to horizontal (Wilkinson, 1967). Since the diameter of the LHe load was only about 12 cm, there was significant emission from the walls. The largest source of systematic error in their measurements was the uncertainty of the temperature of the LHe load.

Combining the good features of Wilkinson's techniques and ours would allow an improved measurement. First, our large LHe load is necessary to keep the wall emission low. Second, the atmosphere must be measured using a reflector.

The radiometer would have a similar design to that in the present experiment. Only three rotation positions would be used : straight up to view the vertical sky; straight down to view the LHe load; and horizontally to view a reflector for zenith scans. The atmospheric emission would be measured without moving the radiometer. The flip asymmetry would still be present, but it would

not be multiplied by the factor $1/F_o$ that appears in Eq. (V.5). Thus the error in T_{VA} would be greatly reduced.

The disadvantage of this system is that a large reflector and extensive shielding would be required to prevent reception of ground radiation during zenith scans at large angles. But the effort required would be offset by the accuracy of the measurement, which could be more than a factor of two better than has been achieved before.

Appendix A - Intensity-Temperature Relations

The intensity I of the radiation emitted by a blackbody at a thermodynamic temperature T is (Kraus, 1966; Ulaby et al., 1981)

$$I = \frac{2h\nu^3}{c^2} (e^x - 1)^{-1} \text{ erg cm}^{-2} \text{ sec}^{-1} \text{ Hz}^{-1} \text{ st}^{-1} ,$$

where $$x = \frac{h\nu}{kT} = \frac{hc}{\lambda kT} .$$

For $x << 1$, called the Rayleigh-Jeans limit, this reduces to

$$I = 2kT \frac{\nu^2}{c^2} = 2 \frac{kT}{\lambda^2} .$$

The antenna temperature T_A is defined such that a blackbody source at a temperature T_A, which fills the antenna beam, would emit radiation at an intensity I in the Rayleigh-Jeans limit. Therefore

$$T_A = \frac{\lambda^2}{2k} I .$$

It is this linear relationship between I and T_A which allows us to speak of the intensity of sources in terms of temperature.

It follows from these relations that

$$T_A = \frac{x}{e^x - 1} T .$$

For example, with $\lambda = 3$ cm and $T = 2.64$ K

$$x = 0.182 ;$$

$$\frac{x}{e^{x}-1} = 0.912 ;$$

and

$$T_A = 2.41 \text{ K} .$$

Appendix B - Ouarter Wave Plate

The horizontal antenna of the radiometer views the vertical sky by means of a mirror at a 45° angle. The virtue of this arrangement is that it provides a convenient, stable, low temperature signal. This advantage is lost, however, if this signal changes as the radiometer is rotated.

Radiation from an unpolarized source, in general, becomes partially linearly polarized upon reflection from an imperfect conductor. Since the feed of the antenna accepts one linear polarization state and reflects the orthogonal state, there is a modulation of the signal intensity into the secondary antenna as a function of radiometer rotation position. This modulation makes a direct contribution to the systematic error in the measurement of the atmospheric temperature.

To calculate the magnitude of the polarized signal, consider first the case in which the the electric field **E** is normal to the plane of incidence (Figure B.1a). The ratio of the reflected to incident electric fields is (Lorrain and Corson, 1970)

$$\frac{E_r}{E_i} = \frac{(A - B) + iB}{(A + B) - iB}$$

$$= \frac{(A^2 - 2B^2) + 2iAB}{(A + B)^2 + B^2} ,$$

where $A = \cos\theta_i$;

$B = \frac{\lambda}{2\pi\delta} = 5.78 \times 10^3$;

θ_i = angle of incidence ;

and $\delta = 8.46 \times 10^{-5}$ cm = skin depth for aluminum.

We have made the approximations that the index of refraction for air is unity,

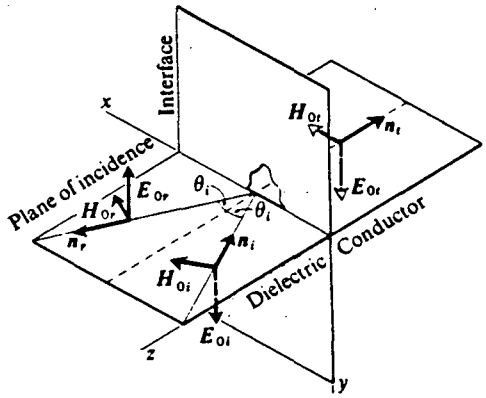

Figure B.1a - Reflection with electric field normal to the plane of incidence

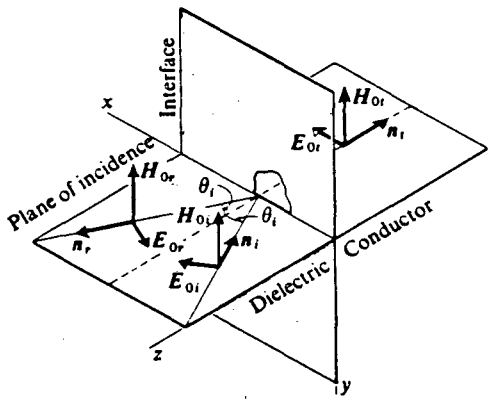

Figure B.1b - Reflection with electric field parallel to the plane of incidence.

(From Electromagnetic Fields and Waves by P. Lorrain and D. Corson, 2nd ed., W. H. Freeman and Company. Copyright © 1970.)

and that the magnetic permeability of the aluminum reflector is unity. Since $B \gg A$, the ratio of the reflected to incident intensities is

$$\left| \frac{E_r}{E_i} \right|_{\perp}^2 = \left(1 + 2\frac{A}{B}\right)^{-1}$$

$$\simeq 1 - 2\frac{A}{B}$$

$$\simeq 1 - 4\pi \frac{\delta}{\lambda} \cos\theta_i \, .$$

If the electric field is parallel to the plane of incidence (Figure B.1b) then

$$\frac{E_r}{E_i} = \frac{(1 - AB) + iAB}{(1 + AB) - iAB}$$

$$= \frac{(1 - 2A^2B^2) + 2iAB}{(1 + AB)^2 + (AB)^2} \, .$$

The reflected intensity is

$$\left| \frac{E_r}{E_i} \right|_{\parallel}^2 \simeq \left(1 + \frac{2}{AB}\right)^{-1}$$

$$\simeq 1 - \frac{2}{AB}$$

$$\simeq 1 - 4\pi \frac{\delta}{\lambda} \sec\theta_i \, .$$

Since the mirror is at a 45° angle with respect to the antenna, $\theta_i = 45^\circ$ for all rotation positions. The effective perpendicular and parallel emissivities of the reflector may now be written

$$\varepsilon_{\perp} = 1 - \left| \frac{E_r}{E_i} \right|_{\perp}^{2} = 2.5 \times 10^{-4} ,$$

$$\varepsilon_{\parallel} = 1 - \left| \frac{E_r}{E_i} \right|_{\parallel}^{2} = 5.0 \times 10^{-4} .$$

The total emissivity is

$$\varepsilon = \varepsilon_{\perp} \cos^2\theta + \varepsilon_{\parallel} \sin^2\theta ,$$

where θ is now the rotation angle of the radiometer ($\theta = 0^{\circ}$ when the primary antenna is toward the zenith). Table B.1 gives values of the emissivity and the effective emission temperature of an aluminum reflector at 275 K.

If no corrections were made for this polarization effect, then the error in the computed atmospheric temperature would be approximately (86mK - 69mK)(sec(30°) - 1) = 110mK at a rotation angle of 30°, and 92mK at 40°. To avoid such a large systematic error a quarter wave plate (QWP) was installed in the feed of the horizontal antenna.

The QWP (Figure B.2) is simply a flat piece of Teflon. It is in the cylindrical waveguide feed of the antenna, just in front of the step transition to the rectangular waveguide. The QWP makes a 45° angle with respect to the walls of the rectangular waveguide.

The dielectric constant of Teflon is 2.1. Thus, the propagation velocity of electromagnetic radiation is about 30% lower in Teflon than in free space. Consider a circularly polarized wave received by the antenna. This wave is the superposition of two orthogonal, linearly polarized waves, out of phase by 90°. One of these is normal to the Teflon, and is essentially unaffected as it passes by the QWP. The other is parallel to the Teflon, and slows when it reaches the QWP. If the length of the QWP is properly chosen then the two waves emerge in

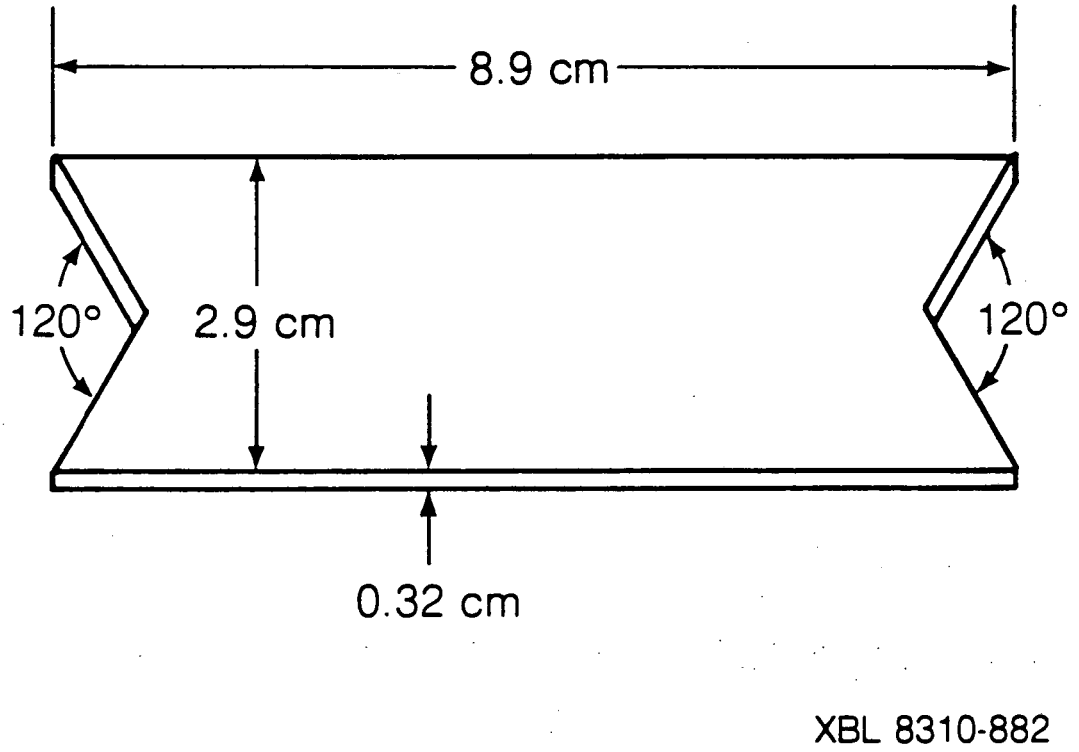

Figure B.2 - Quarter wave plate

phase, and form a single linearly polarized wave which is accepted by the radiometer. The circularly polarized wave of the opposite sense is reflected back out of the radiometer.

The tapered edges of the QWP help reduce the reflections of the accepted polarization state to a small level. The insertion loss was measured to be only 60 mK, so it was not necessary to thermally regulate the plate.

The effectiveness of the QWP is measured by using a polarizer, originally designed for the calibration of a microwave polarimeter (Lubin and Smoot, 1981). The polarizer transmits radiation of one linear polarization state from the vertical sky into the antenna, and reflects radiation of the orthogonal linear state from a room temperature Eccosorb load into the antenna. With the primary antenna viewing the zenith the polaroid is rotated about the axis of the secondary antenna, and in front of it. The maximum and minimum output voltages from the radiometer observed during this rotation are a measure of the quality of the QWP. Defining

$$R = \frac{V_{max}}{V_{max} + V_{min}} ,$$

then R = 0.5 corresponds to a perfect QWP, and R = 1.0 corresponds to a QWP that has no effect at all. The length of the QWP was empirically chosen to minimize R.

On White Mountain we measured V_{max} = 5.25 V, V_{min} = 4.60 V, giving R = 0.53 .

The emissivity of the reflector is now

$$\varepsilon = R(\varepsilon_{\perp} \cos^2\theta + \varepsilon_{\parallel} \sin^2\theta) + (1 - R)(\varepsilon_{\perp} \sin^2\theta + \varepsilon_{\parallel} \cos^2\theta) .$$

Various values of the emissivity as a function of rotation angle are given in Table B.2 for R = 0.53, and displayed in Figure B.3.

Table B.1 - Emission from an aluminum reflector at temperature T = 275 K.

θ	ε	εT
0°	2.50×10^{-4}	69 mK
30	3.13	86
40	3.53	97
90	5.00	138

Table B.2 - Emission from an aluminum reflector for R = 0.53 .

θ	ε	εT
0°	3.68×10^{-4}	101 mK
30	3.71	102
40	3.74	103
90	3.83	105

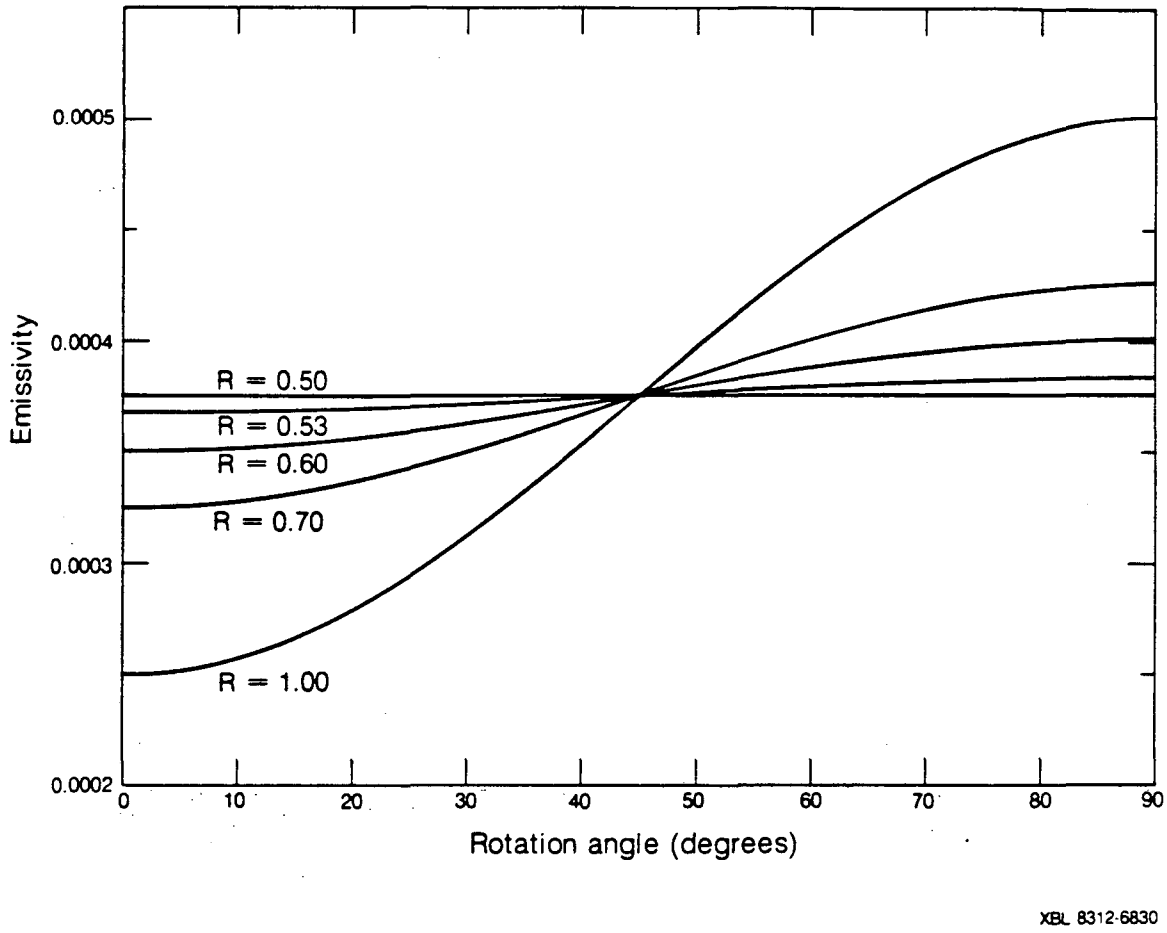

Figure B.3 - Emissivity of reflector versus radiometer rotation angle

Appendix C - Emission From LHe Reference Load

The temperature of the CBR is found by comparing the power from the vertical sky with the power from the LHe-cooled reference load, as shown in Eq. (V.1). An error in the temperature of this load causes an identical error in the CBR temperature. Thus it is important to know the emissive properties of the load.

The dominant emission source is the Eccosorb, which is immersed in the LHe. The emissivity of the Eccosorb is greater than 0.999 . Thus the effective radiometric temperature of the Eccosorb departs from its physical temperature by less than (0.001)(3.773 K) $\simeq$ 4 mK.

There are three additional sources of radiation, all of which are small compared to the Eccosorb. These are emission from the walls of the load, reflected power from the load, and emission from the windows.

C.1 Wall Emission

An upper limit on the emission from the walls can be estimated by assuming that the load is a large cylindrical waveguide. The antenna responds primarily to the TE_{11} mode. The attenuation per unit length for this mode is (Ramo et al., 1965)

$$a = \frac{1}{r\eta}\left(\frac{\pi c \rho}{\lambda}\right)^{1/2} \left(1 - \lambda_r^2\right)\left(\lambda_r^2 + 0.420\right) \tag{C.1}$$

where r = 0.35 meters = radius of the waveguide ;

η = 376.7 ohms = impedence of waveguide dielectric (He gas) ;

ρ = resistivity of aluminum ;

$\lambda_r = \lambda/\lambda_c = 2.510 \times 10^{-2}$ = normalized wavelength ;

and $\lambda_c = 3.415r = 1.195$ meters = cutoff wavelength.

The wall emission is found by dividing the cylinder into annular strips, and summing the contributions of each strip from the bottom to the top of the walls. The effective temperature from a strip of width d is

$$T_{ann} = adT_{wl} + T_b e^{-ad} , \qquad (C.2)$$

where T_{wl} = the physical wall temperature of the annulus ;

and T_b = the effective temperature radiated by the cold load from below the strip.

The first term represents the emissive power contributed by the strip itself, and the second term represents the attenuation by the strip of radiation from below. The width d of the strip is taken to be 1 cm.

The temperature of the wall was a function of the height above the LHe. The temperature is known at three locations.

At the bottom, or height h = 0 cm, the temperature was $T_{wl} = T_{LHe}$ = 3.773 K.

Above the level of the shutter, h = 116 cm, external heaters maintained a wall temperature of 275 K, to prevent frost from forming on the outside of the load.

The third location was at the level h = 81 cm, where a temperature sensor indicated $T_{wl} = 60 \pm 5$ K. The uncertainty arises because the temperature changed depending on which radiometer was viewing the load, which affected the LHe boil-off rate.

The wall temperature was assumed to vary linearly with height in the two regions below the level of the shutter, and stay constant above it.

$$T_{wl} = (0.694h) + 3.773 \text{ K}, \qquad 0 \leq h \leq 81 \text{ cm};$$

$$T_{wl} = (6.143h) - 437.6 \text{ K}, \qquad 81 \leq h \leq 116 \text{ cm};$$

$$T_{wl} = 275 \text{ K}, \qquad 116 \leq h \leq 130 \text{ cm}.$$

The resistivity of aluminum depends on its temperature. At low temperatures $\rho \propto T$, and at high temperatures $\rho \propto T^5$. An empirical relation called the Gruneisen formula (Bardeen, 1940) fits both of these, and the transition region, to an accuracy better than 0.5% in the required temperature range.

Table C.1 gives values of ρ and a for several temperatures.

Summing the contributions from all annular strips gives the total wall emission, $T_w = 9 \pm 5$ mK. This result is not very sensitive to the wall temperature distribution. For example, a linear distribution for $0 < h < 116$ cm, certainly an overestimate of the temperature, increases the emission only to 15 mK.

An error of 50% is assumed because our estimate of T_w is almost certainly an upper limit, since only about 1% of the beam solid angle is intercepted by the walls.

An exact calculation of the loss due to the walls is difficult because the top of the load, where the walls are warmest, is in the near field of the antenna. Only the far field gain pattern is known. However, this calculation is not necessary since the upper limit on the emission determined here is so small.

C.2 Reflected Power

The Dicke switch is a circulator. Thus when the radiometer views the LHe load through the primary antenna, power is being directed toward the load from the secondary antenna arm of the radiometer. This power can be expressed in terms of temperature as

$$T_{in} = T_{sa}e^{-s} + T_g s ,$$

where T_{sa} = temperature of the radiation entering the secondary antenna ;

$T_g \simeq$ 290 K = physical temperature of waveguide and Dicke switch ;

and s = attenuation of T_{sa} by the waveguide, Dicke switch, and antennas .

Table C.1 - Resistivity of aluminum and attenuation of an annulus.

Temperature (K)	ρ (ohm meters)	a (nepers/meter)
3.773	1.68×10^{-15}	2.59×10^{-8}
30	5.37×10^{-11}	4.65×10^{-6}
60	1.06×10^{-9}	2.07×10^{-5}
100	5.27×10^{-9}	4.60×10^{-5}
150	1.13×10^{-8}	6.74×10^{-5}
200	1.73×10^{-8}	8.35×10^{-5}
275	2.62×10^{-8}	1.03×10^{-4}

$T_{sa} \simeq 4$ K is the sum of the CBR and the vertical atmospheric temperatures.

The insertion loss is about 0.25 dB for the Dicke switch, and 0.1 dB for each antenna. There are six inches of WR90 waveguide, which has 0.025 dB insertion loss. The total is s = 0.475 dB = 0.116. Thus the effective temperature of the power entering the LHe load is $T_{in} = 37$ K.

The reflection coefficient of the LHe load with no cryogen in it was measured to be 1.5×10^{-4}. This was never measured with LHe in the load. The theoretical reflection coefficient from the LHe surface is

$$R_{LHe} = \left(\frac{n-1}{n+1}\right)^2 = 1.29 \times 10^{-4},$$

where n = 1.023 is the index of refraction for LHe. The true reflection coefficient from the surface is expected to be somewhat less than this since the liquid surface is broken due to boiling, and only a fraction of the incoming power is reflected back into the antenna. This fraction is roughly estimated by assuming that the flux out of the antenna is uniform within a cone whose half angle is the HPBW of the antenna (12.5°). If this radiation were perfectly reflected from the cryogen surface then it would illuminate a circle of radius (2 x 130 cm) x tan(12.5°) ≃ 58 cm. The radius of the antenna aperture is 9 cm. Thus the fraction of power that re-enters the antenna is $(9/58)^2 \simeq 0.02$.

We verified this effect using LN. The theoretical reflection coefficient is $R_{LN} = 8.72 \times 10^{-3}$, but the measured reflection from the load was in the range 1.5×10^{-4} to 1.1×10^{-3}, depending on the LN level.

We take the reflection coefficient of the LHe load to be $R = 2 \times 10^{-4}$.

The contribution of the reflected power to the temperature of the LHe load is

$$T_{ref} = (37\ K) \times (2 \times 10^{-4}) = 7 \pm 4\ mK\ ,$$

where the error is primarily due to the uncertainties of the reflection coefficient.

C.3 Windows

Two polyethylene windows are the only objects between the LHe and the antenna. Each window is 23 microns thick. Their insertion loss was estimated by directing the primary antenna toward the vertical sky and comparing the radiometer output when 32 windows were alternately put in front of the antenna, and then removed. Thirty-two windows were used simply to enhance the signal. The result was an insertion loss of 3 mK for a single ambient temperature window. Since the bottom window in the LHe load is cooled by the He gas, we take the contribution from the windows to be $T_{win} = 5 \pm 2$ mK. The error is dominated by the uncertainty in the temperature of the windows.

The reflection coefficient from the windows alone was too small to measure.

C.4 LHe Reference Load Temperature

The antenna temperature of the LHe-cooled load is the sum of the antenna temperature of the LHe (3.538 ± 0.004 K) and the contributions of the terms discussed above. The result is

$$T_{cla} = 3.538\ \mathrm{K} + T_w + T_{ref} + T_{win}$$

$$= 3.56 \pm 0.01\ \mathrm{K}\ .$$

The error is the quadrature sum of the individual errors.

We observed some solid nitrogen frost at various places on the walls after the CBR measurements were completed. This had a negligible effect on T_{cla} because solid nitrogen has low emissivity over the relevant wavelengths. In support of this the emissivity of a 1 mm thick layer of liquid nitrogen, which is expected to have a higher emissivity than solid nitrogen, was measured to be approximately 10^{-3} at a wavelength of 0.33 cm. It would be less than this at wavelength of 3 cm. Furthermore, the frost on the walls was probably thinner than 1 mm. This measured emissivity is comparable to that of the aluminum walls themselves.

There were tremendous problems in using such a large LHe reference load. The compensating benefits are that the temperature T_{cla} can be very accurately determined because the correction terms are so small.

Appendix D - Galactic Background

Synchrotron and HII thermal emission are the only sources of galactic radiation that are important at a wavelength of 3 cm. Sources such as stars, although hot, make a negligible contribution because the wide-beam antennas average over extended regions of the sky, and the solid angle of these objects is small.

The synchrotron flux is estimated using the 408 MHz sky survey of Haslam et al. (1982). It is scaled with frequency as $\nu^{-2.8}$. The HII flux is estimated from a collection of surveys compiled by Witebsky (1978), and is scaled according to $\nu^{-2.1}$.

A map of the total intensity due to these sources is shown in Figure D.1, and the numerical values are listed in Table D.1. These numbers represent the estimated effective temperature of the galactic background convolved with a 12.5° HPBW antenna beam, whose axis is in the specified direction.

The latitude of White Mountain is 38°N, so observations at zenith were at a declination of +38°. Zenith scans were made in the east-west direction. Tilting ±30° from zenith changes the relative right ascension by ±36.2°, and changes the declination to +32.2° (Smart, 1977). Tilting ±40° from zenith changes the relative RA by ±46.8°, and changes the declination to +28.1°. Thus all observations were made at declinations of approximately 38°, 32°, and 28°, and in the range RA = 165° to 60° (11 hours to 4 hours). The numbers in Table D.1 cover this portion of the sky.

The only strong source in this area of the sky is Cygnus, centered at RA = 308°, dec = +42°. The maximum effective temperature of this souce is 31 mK. The maximum galactic correction applied to the data is 14 mK, for observations closest (17°) to Cygnus. Most of the corrections are less than

8 mK.

The results are very insensitive to the accuracy of the galactic model. If all values of the model were in error by 50% the computed final value of the CBR temperature would change by only 2 mK. Thus, although there is some disagreement about the precise values of the spectral indices for the synchrotron and HII emission, the possible errors have a negligible effect on the measured value of T_{CBR}.

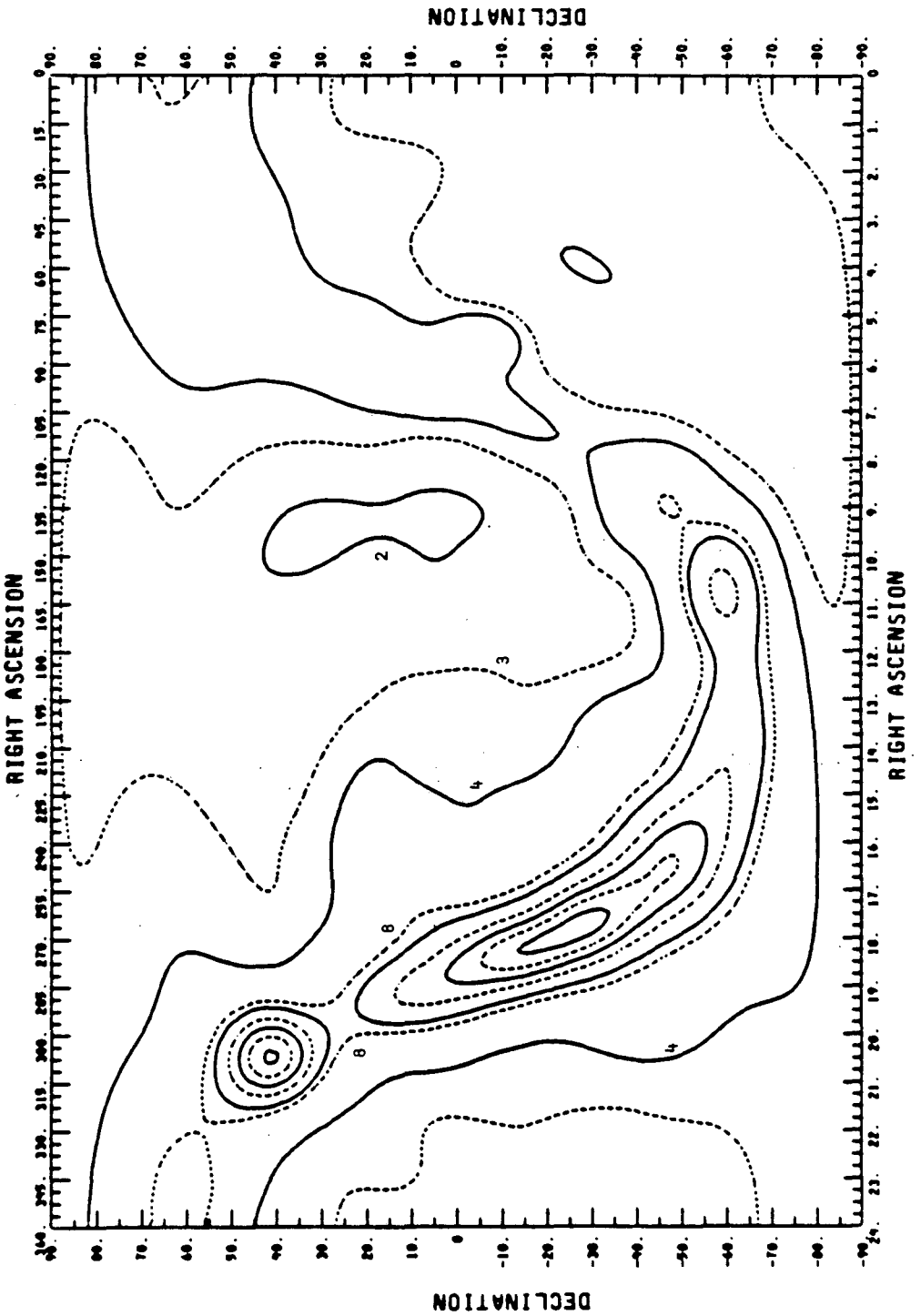

Figure D.1 - Estimated galactic background temperature at 3.0 cm. Contour levels are in mK. The contours near Cygnus (RA = 308° , dec = +42°) and the galactic center (RA = 265° , dec = -30°) are 30, 25, 20, 15, 10, 8 mK.

Table D.1 - Estimated galactic background temperature (in mK) at 3.0 cm

Dec	RA = 0				10				20				30				40				50			
38	3	3	3	3	3	3	3	3	3	3	3	4	4	4	4	4	4	4	4	4	4	4	4	5
32	3	3	3	3	3	3	3	3	3	3	3	3	3	3	3	3	4	4	4	4	4	4	4	4
28	3	3	3	3	3	3	3	3	3	3	3	3	3	3	3	3	3	4	4	4	4	4	4	4

Dec	RA = 60				70				80				90				100				110			
38	5	5	5	5	5	5	5	5	5	5	5	5	5	5	5	4	4	4	4	4	4	4	4	3
32	4	4	4	4	4	5	5	5	5	5	5	5	5	5	5	5	5	4	4	4	4	4	4	4
28	4	4	4	4	4	4	5	5	5	5	5	5	5	5	5	5	5	5	4	4	4	4	4	4

Dec	RA = 120				130				140				150				160				170			
38	3	3	2	2	2	2	2	2	2	2	2	2	2	2	2	2	2	2	2	2	2	2	2	2
32	3	3	2	2	2	2	2	2	2	2	2	2	2	2	2	2	2	2	2	2	2	2	2	2
28	3	3	2	2	2	2	2	2	2	2	2	2	2	2	2	2	2	2	2	2	2	2	2	2

Dec	RA = 180				190				200				210				220				230			
38	2	2	2	2	2	2	2	2	2	2	2	2	2	2	3	3	3	3	3	3	3	3	3	3
32	2	2	2	2	2	2	2	2	2	3	3	3	3	3	3	3	3	3	3	3	3	3	3	3
28	2	2	2	2	2	2	3	3	3	3	3	3	3	3	3	3	3	3	3	3	4	4	4	4

Dec	RA = 240				250				260				270				280				290			
38	3	3	3	3	3	3	3	3	3	3	3	3	3	3	3	4	4	4	4	5	5	6	7	8
32	3	3	4	4	4	4	4	4	4	4	4	4	4	4	4	4	4	5	5	5	6	6	7	8
28	4	4	4	4	4	4	4	4	4	4	4	4	4	4	4	5	5	5	5	6	6	6	7	7

Dec	RA = 300				310				320				330				340				350			
38	22	25	27	28	27	26	23	20	17	14	11	9	7	6	5	5	5	4	4	4	4	4	4	4
32	13	14	14	14	14	13	12	10	9	7	6	6	5	5	4	4	4	4	4	4	3	3	3	3
28	10	9	9	9	8	8	7	6	6	5	5	5	4	4	4	4	4	4	3	3	3	3	3	3

Dec	RA = 10				20				30				40				50			
38	3	3	3	3	3	3	3	3	3	3	3	4	4	4	4	4	4	4	4	4
32	3	3	3	3	3	3	3	3	3	3	3	3	3	3	3	3	4	4	4	4
28	3	3	3	3	3	3	3	3	3	3	3	3	3	3	3	3	3	4	4	4

Dec	RA = 60				70				80				90				100				110			
38	5	5	5	5	5	5	5	5	5	5	5	5	5	5	5	4	4	4	4	4	4	4	4	3
32	4	4	4	4	4	5	5	5	5	5	5	5	5	5	5	5	5	4	4	4	4	4	4	4
28	4	4	4	4	4	4	5	5	5	5	5	5	5	5	5	5	5	5	4	4	4	4	4	4

Dec	RA = 120				130				140				150				160				170			
38	3	3	2	2	2	2	2	2	2	2	2	2	2	2	2	2	2	2	2	2	2	2	2	2
32	3	3	2	2	2	2	2	2	2	2	2	2	2	2	2	2	2	2	2	2	2	2	2	2
28	3	3	2	2	2	2	2	2	2	2	2	2	2	2	2	2	2	2	2	2	2	2	2	2

Dec	RA = 180				190				200				210				220				230			
38	2	2	2	2	2	2	2	2	2	2	2	2	2	2	3	3	3	3	3	3	3	3	3	3
32	2	2	2	2	2	2	2	2	2	3	3	3	3	3	3	3	3	3	3	3	3	3	3	3
28	2	2	2	2	2	2	3	3	3	3	3	3	3	3	3	3	3	3	3	3	4	4	4	4

Dec	RA = 240				250				260				270				280				290			
38	3	3	3	3	3	3	3	3	3	3	3	3	3	3	3	4	4	4	4	4	5	5	6	7
32	3	3	4	4	4	4	4	4	4	4	4	4	4	4	4	4	4	5	5	5	5	6	6	7
28	4	4	4	4	4	4	4	4	4	4	4	4	4	4	4	5	5	5	5	6	6	6	7	7

Dec	RA = 300				310				320				330				340				350			
38	22	25	27	28	27	26	23	20	17	14	11	9	7	6	5	5	5	4	4	4	4	4	4	4
32	13	14	14	14	14	13	12	10	9	7	6	6	5	5	4	4	4	4	4	4	3	3	3	3
28	10	9	9	9	8	8	7	6	6	5	5	5	4	4	4	4	4	4	3	3	3	3	3	3

Appendix E - Atmospheric Correction

The total sky temperature T_{sky} at an angle z from the zenith is

$$T_{sky}(z) = T_{atm}B(\tau,z) + T_{ext}\{1 - B(\tau,z)\} \tag{E.1}$$

where $$B(\tau,z) = \iint d\Omega\, g(\theta,\phi)\left(1 - e^{-\tau H(z)}\right), \tag{E.2}$$

and $g(\theta,\phi)$ = normalized gain pattern of the antenna,

$H(z)$ = thickness of the atmosphere,

τ = mean optical depth of the atmosphere,

T_{atm} = physical temperature of the amosphere $\simeq$ 240 K,

T_{ext} = combined temperature of all sources beyond the atmosphere,

(Stokes, 1968; Witebsky, 1984). Expanding the exponential in Eq. (E.2), and keeping terms to third order, we get

$$B(\tau,z) = \tau B_1(z) - \frac{1}{2}\tau^2 B_2(z) + \frac{1}{6}\tau^3 B_3(z), \tag{E.3}$$

where $$B_n(z) = \iint d\Omega\, g(\theta,\phi)\left(H(z)\right)^n.$$

Inserting Eq. (E.3) into Eq. (E.1) gives

$$T_{sky}(z) = T_{ext} + (T_{atm} - T_{ext})\left\{\tau B_1(z) - \frac{1}{2}\tau^2 B_2(z) + \frac{1}{6}\tau^3 B_3(z)\right\}.$$

An expression for τ is obtained as follows. If one measurement of the intensity of the sky emission is made at an angle z from vertical and another

measurement is made at vertical, then the difference between them is

$$\Delta T = (T_{atm} - T_{ext})\{\tau \Delta B_1 - \frac{1}{2}\tau^2 \Delta B_2 + \frac{1}{6}\tau^3 \Delta B_3\} \tag{E.4}$$

where $\Delta B_n = B_n(z) - B_n(0)$.

Let $$\varepsilon = \frac{\Delta T}{(T_{atm} - T_{ext})\ \Delta B_1} .$$

Then Eq. (E.4) becomes

$$\varepsilon = \tau - \frac{1}{2}\tau^2 \frac{\Delta B_2}{\Delta B_1} + \frac{1}{6}\tau^3 \frac{\Delta B_3}{\Delta B_1} .$$

This can be inverted to yield

$$\tau = \varepsilon + \frac{1}{2}\left(\frac{\Delta B_2}{\Delta B_1}\right)\varepsilon^2 + \left\{\frac{1}{2}\left(\frac{\Delta B_2}{\Delta B_1}\right)^2 - \frac{1}{6}\left(\frac{\Delta B_3}{\Delta B_1}\right)\right\}\varepsilon^3 . \tag{E.5}$$

Inserting Eq. (E.5) into Eq. (E.4) gives

$$T_{sky}(0) = T_{ext} + (T_{atm} - T_{ext})\left\{\varepsilon B_1 + \frac{1}{2}\varepsilon^2\left(\frac{\Delta B_2}{\Delta B_1} B_1 - B_2\right)\right.$$

$$\left. + \frac{1}{2}\varepsilon^3\left(\frac{\Delta B_2}{\Delta B_1}\left(\frac{\Delta B_2}{\Delta B_1} B_1 - B_2\right) + \frac{1}{3}\left(B_3 - \frac{\Delta B_3}{\Delta B_1} B_1\right)\right)\right\} ,$$

where B_1, B_2, and B_3 are evaluated at $z = 0$.

The vertical atmospheric antenna temperature is

$$T_{VA} = T_{sky}(0) - T_{ext}$$

$$= \frac{\Delta T}{\Delta B_1}\{ B_1 + \frac{1}{2}(\frac{\Delta T}{\Delta B_1 T_{atm}})(\frac{\Delta B_2}{\Delta B_1} B_1 - B_2)$$

$$+ \frac{1}{2}(\frac{\Delta T}{\Delta B_1 T_{atm}})^2 (\frac{\Delta B_2}{\Delta B_1}(\frac{\Delta B_2}{\Delta B_1} B_1 - B_2) + \frac{1}{3}(B_3 - \frac{\Delta B_3}{\Delta B_1} B_1))\}$$

$$= \frac{\Delta T}{F_o}\{F_1 + (\frac{\Delta T}{F_o T_{atm}})F_2 + (\frac{\Delta T}{F_o T_{atm}})^2 F_3\},$$

where $F_o = \Delta B_1$;

$$F_1 = B_1;$$

$$F_2 = \frac{1}{2}\{\frac{\Delta B_2}{\Delta B_1} B_1 - B_2\};$$

$$F_3 = \frac{1}{2}\{\frac{\Delta B_2}{\Delta B_1}(\frac{\Delta B_2}{\Delta B_1} B_1 - B_2) + \frac{1}{3}(B_3 - \frac{\Delta B_3}{\Delta B_1} B_1)\},$$

and we have made the approximation $T_{atm} - T_{ext} \simeq T_{atm}$, since $T_{atm} \simeq 240$ K and $T_{ext} \simeq 3$ K. This is the same as Eq. (V.5).

The function H(z) is the ratio of the thickness of the atmosphere at an angle z from vertical, to the vertical thickness. If the atmosphere were a flat slab then H(z) = sec(z). It is easily shown that the generalization to this expression, due to its curvature, is

$$H(z) = \sec(z) - \frac{1}{2}\frac{r}{R}\sec^3(z)$$

where r = mean scale height of the atmosphere ;

R = radius of the earth,

and we have kept only the second order correction term. Approximately 90% of the atmospheric emission at $\lambda = 3$ cm is due to oxygen, and 10% due to water vapor (Partridge et al., 1984). Therefore, we take $r = 7$ km, the scale height for oxygen, giving $(r/R) \simeq 1.09 \times 10^{-3}$.

The values of the constants $F_o - F_3$ are found for the zenith angles 30° and 40° by numerical integration. For the purposes of this integration the E-plane beam pattern (Figure II.5a) has been used. This pattern is split into three regions. For the inner 10° portion it is well fit by a Gaussian,

$$g(\theta,\phi) = (15.50)e^{-(0.01775)\theta^2} ,$$

where θ is in degrees. For the range $10^o < \theta < 34^o$ values for the gain were taken directly from Figure II.5a. For $34^o < \theta < 45^o$ another Gaussian is used,

$$g(\theta,\phi) = (15.50)e^{-(0.00697)\theta^2} ,$$

which smoothly joins the intermediate region. The leading factor in the Gaussian profiles was chosen to properly normalize the gain to unity.

Just prior the Series III runs the radiometer shifted on its bearings 3.4^o toward the east. This series therefore required slightly different values for the terms $F_o - F_3$. The angles for the series I, II, and IV - IX runs were within four arcminutes of their nominal values.

The numerical values of $F_o - F_3$ are given in Table E.1.

Table E.1 - Atmospheric numerical constants

Series I, II, and IV - IX

	F_o	F_1	F_2	F_3
30°	0.16286	1.01419	0.62287	0.92838
40°	0.32441	1.01419	0.71756	1.15316

Series III

30°	0.15391	1.01604	0.65513	1.07820
40°	0.31367	1.01604	0.73860	1.26221

Appendix F - Error Analysis

The total experimental error was determined by considering separately the systematic errors and the statistical errors.

F.1 Systematic Errors

The three fundamental equations for the calibration constant, vertical atmospheric antenna temperature, and cosmic background antenna temperature are :

$$\alpha = g \frac{T_{amb} - T_{cla}}{V_{amb} - V_{cla}} ;$$

$$T_{VA} = \frac{\Delta T}{F_o} \left\{ F_1 + \frac{\Delta T}{F_o T_{atm}} F_2 + \left(\frac{\Delta T}{F_o T_{atm}} \right)^2 F_3 \right\} ;$$

$$T_{CBRa} = \alpha(V_o - V_{cla}) + T_{cla} - (T_{VA} + T_{go} + T_{so}) ;$$

where $\Delta T = \alpha(V_1 - V_o) - (T_{g1} + T_{s1}) + (T_{go} + T_{so})$.

The formal systematic errors for α, T_{VA} , and T_{CBRa} were calculated for each run, and are listed in Table F.1. The terms used to compute these errors appear in Table F.2. The total systematic error was found by combining in quadrature the individual errors that appear in the error equations given below.

F.1.a Calibration Constant

The systematic error in the calibration constant is given by

$$\sigma_\alpha^2 = \sigma_g^2 \left\{ \frac{T_{amb} - T_{cla}}{V_{amb} - V_{cla}} \right\}^2$$

$$+ g^2 \left\{ \frac{T_{amb} - T_{cla}}{V_{amb} - T_{cla}} \right\}^2 (\delta_\alpha \delta_T)^2$$

$$+ \left\{ \sigma_{Tamb}^2 + \sigma_{Tcla}^2 \right\} \left\{ \frac{g}{V_{amb} - V_{cla}} \right\}^2$$

$$+ \left\{ \sigma_{Vamb}^2 + \sigma_{Vcla}^2 \right\} \left\{ g \frac{T_{amb} - T_{cla}}{(V_{amb} - V_{cla})^2} \right\}^2 .$$

These terms are listed in decreasing order of importance. The first term arises because of the uncertainty in the gain saturation g, and accounts for more than 95% of the error. Since $\sigma_g = 0.01$ is a constant, σ_α has the same value for each run :

$$\sigma_\alpha = 9 \times 10^{-5} \text{ K/du} .$$

Since the inputs into the two antennas of the radiometer were always at nearly the same power level, the output of the radiometer was close to zero. Thus the systematic error in the calibration constant caused a very small error in T_{CBRa}. This is the reason that it was advantageous for the secondary antenna to view a cold stable source instead of a warm stable source.

F.1.b Vertical Atmospheric Temperature

The error in the vertical atmospheric antenna temperature is calculated separately for data taken at the zenith angles ±30° and ±40°. At ±40° this error is

$$\sigma_{40}^2 = \{ \alpha^2 (\sigma_{V1}^2 + \sigma_{Vo}^2) + \sigma_{g1}^2 + \sigma_{s1}^2 + \sigma_{go}^2 + \sigma_{so}^2 \}$$

$$\times \left\{ \frac{F_1}{F_o} + 2\frac{F_2}{F_o^2} \frac{\Delta T}{T_{atm}} \right\}^2$$

$$+ \sigma_\alpha^2 \left\{ \frac{F_1}{F_o} (V_1 - V_o) + \frac{2}{F_o^2} \frac{F_2}{T_{atm}} \Delta T (V_1 - V_o) \right\}^2$$

$$+ \sigma_{F_o}^2 \left\{ \frac{F_1}{F_o^2} (\Delta T) + \frac{2}{F_o^3} \frac{F_2}{T_{atm}} (\Delta T)^2 \right\}^2$$

$$+ \sigma_{F_1}^2 \left\{ \frac{\Delta T}{F_o} \right\}^2$$

$$+ \sigma_{F_2}^2 \left\{ \frac{1}{T_{atm}} \left(\frac{\Delta T}{F_o}\right)^2 \right\}^2$$

$$+ \sigma_{atm}^2 \left\{ F_2 (T_{atm})^{-2} \left(\frac{\Delta T}{F_o}\right)^2 \right\}^2 .$$

The same formal expression holds for σ_{30}, except that different values for the atmospheric constants F_o, F_1, and F_2 must be used. In this expression we have neglected the terms involving F_3 since they are less than 10^{-4} as large as the terms involving F_1.

The first term on the right hand side is the largest. It is dominated by the flip asymmetry, of magnitude $(\sigma_{Vo})\alpha = (\sigma_{V1})\alpha = 30$ mK. However, σ_{30} is about twice as large as σ_{40} since the term $1/F_o$ is twice as large for 30° as it is for 40°. These errors appear in Table F.1 under the headings "SIG30" and "SIG40", respectively.

The error in the vertical atmospheric temperature is given by the weighted mean of σ_{30} and σ_{40},

$$\sigma_{VA}^2 = \{ \sigma_{30}^{-2} + \sigma_{40}^{-2} \}^{-1} .$$

This is listed under the heading "SIGVA" in Table F.1.

The measured CBR temperature was more accurate in 1983 than in 1982 because σ_{40} is considerably less than σ_{30}, which causes a corresponding decrease in σ_{VA}.

F.1.c Cosmic Background Temperature

The error in the cosmic background radiation antenna temperature is

$$\begin{aligned}\sigma^2_{CBRa} = \; & \sigma^2_{VA} \\ & + \alpha^2 \; (\sigma^2_{Vo} + \sigma^2_{Vcla}) \\ & + \sigma^2_{Tcla} + \sigma^2_{go} + \sigma^2_{so} \\ & + \sigma^2_{\alpha} \; (V_o - V_{cla})^2 .\end{aligned}$$

By far the largest contribution is from the error in the vertical atmospheric temperature, σ_{VA}. The second term, about a factor of ten lower than the first, is primarily due to the flip asymmetry. The last two terms are negligibly small.

The error in the CBR antenna temperature is listed in Table F.1 under the heading "SIGCBRa".

Adding these errors in quadrature is not strictly correct because some of them are correlated. However, tests in which the parameters are varied indicate that this formula is a reasonable approximation, because the error σ_{VA} is much larger than the others.

The error σ_{CBRa} varies slightly from series to series because the atmospheric temperature and the galactic background are not constant. The mean value of σ_{CBRa} is 0.13 K

Zenith scans were made only at $\pm 30^{o}$ in 1982. If the flip asymmetry were the same then as in 1983 then the error in σ_{VA} for 1982 would be about the same as σ_{30} in Table F.1. The error in the CBR antenna temperature would be about twice as large as the values of σ_{CBRa} shown in Table F.1. However, as was discussed earlier, the true magnitude of the flip asymmetry was probably greater than 30 mK in 1982. Since we are uncertain of its magnitude we include only the 1983 data in Table F.1 and in this error analysis.

F.2 Statistical Errors

The RMS of the 59 measurements of T_{CBRa} is 0.07 K. The standard deviation in the mean is $(0.07\ K)/59^{1/2} \simeq 0.01$ K.

An ideal radiometer with a sensitivity of 46 $mK/Hz^{1/2}$ which measures the atmosphere at two pairs of zenith angles would have an RMS variation of 0.04 K in T_{CBRa}. This assumes that the radiometer is subject to no systematic errors. The observed RMS is higher primarily because of atmospheric fluctuations. For the Series III runs, when the atmosphere was most stable, the RMS was only 0.04 K, in agreement with the ideal value.

F.3 Total Experimental Error

The sum of the estimated systematic error (0.13 K) and the statistical deviation in the mean (0.01 K) gives the total experimental error of 0.14 K. Thus the final value for the temperature of the cosmic background radiation at a wavelength of 3.0 cm is

$T_{CBRa} = 2.41 \pm 0.14$ K (antenna temperature) ;

$T_{CBR} = 2.64 \pm 0.14$ K (thermodynamic temperature) .

Table F.1 - Systematic errors

1983		TIME (UT)	SIGALPHA	SIG30	SIG40	SIGVA	SIGCBRa
SERIES I	1	4: 8:25:53	0.00009	0.263	0.136	0.121	0.129
	2	4: 8:29:37	0.00009	0.263	0.136	0.121	0.130
	3	4: 8:33:21	0.00009	0.262	0.135	0.120	0.129
	4	4: 8:37: 5	0.00009	0.263	0.136	0.121	0.129
	5	4: 8:40:49	0.00009	0.263	0.136	0.121	0.129
	6	4: 8:44:33	0.00009	0.263	0.136	0.121	0.129
	7	4: 8:48:17	0.00009	0.263	0.136	0.121	0.130
	8	4: 8:52: 1	0.00009	0.263	0.136	0.121	0.130
	9	4: 8:55:45	0.00009	0.263	0.135	0.120	0.129
	10	4: 8:59:29	0.00009	0.262	0.135	0.120	0.129
	11	4: 9: 3:13	0.00009	0.263	0.135	0.120	0.129
	12	4: 9: 6:57	0.00009	0.264	0.136	0.121	0.129
	13	4: 9:10:41	0.00009	0.263	0.135	0.120	0.129
	14	4: 9:14:25	0.00009	0.263	0.136	0.121	0.129
	15	4: 9:18: 9	0.00009	0.263	0.136	0.121	0.129
SERIES II	16	5: 3:31:50	0.00009	0.263	0.136	0.121	0.129
	17	5: 3:35:34	0.00009	0.263	0.136	0.121	0.129
	18	5: 3:39:18	0.00009	0.263	0.136	0.121	0.129
	19	5: 3:43: 2	0.00009	0.263	0.135	0.120	0.129
	20	5: 3:46:46	0.00009	0.263	0.136	0.120	0.129
	21	5: 3:50:30	0.00009	0.264	0.136	0.121	0.129
	22	5: 3:54:14	0.00009	0.263	0.136	0.121	0.130
	23	5: 3:57:58	0.00009	0.263	0.135	0.120	0.129
	24	5: 4: 1:42	0.00009	0.264	0.135	0.120	0.129
	25	5: 4: 5:26	0.00009	0.263	0.135	0.120	0.129
	26	5: 4: 9:10	0.00009	0.263	0.136	0.121	0.130
	27	5: 4:12:54	0.00009	0.264	0.136	0.121	0.130
	28	5: 4:16:38	0.00009	0.264	0.135	0.120	0.129
SERIES III	29	5: 9: 0:38	0.00009	0.278	0.140	0.125	0.133
	30	5: 9: 8: 6	0.00009	0.277	0.140	0.125	0.133
	31	5: 9:11:50	0.00009	0.277	0.140	0.125	0.133
	32	5: 9:15:34	0.00009	0.277	0.140	0.125	0.133
	33	5: 9:19:18	0.00009	0.277	0.140	0.125	0.133
	34	5: 9:23: 2	0.00009	0.277	0.139	0.125	0.133
	35	5: 9:26:46	0.00009	0.277	0.139	0.124	0.133
	36	5: 9:30:30	0.00009	0.278	0.140	0.125	0.133
	37	5: 9:34:15	0.00009	0.278	0.140	0.125	0.133
	38	5: 9:37:59	0.00009	0.278	0.140	0.125	0.133
SERIES IV	39	6: 7: 2:35	0.00009	0.260	0.134	0.119	0.128
	40	6: 7: 6:19	0.00009	0.261	0.134	0.120	0.128
	41	6: 7:10: 3	0.00009	0.262	0.135	0.120	0.129
	42	6: 7:13:47	0.00009	0.262	0.134	0.119	0.128
	43	6: 7:17:31	0.00009	0.263	0.135	0.120	0.128
	44	6: 7:21:15	0.00009	0.262	0.135	0.120	0.128
	45	6: 7:24:59	0.00009	0.263	0.135	0.120	0.128
	46	6: 7:28:43	0.00009	0.263	0.135	0.120	0.129
	47	6: 7:32:27	0.00009	0.261	0.134	0.120	0.128
	48	6: 7:36:11	0.00009	0.262	0.134	0.120	0.128
	49	6: 7:39:55	0.00009	0.262	0.135	0.120	0.128
	50	6: 7:43:39	0.00009	0.263	0.135	0.120	0.129
	51	6: 7:47:23	0.00009	0.263	0.135	0.120	0.129
	52	6: 7:51: 7	0.00009	0.262	0.135	0.120	0.129
	53	6: 7:54:51	0.00009	0.262	0.135	0.120	0.128
	54	6: 7:58:35	0.00009	0.262	0.135	0.120	0.128
	55	6: 8: 2:19	0.00009	0.262	0.135	0.120	0.128
	56	6: 8: 6: 3	0.00009	0.262	0.135	0.120	0.128
	57	6: 8: 9:47	0.00009	0.261	0.134	0.119	0.128
	58	6: 8:13:31	0.00009	0.262	0.135	0.120	0.128
	59	6: 8:17:15	0.00009	0.262	0.135	0.120	0.128

Table F.2 - Parameters used in error analysis

Parameter	Error	Value of Error	Description
α	σ_α	——	Calibration constant
T_{VA}	σ_{VA}	——	Vertical atmos. antenna temp.
T_{CBRa}	σ_{CBRa}	——	CBR antenna temp.
g	σ_g	0.01	gain saturation factor
T_{amb}	σ_{Tamb}	0.3 K	antenna temp. of ambient load
T_{cla}	σ_{Tcla}	0.01 K	antenna temp. of LHe load
V_{amb}	σ_{Vamb}	3.3 du	radiometer output, ambient load
V_{cla}	σ_{Vcla}	3.3 du	radiometer output, LHe load
V_1	σ_{V1}	3.3 du	radiometer output, $\theta = \pm 30^o, \pm 40^o$
T_{g1}	σ_{g1}	$(0.5)T_{g1}$	galactic back. temp., $\theta = \pm 30^o, \pm 40^o$
T_{s1}	σ_{s1}	3 mK	sidelobe temp., $\theta = \pm 30^o, \pm 40^o$
V_o	σ_{Vo}	3.3 du	radiometer output, $\theta = 0^o$
T_{go}	σ_{go}	$(0.5)T_{go}$	galactic background temp., $\theta = 0^o$
T_{so}	σ_{so}	3 mK	sidelobe temp., $\theta = 0^o$
T_{atm}	σ_{atm}	20 K	mean physical temp. of atmosphere
F_o	σ_{F_o}	$(0.03)F_o$	atmospheric numerical constant
F_1	σ_{F_1}	$(0.01)F_1$	atmospheric numerical constant
F_2	σ_{F_2}	$(0.03)F_2$	atmospheric numerical constant
—	δ_α	$0.02/^oC$	gain temperature coefficient
—	δ_T	0.1^oC/run	temperature drift of receiver

Acknowledgments

The international scope of this experiment has made for a most interesting graduate career. I have profited greatly from my exposure to physicists with different backgrounds, and who have different approaches to research. George Smoot set the style and direction of the Berkeley portion of the experiment. He showed me how to identify the important tasks, and how to pursue the solutions. I am grateful to him for teaching me to think and act independently. I thank Reno Mandolesi, Bruce Partridge, Giorgio Sironi, and Gigi Danese for an enjoyable collaboration. I have learned from each of them, and now have friends to visit on my first trip to Italy.

I have been fortunate to work with Chris Witebsky, Giovanni De Amici, and Steve Levin on this experiment. The successful operation of the LHe-cooled load, perhaps the single most important piece of equipment in the experiment, was primarily due to Chris' determined efforts. Hal Dougherty and John Gibson provided mechanical and electronics support at their standard level of excellence. The experiment would not have been possible without their contributions.

Clarence Hall, Dave Trydahl, and the staff at the White Mountain Research Station could not have been more helpful and pleasant to work with. They made our long visits to Barcroft memorable, although I may have used a different description if asked at the time. I especially appreciate the long nights they spent taming a rogue electrical generator.

Terry Mast, Rich Muller, Phil Lubin, Jerry Epstein, and Luis Alvarez have made my working environment very interesting and educational. I have enjoyed my association with each of them. I thank Luis in particular for providing me with the only twin engine piloting time that I have logged to date. Nancy Gusack

and Faye Mitschang have provided excellent administrative and secretarial services, and are really responsible for the successful operation of the astrophysics group.

The Lawrence Berkeley Laboratory has been a wonderful place to work, with many resources at my disposal. One can always locate someone who knows something about anything at LBL. I also thank the staff of the Space Sciences Laboratory for their support. This work has been supported by the National Science Foundation, the Department of Energy, and the White Mountain Research Station of the University of California.

Finally I owe many thanks to my parents, who have given me constant support and encouragement throughout my education.

References

Bardeen, J., J. Appl. Phys. 11, 88 (1940).

Barrow, J. D. and Turner, M. S., Nature 298, 801 (1982).

Bohm-Vitense, E. and Szkody, P., Ap. J. 184, 211 (1973).

Bontz, R. J., Price, R. H., and Haugan, M. P., Ap. J. 246, 592 (1981).

Buta, R. and de Vaucouleurs, G., Ap. J. 266, 1 (1983).

Chan, K. L. and Jones, B. J. T., Ap. J. 195, 1 (1975).

Danese, L. and De Zotti, G., Rivista Del Nuovo Cimento 7, 277 (1977).

Danese, L. and De Zotti, G., Astron. Astrophys. 68, 157 (1978).

Danese, L. and De Zotti, G., Unpublished report (1979).

De Amici, G., Witebsky, C., Smoot, G. F., and Friedman, S. D., submitted to Phys. Rev. D (1984).

Dicke, R. H., Peebles, P. J. E., Roll, P. G., and Wilkinson, D. T., Ap. J. 142, 414 (1965).

Donnelly, R. J., Experimental Superfluidity (University of Chicago Press, Chicago, Il., 1967).

Doroshkevich, A. G., Zeldovich, Ya B., and Novikov, I. D., Sov. Phys.-JETP 26, 408 (1968).

Epstein, G. L., Ph.D. Thesis, University of California, Berkeley, 1983.

Fixsen, D. J., Cheng, E. S., and Wilkinson, D. T., Phys. Rev. Lett. 50, 620 (1983).

Friedman, S. D., Smoot, G. F., De Amici, G., and Witebsky, C., submitted to Phys. Rev. D (1984).

Guth, A. H., Phys. Rev. D 23, 347 (1981).

Harrison, E. R., Phys. Rev. Lett. 18, 1011 (1967).

Harrison, E. R., Ann. Rev. Astron. Astrophys. 11, 155 (1973).

Haslam, C. G. T., Salter, C. J., Stoffel, H., and Wilson, W. E., Astron. Astrophys. Suppl. Ser. 47, 1 (1982).

Hubble, E., Proc. Nat. Acad. Sci. 15, 168 (1929).

Illarionov, A. F. and Sunyaev, R. A., Sov. Astron 18, 691 (1975).

Jones, B. J. T., Physica Scripta 21, 732 (1980).

Kompaneets, A. S., Sov. Phys.-JETP 4, 730 (1957).

Kraus, J. D., Radio Astronomy (McGraw-Hill, 1966).

Lorrain, P. and Corson, D. R., Electromagnetic Fields and Waves, 2nd Edition (W. H. Freeman and Co., San Francisco, Ca., 1970).

Lorentz, H. A., Einstein, A., Minkowski, H., and Weyl, H, The Principle of Relativity (Dover Publications, Inc., New York, 1952).

Lubin, P. M., and Smoot, G. F., Ap. J. 245, 1 (1981).

Lubin, P. M., Epstein, G. L., and Smoot, G. F., Phys. Rev. Lett. 50, 616 (1983a).

Lubin, P., Melese, P., and Smoot, G., Ap. J. 273, L51 (1983b).

Mandolesi, N., Calzolari, P., Cortiglioni, S., and Morigi, G., submitted to Phys. Rev. D (1984).

Matsuda, T., Sato, H., and Takeda, H., Progr. Theor. Phys. (Japan) 46, 416 (1971).

Meyer, D. M. and Jura, M., Ap. J. Lett. 276, L1 (1984).

Negroponte, J., Powan-Robinson, M., and Silk, J., Ap. J. 248, 38 (1981).

Partridge, R. B., Cannon, J., Foster, R., Johnson, C., Rubinstein, H., Rudolph, A., Danese, L., and De Zotti, G., submitted to Phys. Rev. D (1984).

Peebles, P. J. E., Phys. Rev. D 1, 397 (1970).

Peebles, P. J. E., Physical Cosmology (Princeton University Press, Princeton, N. J., 1971).

Penzias, A. A. and Wilson, R. W., Ap. J. 142, 419 (1965).

Press, W. H., in Cosmology and Particles, Audouze et al., editors, Proceedings of the Sixteenth Recontre de Moriond Astrophysics Meeting (Singapore National Printers, 1981).

Ramo, S., Whinnery, J. R., and Van Duzer, T., Fields and Waves in Communication Electronics (John Wiley & Sons, Inc., NY., 1965).

Roll, P. G. and Wilkinson, D. T., Phys. Rev. Lett. 16, 405 (1966).

Rood, R. T., Ap. J. 184, 815 (1973).

Sandage, A. and Tammann, G. A., Ap. J. 256, 339 (1982).

Sironi, G., Inzani, P., and Ferrari, A., submitted to Phys. Rev. D (1984).

Smart, W. M., Textbook on Spherical Astronomy, 6th Edition (Cambridge University Press, NY, 1977).

Smoot, G. F., De Amici, G., Friedman, S. D., Witebsky, C., Mandolesi, N., Partridge, R. B., Sironi, G., Danese, L., and De Zotti, G., Phys. Rev. Lett. 51, 1099 (1983).

Stokes, R. A., Ph.D. Thesis, Princeton University, 1968.

Stokes, R. A., Partridge, R. B., and Wilkinson, D. T., Phys. Rev. Lett. 19, 1199 (1967).

Sunyaev, R. A. and Zeldovich, Ya B., Astron. and Ap. 20, 189 (1972).

Ulaby, F. T., Moore, R. K., and Fung, A. K., Microwave Remote Sensing, Volume 1 (Addison-Wesley, Reading, Ma., 1981).

Weinberg, S., Gravitation and Cosmology (John Wiley & Sons, N.Y., 1972).

Weiss, R., Ann. Rev. Astron. Astrophys. 18, 489 (1980).

Weymann, R., Phys. Fluids 8, 2112 (1965).

Weymann, R., Ap. J. 145, 560 (1966).

Wilkinson, D. T., Phys. Rev. Lett. 19, 1195 (1967).

Witebsky, C., COBE Report #5013 (1978), unpublished.

Witebsky, C., Ph.D. Thesis, University of California, 1984.

Woody, D. P. and Richards, P. L., Ap. J. 248, 18 (1981).

Yang, J., Schramm, D. N., Steigman, G., and Rood, R. T., Ap. J. 227, 697 (1979).

Zeldovich, Ya B., Kurt, V. G., and Sunyaev, R. A., Sov. Phys.-JETP 28, 146 (1969).

Zeldovich, Ya B., and Illarionov, A. F., Sov. Phys.-JETP 38, 643 (1975).

This report was done with support from the Department of Energy. Any conclusions or opinions expressed in this report represent solely those of the author(s) and not necessarily those of The Regents of the University of California, the Lawrence Berkeley Laboratory or the Department of Energy.

Reference to a company or product name does not imply approval or recommendation of the product by the University of California or the U.S. Department of Energy to the exclusion of others that may be suitable.

TECHNICAL INFORMATION DEPARTMENT
LAWRENCE BERKELEY LABORATORY
UNIVERSITY OF CALIFORNIA
BERKELEY, CALIFORNIA 94720